2021

A Role for ACSBG1 in Obesity-Accelerated Breast

Olivia Maguire

A ROLE FOR ACSBG1 IN OBESITY-ACCELERATED BREAST CANCER

A Thesis Presented to the Faculty of
The Rockefeller University
in Partial Fulfillment of the Requirements for
the degree of Doctor of Philosophy

by
Olivia Maguire
June 2021

A ROLE FOR ACSBG1 IN OBESITY-ACCELERATED BREAST CANCER

Olivia Maguire, Ph.D.
The Rockefeller University 2021

Overweight and obesity affect more than 70% of American adults and are major risk factors for the development of comorbidities, including cancer. Breast cancer is the most commonly diagnosed malignancy in American women: 1 in 8 women will develop breast cancer in their lifetimes, and more than 40,000 women die from breast cancer each year. Obesity is associated with increased incidence and worse prognosis in breast cancer, including aggressive triple-negative breast cancer, which has a particularly poor prognosis with few treatment options. The goal of this thesis was to elucidate the mechanisms by which obesity promotes breast cancer progression. To that end, we used an orthotopic model of triple-negative murine mammary carcinoma in a diet-induced model of obesity. We found that obesity significantly accelerated tumor growth, which was due to increased proliferation. Upon performing whole-tissue RNA sequencing of tumors isolated from lean or obese animals, we found that many of the transcriptional programs differentially regulated in obesity were immune-related. Since tumors are cellularly heterogeneous and contain tumor-associated cell types, such as immune cells, adipocytes, endothelial cells, and fibroblasts, we devised a fluorescence-based approach to specifically isolate cancer cells prior to analysis. To achieve this, we produced a stable-mCherry expressing breast cancer cell line and utilized fluorescence-activated cell sorting to isolate cancer cells from heterogeneous tumor tissue. RNA sequencing of this pure cancer cell population identified the acyl-CoA synthetase, Acsbg1, as robustly upregulated in cancer cells isolated from tumors in obese compared to lean animals. Overexpression of Acsbg1 in tumor cells further enhanced tumor growth in an obesity-specific manner, which required intact creatine transport. Inhibition of acyl-CoA synthetase activity, on the other hand, significantly attenuated tumor growth in obese animals. This led us to hypothesize that Acsbg1 may reprogram the breast cancer cell metabolome. We performed targeted metabolomic analysis on tumors from lean and obese animals and identified a role for Acsbg1 in promoting mitochondrial ATP production, which was confirmed with plate-based respirometry. We used untargeted lipidomic analysis to identify the lipid substrate and products of Acsbg1 activity and found that phospholipids containing 20:4 and 22:4 side chains were more abundant in Acsbg1-overexpressing tumors in obesity. The most common 20:4 and 22:4 lipid species are arachidonic and adrenic acid, respectively. Since arachidonic and adrenic acid are products of sequential steps of linoleic acid metabolism, an essential fatty acid, this suggests a role for dietary lipids in the pathogenesis of obesity-driven breast cancer progression. These findings further suggest that Acsbg1 supports obesity-related tumor progression through both catabolic ATP generation and anabolic processes to build biomass. Finally, we analyzed a dataset of human tumor gene expression and found that Acsbg1 levels are associated with worse tumor grade and with aggressive, basal-like cancers in overweight and obese individuals. Overall, these studies identified an undescribed, obesity-specific role for Acsbg1 in promoting tumor progression and provide the foundation for further studies investigating Acsbg1 and acyl-coA synthetase activity as a possible target for therapeutic intervention in breast cancer and other obesity-driven cancer types.

For Mason

ACKNOWLEDGMENTS

Thank you, Paul, for your extraordinary mentorship. Choosing to join your lab was easily the best decision that I made during graduate school. Thank you for teaching me how to be scientist and for setting such a tremendous example of a physician-scientist. Watching you seamlessly balance your scientific career, clinical practice, and family life has inspired me more than you could possibly know.

To the other Adiposcientists, past and present: gloves off, party hats on! I could not resist writing that one last time. Thank you all for making graduate school not only educational, but incredibly fun. I will miss our lab celebrations and think of you whenever I listen to the Harry Potter audiobooks. I cannot wait for "The Team Who Must Not Be Named" to rise again! I would especially like to thank my scientific partner, Sarah Ackerman. I will be forever grateful that you helped me put out the metaphorical trash fire (and that one time, a literal flask fire).

Thank you to my faculty advisory committee: Drs Sohail Tavazoie, Barry Coller, and Richard White. Your feedback on this work has been invaluable. Thank you, Dr. Emily Gallagher for being my external examiner, I truly appreciate all of your input. Thank you, Dr. Danielle Friedman, you have been a wonderful collaborator and an exceptional role model.

Thank you to the Rockefeller Resource Centers for your help with this work, so much of it would have been impossible without your assistance and guidance.

Thank you to the MD-PhD program directors, staff, and students. Over the last seven years, 1300 York, C103 has been my on-campus home base, and I am convinced that the candy from the MD-PhD bowl has magical, destressing powers. To the Rockefeller University Dean's office: thank you for keeping me on track.

Thank you to my friends. I have known some of you since preschool, others I met as recently as graduate school, but each of you has been such an important source of support. I am so lucky to have friends like you. Those wine nights, happy hours, and brunches were absolutely necessary to get me through the hard days in graduate school.

To my wonderful family: thank you for supporting me along this fifteen-plus year journey. Thank you for rarely asking when I will have a "real job" and for accepting "One day. Probably." as an answer. Dad, this is as much for you as it is for me. To my husband, Jeff: thank you, ML, for being my strongest support, my loudest cheerleader, and my partner in all things.

Mason, I love you, peanut. Being your mama is the best part of my life.

TABLE OF CONTENTS

LIST OF FIGURES

LIST OF TABLES

LIST OF ABBREVIATIONS

2-DG - 2-deoxyglucose
27-HC - 27-hydroxycholesterol
Acsbg1 - acyl-coA synthetase bubblegum family member 1
Acsbg1 KD - Acsbg1 knockdown
Acsbg1 OE - Acsbg1 overexpressing
Acsl - long chain Acyl-coA synthetase
Acsl4 - acyl-CoA Synthetase Long Chain Family Member 4
Adipo-TRAP - adipocyte-specific Rosa26^{fsTRAP}
AMPK - AMP-activated protein kinase
ANL – azidonorleucine
ATGL – adipose triglyceride lipase
B6 - C57BL6/J
BMI - body mass index
Bmp7 - bone morphogenetic protein 7
BONCAT - bio-orthogonal noncanonical amino acid tagging
Cdo1 - cysteine dioxygenase type 1
CLS – crown-like structures
Cpt1 - carnitine palmitoyltransferase I
CRP - C-reactive protein
ECAR - extracellular acidification rate
EdU - 5-ethynyl-2'-deoxyuridine
EMT - epithelial to mesenchymal transition
ER - estrogen receptor
ETP - endotrophin
FCCP - carbonyl cyanide-4 phenylhydrazone
FFA - free fatty acids
GLUT1 - glucose transporter 1
GSEA - gene set enrichment analysis
H&E - hematoxylin and eosin
HER2 - human epidermal growth factor receptor 2
HFD - high fat diet
HIF1-α - hypoxia inducible factor 1 alpha
IGF-1 - insulin like growth factor 1
IGFBP - insulin like growth factor binding protein
IGFR - insulin like growth factor 1 receptor
IHC - immunohistochemistry
IL-1b - interleukin 1 beta
IL-6 - interleukin 6
IR – insulin receptor
IVIS – in vivo imaging system
LC-MS - liquid chromatography / mass spectroscopy
LDL - low density lipoprotein
LDL-R - low density lipoproteins receptor
LPL - lipoprotein lipase

MAPK - mitogen-activated protein kinase
metRS - methionyl tRNA synthetase
mTOR - mammalian target of rapamycin
NCI - National Cancer Institute
NFκB - nuclear factor kappa-light-chain-enhancer of activated B cells
OCR - oxygen consumption rate
ODC1 - ornithine decarboxylase 1
PAF - population attributable fraction
PCA - principal component analysis
PGE2 - prostaglandin E2
PHH3 - phospho-histone H3
PI3K - phosphatidylinositol-4,5-bisphosphate 3-kinase
PR - progesterone receptor
SAA - serum amyloid A
Slc6a8 - solute Carrier Family 6 member 8
T2DM - type 2 diabetes mellitus
Tgf-β - transforming growth factor beta
TNBC - triple negative breast cancer
TNFα - tumor necrosis factor alpha
VEGF - vascular endothelial growth factor
VLDL - very low density lipoprotein
WAT - white adipose tissue
X-ALD - X-linked adrenoleukodystrophy

CHAPTER 1 Introduction

1.1 The epidemiological links between obesity and cancer

Obesity is defined by a body mass index (BMI) above 30. Obesity develops when energy intake chronically exceeds energy expenditure and is characterized by an accumulation of adipose tissue. The prevalence of obesity is increasing rapidly in the United States and around the world. From 1999 to 2017, the rate of obesity among American adults increased from 30.5% to 42.4%. Furthermore, severe obesity, defined by a BMI above 40, increased from 4.7% to 9.2% over that same timeframe (Hales et al. 2020). By 2030, more than 50% of adults in the United States are predicted to be obese (Ward et al. 2019). The rapidly increasing prevalence of obesity is a major public health concern because excess adiposity is a well-established risk factor for comorbidities like hypertension, type 2 diabetes mellitus (T2DM), dyslipidemia, coronary artery disease, and non-alcoholic fatty liver disease (Goossens 2017; Williams et al. 2015). Additionally, epidemiological studies have firmly linked obesity with increased risk and worse outcomes for a number of cancer types. In 2003, a landmark prospective study demonstrated that cancer patients with a BMI above 40 had cancer-specific mortality rates that were 52% higher for men and 62% higher for women (Calle et al. 2003).

In recent years, several other studies have strengthened the evidence that obesity is associated with adverse effects on cancer outcomes (Bhaskaran et al. 2014; Arnold et al. 2015; Renehan et al. 2008). A population-based study estimated that overweight and obesity were associated with more than 72,000 cases of cancer in American women and 28,000 cases of cancer in American men each year (Arnold et al. 2015). Epidemiologists describe the effects of modifiable risk factors on cancer incidence by reporting the population attributable fraction (PAF) of cancer cases. The PAF quantifies the potential reduction in incidence if these factors were reduced or eliminated. These analyses have consistently demonstrated significant PAFs related to obesity in several cancer types in both men and women. The types of cancers which have the highest PAFs associated with obesity in men include esophageal, colorectal, pancreatic, and gallbladder cancers. In women, esophageal, endometrial, gallbladder and breast cancer, among others, can be most strongly attributed to obesity (Whiteman and Wilson 2016).

1.2 Obesity and breast cancer

Breast cancer is a leading cause of morbidity and mortality in the United States. It is the most common cancer in American women; the National Cancer Institute (NCI) estimates that more than 250,000 women will be newly diagnosed with breast cancer in 2020. Furthermore, the NCI estimates that more than 40,000 breast cancer patients will die in 2020, making it the second deadliest cancer in women (National Cancer Institute 2020). Obesity is a major risk factor for the development of breast cancer in post-menopausal women as well as for worse breast cancer outcomes, independent of menopausal status (White et al. 2015; Neuhouser et al. 2016; Chan et al. 2014; Picon-Ruiz et al. 2017; Protani, Coory, and Martin 2010). In 2012, more than 100,000 cases of breast cancer were attributed to overweight and obesity worldwide (Arnold et al. 2015). A retrospective study analyzing more than 18,000 Danish breast cancer patients found that compared to women with a BMI below 25, those patients who had a BMI above 30 had a 46%

higher risk of developing distant metastases and a 38% higher risk of death due to breast cancer (Ewertz et al. 2011). Furthermore, analysis of participants in the Women's Health Initiative, which included 67,142 postmenopausal women with a median follow-up of 13 years, demonstrated that BMI above 35 is significantly associated with advanced breast cancer, including larger tumor size, lymph node infiltration, distant metastasis, and mortality (Neuhouser et al. 2015; I. Barone et al. 2020). Moreover, a systematic review and meta-analysis of 82 studies, comprising more than 200,000 individuals, concluded that obesity is associated with poorer overall and breast-cancer specific survival (Chan et al. 2014).

Breast cancer can be divided into subtypes based on the expression of molecular markers: estrogen receptor (ER), progesterone receptor (PR), and human epidermal growth factor receptor 2 (HER2). Each of these receptors is the target of effective therapeutics, and their expression is used to inform treatment strategies. Estrogen receptor positive cancers represent more than 80% of all breast cancers, and ER positive breast cancer is significantly associated with obesity in postmenopausal women, in part because obese adipose tissue produces estrogen through the action of aromatase (Chapter 1.4.2). Breast cancers that do not express any of these molecular markers are called triple negative breast cancer (TNBC). TNBC represents 10-20% of all breast cancers and is associated with advanced disease and increased mortality, with fewer treatment options than ER/PR/HER2 positive breast cancers. In contrast to ER positive breast cancer, TNBC is associated with higher BMI in premenopausal women (Gaudet et al. 2011; F. Y. Chen et al. 2013; L. Chen et al. 2016).

The molecular mechanisms that causally link obesity with worse breast cancer progression have not been fully elucidated. Some proposed mechanisms involve systemic changes in obesity, like dysregulated glucose and insulin signaling, alterations in circulating hormone levels, chronic inflammation, and dyslipidemia. Other possible mechanisms involve local changes to the adipose tissue in the breast tumor microenvironment including inflammation, increased hypoxia, and increased estrogen levels through enhanced expression and action of aromatase in extraovarian adipose tissue. The following sections will describe the evidence supporting these molecular mechanisms linking obesity and breast cancer progression.

1.3 Systemic factors linking obesity and breast cancer

Obesity leads to changes in whole-body metabolism, affecting the functions of several organs including the liver, pancreas, adipose, and brain (Font-Burgada, Sun, and Karin 2016). These changes are associated with dysregulation in circulating factors secreted from these organs that can have protumorigenic effects in distant sites (N. M. Iyengar, Hudis, and Dannenberg 2015).

1.3.1 Insulin, Insulin-like growth factor 1, and glucose

Insulin resistance and type 2 diabetes mellitus (T2DM) are among the best recognized comorbidities of obesity. These conditions are characterized by decreased insulin-stimulated glucose uptake in adipose tissue and skeletal muscle as well as by hyperinsulinemia and hyperglycemia (Kahn et al. 2000). These pathological changes may have roles in promoting breast cancer in obese patients. Hyperinsulinemia has been identified as an independent risk factor for breast cancer in humans, and insulin-sensitizing therapies can reduce metastatic burden in genetic models of breast cancer in mice (Gunter et al. 2009; Ferguson et al. 2012).

Furthermore, a meta-analysis of 48 studies revealed that breast cancer patients with T2DM are at increased risk of mortality compared to non-diabetic patients (B. B. Barone et al. 2008).

Hyperinsulinemia also promotes increased hepatic production of insulin-like growth factor 1 (IGF-1) and represses secretion of IGF-1 binding proteins (IGFBPs), leading to a further increase in bioavailable IGF-1. High levels of IGF-1 are associated with an elevated risk of breast cancer (W. Chen et al. 2009). The mechanism underlying the connections between insulin and IGF1 and breast cancer may be related to the direct actions of these hormones on cancer cells. Some breast cancer cells express the insulin receptor (IR) and/or the IGF-1 receptor (IGF1R). Ligand binding of these receptors activates the phosphatidylinositol-4,5-bisphosphate 3-kinase (PI3K) and the mitogen-activated protein kinase (MAPK) pathways, initiating a signaling cascade that promotes proliferation and tumor progression (Ulanet et al. 2010; LeRoith and Roberts 2003; Cohen and LeRoith 2012).

Obese, insulin resistant and diabetic individuals also have persistent hyperglycemia. Enhanced glucose uptake to preferentially fuel anerobic metabolism is termed the Warburg effect and is a described phenotype of many cancer types, including breast cancer (Liberti and Locasale 2016). Thus, hyperglycemia may have a role in promoting cancer cell viability and proliferation. Analysis of a prospective patient cohort revealed that women with the highest fasting glucose had a significantly elevated risk of developing breast cancer compared to those with the lowest glucose levels. This finding was independent of BMI; however, this analysis was not adjusted for circulating insulin levels (Sieri et al. 2012). In humans, breast cancer cells have higher expression of the glucose transporter GLUT1 than normal breast tissue (R. S. Brown and Wahl 1993). *In vitro*, increasing concentrations of glucose in cell culture medium leads to a dose-dependent increase in human breast cancer cell line proliferation (Sun et al. 2019). Together, these findings suggest that glucose may directly promote breast cancer viability and proliferation.

1.3.2 Circulating lipids

Dyslipidemia, including elevated circulating triglycerides and cholesterol-containing low density lipoproteins (LDL), is a common comorbidity of obesity (Klop, Elte, and Cabezas 2013; Jung and Choi 2014). Dyslipidemia is associated with an increased risk of cancers, including breast cancer, and the use of statin drugs, which inhibit cholesterol production, is associated with reduced cancer-specific mortality (Melvin et al. 2013; Kitahara et al. 2011; Nielsen, Nordestgaard, and Bojesen 2012).

In the $ApoE^{-/-}$ mouse model of hyperlipidemia, orthotopically implanted breast cancer cells have accelerated tumor growth and produce an increased number of lung metastases (Alikhani et al. 2013). The mechanism by which hyperlipidemia potentiates breast tumor progression may be related to the expression of lipoprotein lipase (LPL), an enzyme that hydrolyzes circulating chylomicrons and VLDL to release free fatty acids. LPL is more highly expressed in human breast cancers compared to healthy mammary tissue, and *in vitro*, human breast cancer cell lines express the fatty acid transporter, CD36, enabling them to import fatty acids from the environment (Zaidi et al. 2013; Kuemmerle et al. 2011).

Furthermore, there is strong evidence that breast cancer cells can take up LDL particles through expression of the LDL receptor (LDL-R) to promote tumor growth. When human breast cancer cells which highly express LDL-R are implanted into mouse models of hyperlipidemia ($ApoE^{-/-}$ and $LDL\text{-}R^{-/-}$), they produce significantly larger tumors than in wildtype controls

(Gallagher et al. 2017). Moreover, elevated expression of LDL-R in breast cancer was associated with decreased recurrence-free survival in a cohort of breast cancer patients (Gallagher et al. 2017).

Additionally, cholesterol is metabolized to 27-hydroxycholesterol (27-HC) through the P450 enzyme, CYP27A1. Elevated 27-HC increases tumor growth in orthotopic and genetic mouse models of breast cancer. When CYP27A1 is inhibited genetically or pharmacologically, tumor growth is attenuated (Nelson et al. 2013). These findings provide strong evidence that circulating lipids play an important role in the pathogenesis of breast cancer in the setting of dyslipidemia.

1.3.3 Circulating adipokines

Adipose tissue is an endocrine organ that secretes hormones, termed adipokines, that have profound effects on the functions of distant organs, like the liver. The amount and balance of these adipokines is altered in obesity, which can promote breast tumor progression. Leptin is an adipokine that coordinates energy homeostasis by signaling from adipose to the hypothalamus (Vaisse et al. 1996). Serum leptin levels positively correlate with fat mass. Patients with breast cancer that overexpresses the leptin receptor have an unfavorable prognosis, independent of other risk factors (Miyoshi et al. 2006). When peripheral leptin signaling is disrupted in a mouse model of spontaneous breast cancer, there is dramatically reduced tumor burden compared to mice with intact leptin signaling (Park et al. 2010). Mechanistically, leptin can signal directly to cancer cells through the leptin receptor (OB-R) and activate downstream PI3K and MAPK pathways. This suggests that in addition to systemic effects, enhanced leptin levels in obesity can signal directly to some cancer types to promote growth.

Adiponectin is an adipokine that can signal to other tissues to increase insulin sensitivity and reduce inflammation (Berg et al. 2001; Kadowaki et al. 2006). In contrast to leptin, serum adiponectin levels are reduced in obese individuals and are inversely correlated with the progression of several cancers, including breast cancer (Shahar et al. 2010). Furthermore, adiponectin directly signals to cancer cells which express the adiponectin receptor, reducing cellular proliferation and inducing apoptosis (Bråkenhielm et al. 2004). Adiponectin signals through several pathways, including the AMP-activated protein kinase (AMPK), mammalian target of rapamycin (mTOR), and nuclear factor kappa-light-chain-enhancer of activated B cells (NF-κB) pathways (Dalamaga, Diakopoulos, and Mantzoros 2012; A. Y. Kim et al. 2010; Ackerman et al. 2017).

1.3.4 Systemic inflammation

Chronic inflammation is a risk factor for the development of cancer, and obesity is characterized by chronic, low-grade systemic and local adipose inflammation. Obese patients have elevated circulating C-reactive protein (CRP), a hepatic acute phase reactant that is used as a clinical biomarker of inflammation. In a prospective study of 130 women with a median 14.6 year follow-up, individuals with high initial CRP had an increased risk of developing breast cancer (Frydenberg et al. 2016). Furthermore, elevated serum amyloid A (SAA), another hepatic acute phase reactant and circulating biomarker for inflammation, was associated with worse survival in breast cancer patients, independent of BMI (Pierce et al. 2009). These data suggest

that systemic inflammation may be related to breast cancer outcomes, but the mechanisms linking these states are unclear.

1.4 Local factors linking obesity and breast cancer

Chronic excess energy intake leads to white adipose tissue (WAT) hyperplasia and hypertrophy. When WAT surpasses its ability to safely expand for energy storage, there is ensuing adipocyte dysfunction and cell death, leading to immune cell infiltration and local inflammation. Additionally, obesity results in impaired adipose vascularization, leading to tissue hypoxia and oxidative stress. Increased hypoxia inducible factor 1 alpha (HIF1α) expression alters the extracellular matrix produced around adipocytes, leading to adipose tissue fibrosis (Fuster et al. 2016). Obesity also alters the local concentrations of adipose-derived factors like endotrophin, aromatase, and fatty acids. These pathologic changes in the mammary adipose microenvironment may contribute to breast cancer progression.

1.4.1 Adipose tissue inflammation

Chronic local inflammation is an important factor in the development of cancers (Coussens and Werb 2018). Obesity is associated with chronic adipose tissue inflammation, characterized by an increase in concentration of pro-inflammatory cytokines and the accumulation of pro-inflammatory immune cells, like macrophages, natural killer cells, and T-cells. Crown like structures (CLS) are macrophages which surround dead or dying adipocytes and represent a characteristic histologic finding associated with inflamed adipose tissue in both obese humans and mice (Murano et al. 2008; N. M. Iyengar, Hudis, and Dannenberg 2013). In a genetic model of murine mammary cancer, diet-induced obesity was associated with increased CLS, infiltrating macrophages, and vascular growth (Cowen et al. 2015). In humans, there are more CLS in the mammary adipose of obese individuals compared to lean, and in obese breast cancer patients, CLS occur in close proximity to the tumor (Vaysse et al. 2017; Morris et al. 2011). Furthermore, high density of CLS in the mammary adipose portends worse breast cancer outcomes in both lean and obese patients (N. M. Iyengar et al. 2016). Adipose tissue macrophages may have an important role in the pathogenesis of breast cancers in obese individuals. When activated, these cells secrete pro-inflammatory cytokines that promote breast cancer progression. For example, adipose-derived macrophages secrete interleukin 6 (IL-6), which can promote cancer progression by signaling directly to cancer cells to enhance survival and migration (Chang, Daly, and Bromberg 2014). Additionally, activated adipose tissue macrophages secrete interleukin 1-beta (IL-1β) which stimulates vascular endothelial growth factor (VEGF) production and promotes angiogenesis (Kolb et al. 2016; Chang, Daly, and Bromberg 2014).

1.4.2 Adipose derived estrogen

Obesity is associated with increased incidence of ER positive cancer in postmenopausal women. After menopause, estrogen is produced mainly by non-ovarian tissues, like adipose, through the actions of aromatase, a P450 enzyme which aromatizes androgen precursors to estrogen. Importantly, there is increased aromatase expression and activity in the mammary adipose of obese women compared to lean, and the increased local concentration of estrogen

may drive proliferation in estrogen-receptor positive breast cancers (Morris et al. 2011). Increased circulating levels of estrogen are associated with increased risk of breast cancer in post-menopausal women (Baglietto et al. 2010).

Aromatase is expressed in the mammary adipose by adipocyte precursors. It is a transcriptional target of HIF1α, the master regulator of the hypoxic response, and it is induced by tumor-derived factors like prostaglandin E2 (PGE2), tumor necrosis factor alpha (TNFα), and IL-6. This bi-directional interaction between adipose and breast cancer cells produces a feed-forward loop that potentiates tumor progression (Simpson and Brown 2013). Aromatase inhibitors are used clinically to block estrogen production in patients with estrogen receptor positive breast cancers (Smith and Dowset 2003). However, obesity is also significantly associated with worse prognosis of estrogen receptor negative cancers, including aggressive triple negative breast cancers, and aromatase inhibitors are ineffective in treating these cancer types (Gérard and Brown 2018; Pierobon and Frankenfeld 2013).

1.4.3 Adipocyte derived endotrophin

Adipocytes are a major cell type in immediate proximity to cancer cells in the breast cancer microenvironment. In obesity, adipocytes highly express and secrete collagen 6A3, which is cleaved to produce endotrophin (ETP). ETP has pro-tumor effects on breast cancer cells *in vitro* and *in vivo*. In the genetic MMTV-PyMT model of murine mammary carcinoma, Col6a3 knockout mice had attenuated tumor progression (Park and Scherer 2012). ETP can be isolated from human plasma, and in mouse models, neutralizing antibodies targeting ETP can attenuate tumor growth in a human-derived orthotopic model (Bu et al. 2019). The mechanisms by which ETP supports breast cancer progression are multifaceted: it acts on cancer cells to promote epithelial-to-mesenchymal transition, on macrophages to induce inflammation, and on endothelial cells to promote angiogenesis (P. Iyengar, Bonaldo, and Scherer 2005).

1.4.4 Fatty acids

In obesity, adipocytes undergo increased lipolysis, releasing free fatty acids (FFA). This process is implicated in the mechanism underlying insulin resistance in obesity and may also play an important role in obesity-associated breast cancer (Blücher and Stadler 2017; Madak-Erdogan et al. 2019). *In vitro*, breast cancer cells can induce lipolysis in co-cultured adipocytes and take up adipocyte-derived FFA (Dirat et al. 2011; Nieman et al. 2011). In human breast cancer, cancer cells express adipose triglyceride lipase (ATGL) and its expression is associated with tumor aggressiveness (Y. Y. Wang et al. 2017).

1.5 Summary

There is an abundance of epidemiological data that link obesity with breast cancer risk and worse breast cancer outcomes. Obesity is associated with increased mortality from triple-negative breast cancer in premenopausal women, which has fewer therapeutic strategies and portends a poor prognosis, however, there is little known about the mechanisms by which obesity accelerates this breast cancer type. In this thesis, we sought to investigate changes in the cellular and metabolic phenotypes of breast cancer cells that may be responsible for the accelerated tumor progression in obesity. Using a murine model of obesity-accelerated triple-negative breast

cancer, we performed unbiased transcriptomic analyses of the neoplastic cells within the heterogenous tumors in lean or obese animals to identify molecular pathways linking obesity and breast cancer progression. We identified a previously undescribed, obesity-dependent role for the acyl-CoA synthetase, Acsbg1, in cancer cells. Furthermore, we performed metabolomic analysis of Acsbg1 overexpressing tumors in lean and obese animals and identified a role for Acsbg1 in enhancing mitochondrial energy production, which was confirmed with plate-based respirometry. We went on to utilize unbiased lipidomic analysis to identify putative substrates and downstream products of Acsbg1 that may contribute to tumor progression. Finally, gene expression analysis from a large cohort of human breast tumors revealed that high Acsbg1 expression is significantly associated with worse tumor grade. Among overweight and obese individuals, Acsbg1 expression is associated with an aggressive, triple-negative, basal tumor subtype (Toro et al. 2016). These data suggest a novel role for Acsbg1 in the pathogenesis of obesity-accelerated breast cancer and may represent a potential route for therapeutic intervention. Furthermore, these studies provide the basis for future work investigating the role of Acsbg1 in other obesity-induced cancer types.

CHAPTER 2 Characterizing E0771 tumors in an orthotopic model of obesity-accelerated breast cancer

2.1 Introduction

Obesity is linked to worse breast cancer outcomes, and our objective was to better understand the molecular links between these two diseases, with the ultimate goal of discovering insights into this and other obesity-related cancers. Obesity is associated with many systemic and local adipose changes that cannot be adequately recapitulated *in vitro*, so developing a robust *in vivo* model of obesity-driven breast cancer was essential to addressing our goals. We used the C57BL6/J (B6) immunocompetent mouse strain, which is susceptible to diet-induced obesity, its comorbidities, and is commonly used in the fields of metabolism and adipose biology. We used the B6 syngeneic, functionally triple negative E0771 murine breast cancer cell line, which rapidly produces tumors *in vivo* when orthotopically implanted into a mammary adipose depot (Johnstone et al. 2015). E0771 cells are derived from a spontaneous murine mammary tumor and harbor homozygous mutations in Kras and Trp53 (Y. Yang et al. 2017). Importantly, we selected an orthotopic approach rather than a genetic mouse model so that we could use tools such as lentiviral transduction to efficiently modulate gene expression in the cancer cells. This chapter will describe our efforts to characterize the morphological and histological differences between tumors isolated from lean or obese animals.

2.2 E0771 tumors grow larger in obese animals than lean

The first step in this project was to comprehensively characterize E0771 tumors that develop in lean or obese animals, a model which was previously described by a former graduate student in our group (Ackerman 2020). At 6 weeks of age, female B6 animals were randomized to 60% high-fat diet (HFD) or standard chow. After 12 weeks, animals on a HFD gained significantly more body weight than mice fed standard chow, which was attributed to a significant increase in fat mass (Figure 2.2.1 A and B). We implanted 50,000 E0771 cells, suspended in 1:1 serum-free RPMI medium and growth factor reduced Matrigel using a 27-gauge insulin syringe. After seven days, mice in both lean and obese groups had small, but palpable tumors. By day 14, both groups of mice had measurable tumors, but there was no difference in tumor volume between the groups. By day 17, we observed that the obese tumors were significantly larger than the lean tumors, and by day 21, the obese tumors had reached humane endpoint of 2 cm in the largest diameter (Figure 2.2.1 C-E) (Ackerman 2020).

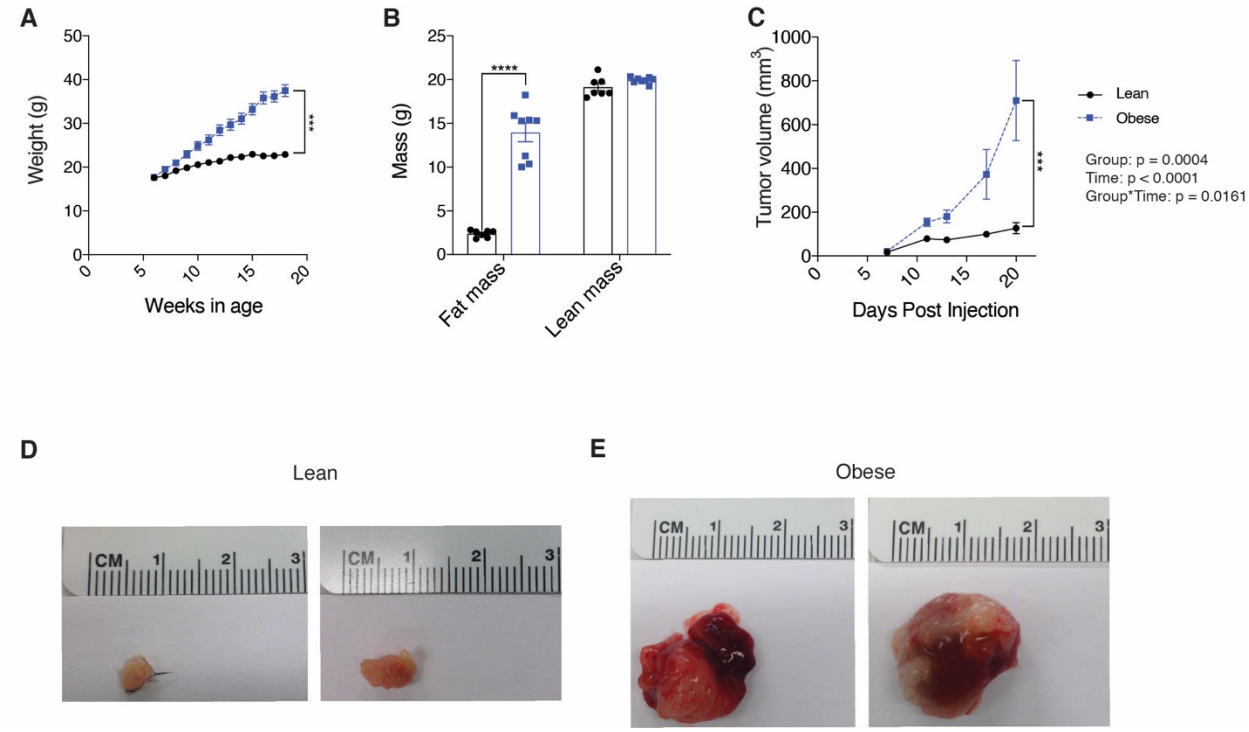

Figure 2.2.1 The E0771 orthotopic model of obesity-accelerated breast cancer.

A. Body weights of B6 animals fed a high fat diet or chow control (n=11 per group) B. Fat and lean mass of animals at endpoint (n=7-8 per group). C. Longitudinal tumor volume in lean or obese mice (n=11 per group). D. Representative images of lean tumors isolated at day 21. E. Representative images of obese tumors at day 21. Data represent mean +/- standard error of the mean (SEM). *** $p<0.001$, **** $p<0.0001$. For panel C, group, time, and group by time p-values are denoted and *** $p<0.001$ by post-hoc analysis at the final time point.

Once we established that the E0771 tumors had accelerated growth in the obese animals compared to lean, we dissociated the tumors from each group and counted the number of live cells from each tumor by trypan blue exclusion. Not surprisingly, obese tumors were comprised of significantly more cells than lean tumors (Figure 2.2.2).

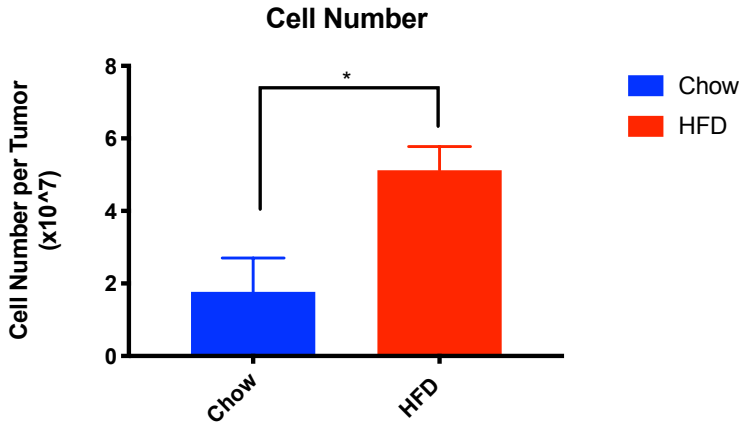

Figure 2.2.2 Average number of cells per tumor.

n=5 tumors per group. Data represent mean +/- standard error of the mean (SEM). *p<0.05

The next step was to determine if this difference in cell number was due primarily to increased cell proliferation or to decreased cell death in the obese group compared to lean. We used three slide-based methods to quantify proliferation: Ki-67 expression by immunohistochemistry (IHC), phospho-histone H3 (PHH3) by IHC, and 5-ethynyl-2'-deoxyuridine (EdU) incorporation.

Ki-67 is a commonly used marker of cell proliferation and aggressiveness in a number of tumor types, including breast cancer (Tőkés et al. 2019; Pathmanathan and Balleine 2013; Gerdes et al. 1991). Ki-67 has robust and well validated antibodies, however it is not specific for mitotic cells, as it marks all cells which are not in interphase (Romar, Kupper, and Divito 2016). When we quantified lean and obese tumors by Ki-67 IHC, we noticed that nearly all cells were Ki-67 positive, and we did not discern any difference in Ki-67 positivity between the groups at midpoint (day 14 after implantation) before the tumors separated in size, or at endpoint (day 21 after implantation) when the tumors reached their maximum volume (Figure 2.2.3). Since Ki-67 is not specific for mitotic cells and will also mark cells in G1, S, and G2 phases of the cell cycle, we reasoned that we may be able to detect more subtle differences between the tumor types with a more specific marker of mitosis.

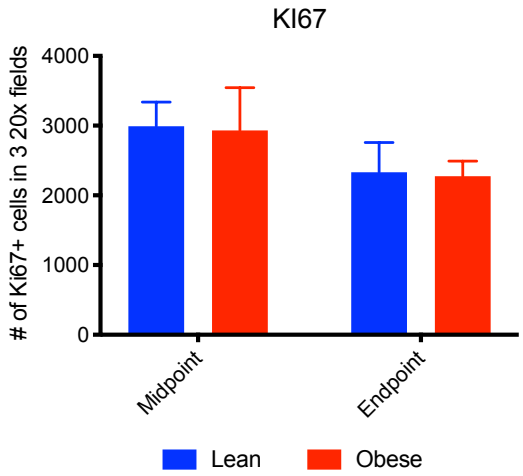

Figure 2.2.3 Ki-67 is not significantly different between tumors isolated from lean and obese animals.

n=3 tumors per group. Data represent mean +/- standard error of the mean (SEM).

Another method of detecting proliferation is IHC for the phosphorylation of Ser10 on histone 3 (PHH3). PHH3 is less commonly used to grade tumors, but is a more specific marker for cell proliferation, as it marks cells in late G2 through prophase (J. Y. Kim et al. 2017; Hao et al. 2018; Fukushima et al. 2009; Hendzel et al. 1997; Chadee et al. 1999). Compared to Ki-67 staining. fewer cells were PHH3 positive in both lean and obese tumors as a percentage of total cells. We counted PHH3 positive cells at midpoint as well as at endpoint. Similar to Ki-67, when we compared the number of PHH3 positive cells in obese tumors compared to lean, we did not detect a significant difference in PHH3 positive cells (Figure 2.2.4 A, B, and C).

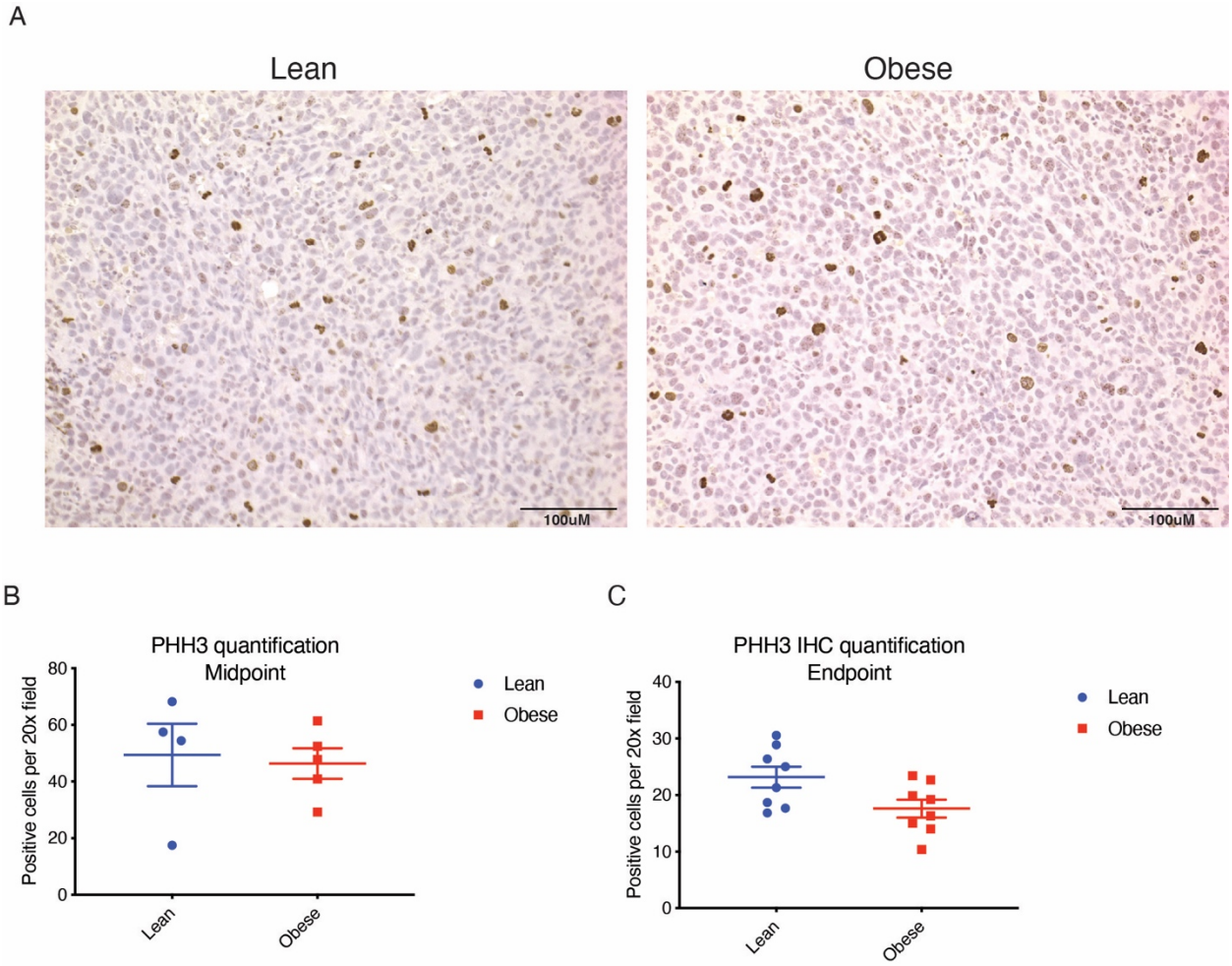

Figure 2.2.4 Phosphohistone H3 (PHH3) is not significantly different between tumors isolated from lean and obese animals.

A. Representative images of PHH3 staining of tumors isolated from lean or obese animals. Scale bars represent 100uM. B. Quantification of PHH3 positive cells in lean or obese animals at midpoint. C. Quantification of PHH3 positive cells in lean or obese animals at endpoint. n= 4-5 tumors per group. Data are presented as mean +/- standard error of the mean (SEM).

The third method we used to quantify proliferation is EdU incorporation. EdU incorporation is a specific method for detecting cells which are actively undergoing DNA synthesis. EdU is a thymidine analog with an alkyne group substituted in place of a terminal methyl group. We administered 25 mg/ kg EdU to tumor bearing animals as a pulse two hours before sacrifice. During the chase period, dividing cells incorporate EdU into newly synthesized DNA. EdU-labeled DNA can then be detected on tumor sections by performing a copper catalyzed click chemistry reaction which results in a covalent bond with a fluorescently conjugated azide dye (Salic and Mitchison 2008; Cavanagh et al. 2011). Finally, we imaged labeled DNA with a fluorescence microscope and quantified the positive cells with ImageJ. We found that obese tumors had significantly more EdU positive cells compared to lean, demonstrating more cell proliferation in obese tumors (Figure 2.2.5).

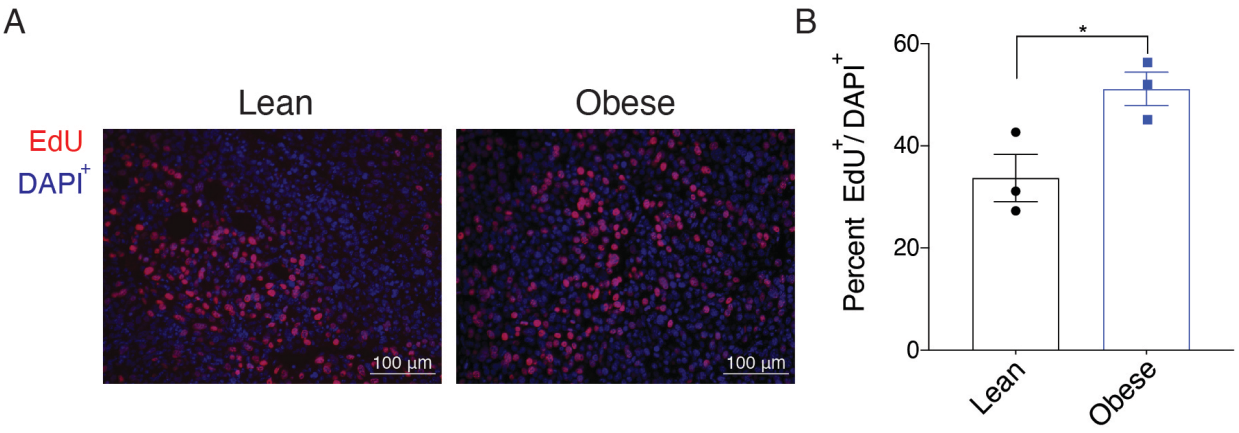

Figure 2.2.5 Obese tumors are more proliferative than lean tumors by EdU incorporation.

A. Representative images of EdU (red) and DAPI (blue) staining in tumors isolated form lean or obese animals. B. Quantification of EdU as a percentage of DAPI nuclei per 20x field (n=3 tumors per group). Data represent mean +/- standard error of the mean (SEM). * $p<0.05$.

In human breast cancer, obese tumors are more hypoxic than lean, and hypoxia is associated with worse outcomes (Petrova et al. 2018; Al Tameemi et al. 2019; Jögi et al. 2019; Schwab et al. 2012; Vaupel et al. 1991). We hypothesized that the rapidly proliferating tumors in obese animals may be more hypoxic than the tumors in lean animals in our model of obesity-accelerated breast cancer. We performed immunoblot assays to detect hypoxia inducible factor 1 alpha (HIF1-α) the master regulator of the hypoxic response and a strong indicator of hypoxia (G. L. Wang et al. 1995; Zhong et al. 1999; Iyer et al. 1998). As expected, tumors from obese animals had significantly more HIF1-α protein than lean, confirming that they are more hypoxic (Figure 2.2.6). This is consistent with large, rapidly growing tumors and raises the possibility that oxygen tension and metabolic reprogramming may play an important role in the obesity-accelerated phenotype of these tumors (Semenza et al. 1994; Schwab et al. 2012; N. S. Brown and Bicknell 2001; Semenza 2013).

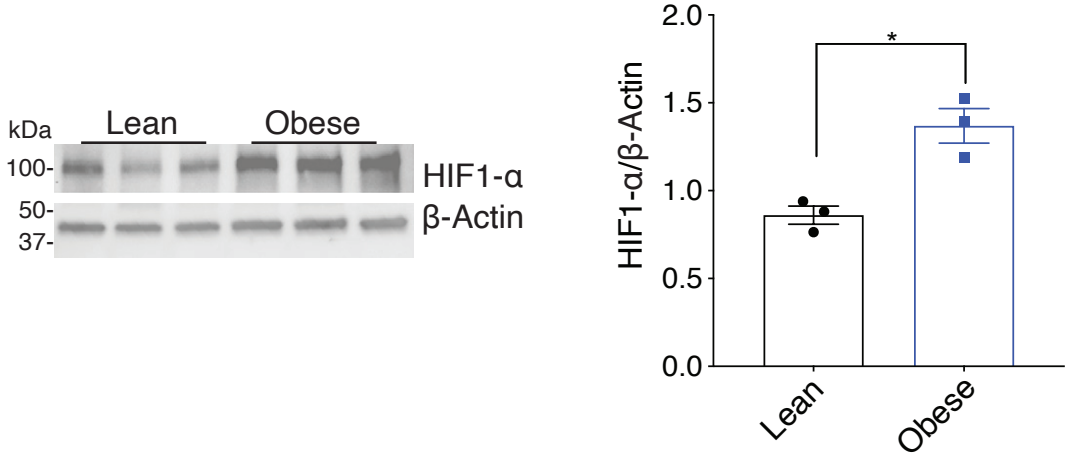

Figure 2.2.6 Immunoblot of HIF1-α from lean or obese tumors.

HIF1α protein levels were quantified using ImageJ and normalized to β-actin (n=3 tumors per group). Data represent mean +/- standard error of the mean (SEM). *$p<0.05$.

We used cleaved caspase 3 reactivity via IHC to assess the contribution of apoptosis to the obesity-accelerated growth of E0771 orthotopic tumors. Caspase 3 is a protease that plays an essential role in the activation of the apoptosis pathway. When cleaved, it promotes a cascade of protease-mediated cleavage events that culminates in the activation of DNA cleavage enzymes and cell death (Porter and Jänicke 1999; Wolf et al. 1999; McIlwain, Berger, and Mak 2015). We used IHC to image and count the number of cleaved-caspase 3 positive cells in tumors from lean and obese animals and found no difference between the groups (Figure 2.2.7). This suggests that the suppression of apoptosis may not play an important role in driving obesity-accelerated growth in this tumor type.

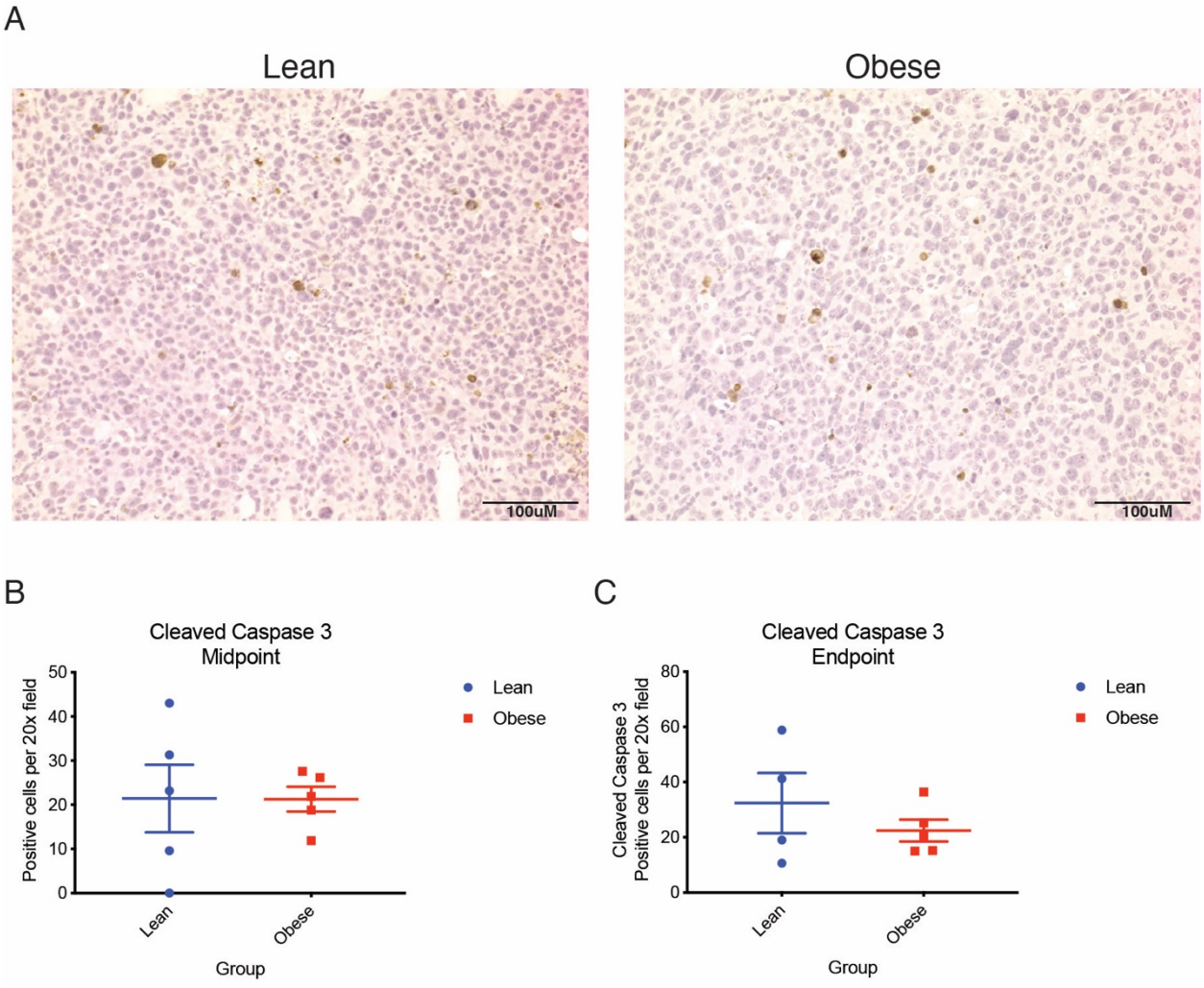

Figure 2.2.7 Obese tumors are not less apoptotic than lean tumors.

A. Representative images of cleaved caspase-3 staining in lean or obese tumors at endpoint. B. Cleaved caspase 3 quantification at midpoint (n=4 or 5 tumors per group). C. Cleaved caspase 3 quantification at endpoint (n=4 or 5 tumors per group). Data are presented as mean +/- standard error of the mean (SEM).

2.3 Obese tumors contain more lipid droplets than lean tumors.

Upon hematoxylin and eosin (H&E) staining, the most obvious histological difference between tumors isolated from lean or obese animals is the number and size of large, empty, circular vacuoles distributed throughout the parenchyma of the tumors (Figure 2.3.1 A-B). To investigate whether these structures are intact adipocytes, we utilized the adipocyte-specific $Rosa26^{fsTRAP}$ (Adipo-TRAP) mice. In the Adipo-TRAP genetic model, mice express GFP under the control of the adiponectin promoter, specifically labeling adipocyte ribosomes. Therefore, any adipocytes located within the parenchyma of the tumor would stain positive by anti-GFP IHC. We were able to detect GFP^{+} ribosomes in the adipose tissue, demonstrating that the technique was effective (Figure 2.3.2 A, arrows). However, we could not detect any GFP in the tumor (Figure 2.3.2 B). These findings suggest that these circular structures may not be intact adipocytes.

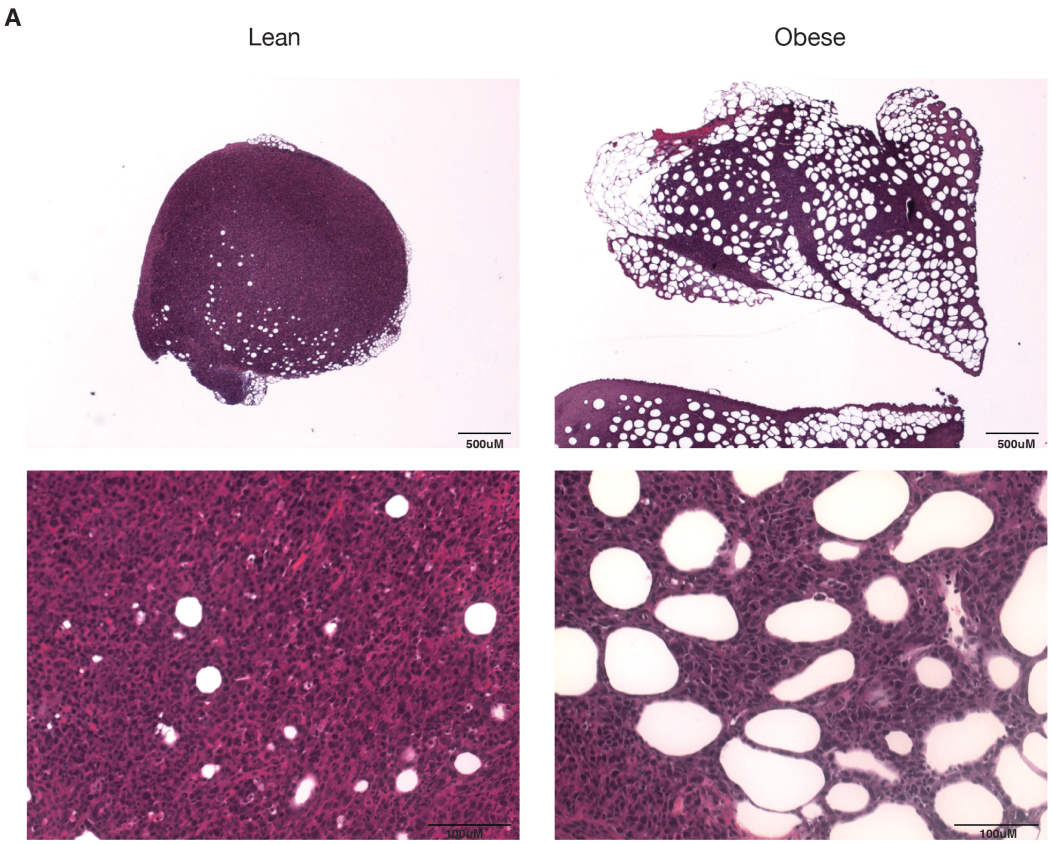

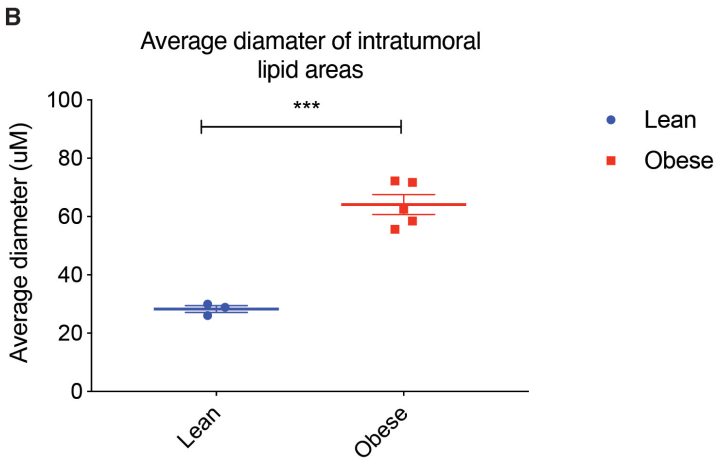

Figure 2.3.1 Obese tumors have more intratumoral lipid areas than lean.

A. Representative H&E staining of lean or obese tumors at 2.5 or 20 x magnification. Scale bars are as noted in the figure. B. Quantification of the average diameter of lipid droplets (n=3 or 5 tumors per group). Data are presented as mean +/- standard error of the mean (SEM). ***p<0.001

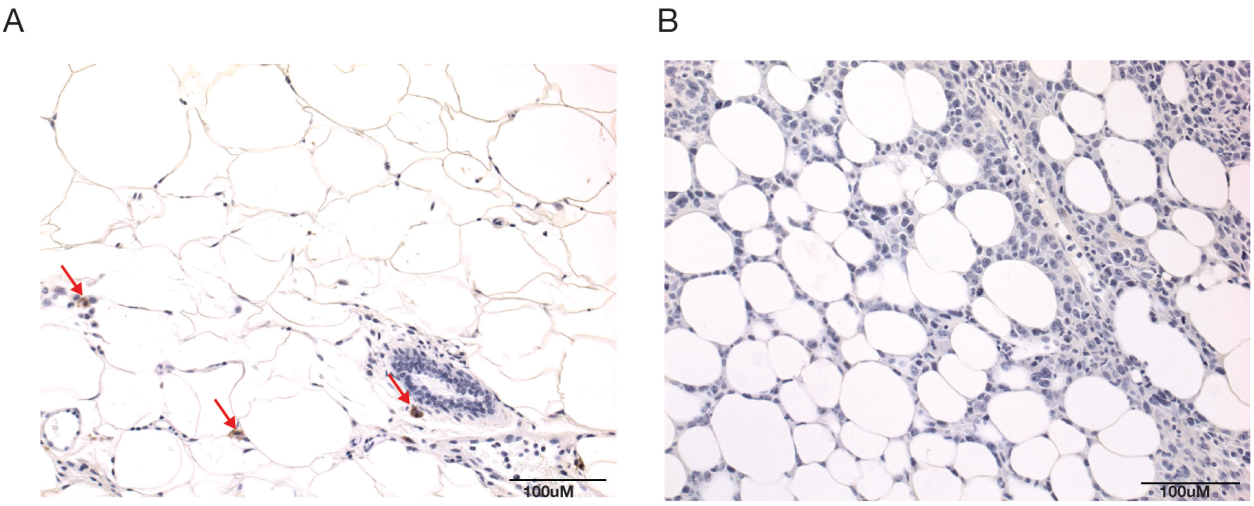

Figure 2.3.2 anti-GFP immunohistochemistry on adipose and tumors isolated from Adipo-TRAP animals.

A. Anti-GFP IHC on adipose from Adipo-TRAP animals. Arrows indicate GFP positive staining. B. Anti-GFP IHC on an E0771 tumor isolated from an Adipo-TRAP animal. Scale bars represent 100uM.

Next, we used IHC to detect perilipin-1, a protein that specifically surrounds lipids droplets, and found that these circular structures are perilipin positive (Figure 2.3.3). We hypothesize that these structures are remnants of adipocyte lipid droplets from the surrounding mammary adipose depot that were subsumed as the tumor invaded the surrounding structures.

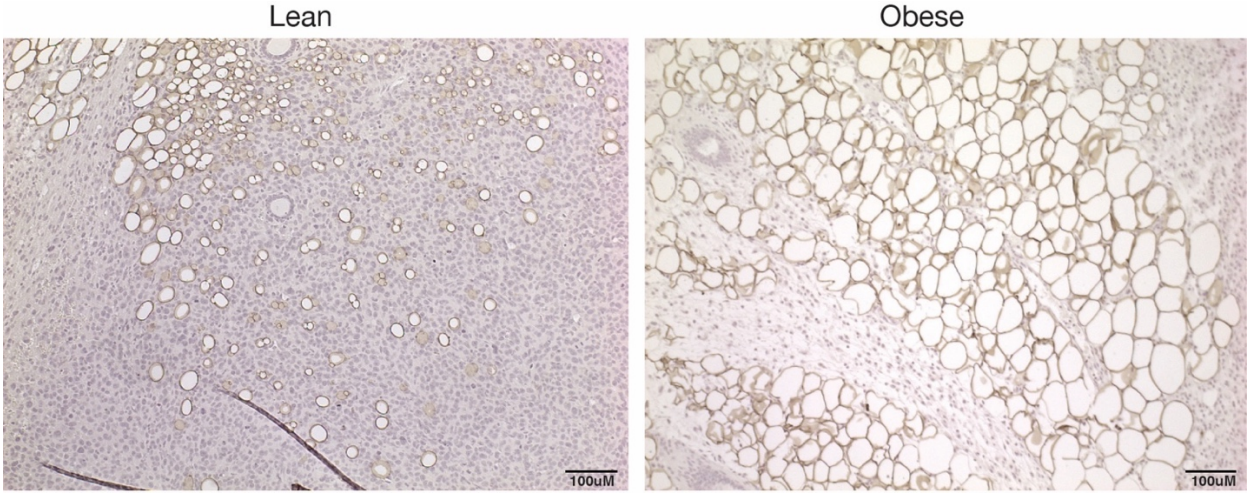

Figure 2.3.3 Perilipin IHC on tumors from lean or obese animals.

Scale bars represent 100uM.

We cryosectioned a representative tumor and performed oil-red-o staining to determine if these perilipin positive structures contain neutral lipids, like triacylglycerides. While these lipid droplets themselves do not contain lipids, the cancer cells which immediately surround them are lipid laden (Figure 2.3.4 B). Interestingly, the lipid content of the cells surrounding these vacuoles appears to decrease with increasing distance from the lipid droplets (Figure 2.3.4 B). Furthermore, cancer cells located in regions of the tumor without these droplets do not stain positive with oil-red-o (Figure 2.3.4 A). Others have shown that breast cancer cells are able to induce lipolysis in adjacent adipocytes to mobilize and take up adipose-derived lipids *in vitro* (Dirat et al. 2011; Nieman et al. 2011). This histological finding suggests that the lipids that were located within these perilipin positive structures may have been mobilized to the surrounding cancer cells, where they have been stored for future use. While technical limitations hindered our ability to cryosection the friable and necrotic obese tumors, the fact that there are more of these droplets in the obese tumors suggests that cancer cells in obese tumors may have increased access to lipids, and we hypothesize that they use these lipids as a source of fuel in times of metabolic stress. This hypothesis is further supported by findings in Chapter 4 which suggest that lipid metabolism plays an essential role in potentiating obesity-driven tumor progression in this model.

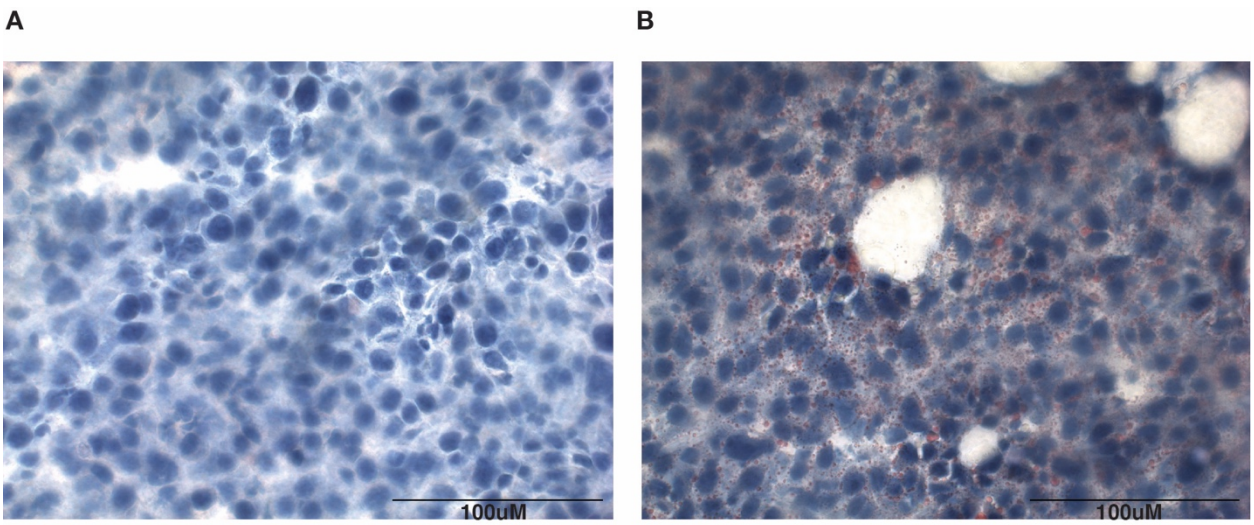

Figure 2.3.4 Oil-Red-O staining on a representative cryosection tumor.

A. A representative image of a region without lipid droplets. B. A representative image of a region with lipid droplets. Scale bars represent 100uM.

2.4 Summary

We utilized a model of obesity-accelerated triple negative breast cancer in female diet-induced obese mice. In this model, orthotopic E0771 tumors grow to be significantly larger in obese animals compared to lean. Obese tumors contain more cells than lean tumors, and this is due to increased proliferation, as quantified by EdU incorporation. There is no difference in cleaved caspase 3, a marker of apoptosis, leaving the enhanced proliferation of cancer cells in obese animals unopposed and producing rapidly growing tumors. In addition to enhanced

proliferation, obese tumors are more hypoxic than lean, and they contain lipid droplets, likely originating from the surrounding adipose. Interestingly, the cancer cells which surround the perilipin positive lipid droplets are lipid laden by oil-red-o staining, suggesting a possible role of lipid metabolism in potentiating obesity related tumor progression. The following chapters will describe our work to identify novel mechanisms which underlie obesity-related tumor growth.

CHAPTER 3 Transcriptomic analysis of bulk E0771 orthotopic tumors from lean or obese animals

3.1 Introduction

Breast cancer and obesity have been epidemiologically linked, yet the mechanisms underlying this connection, particularly in the aggressive triple-negative setting, are not completely understood. Our group has employed a murine model of diet-induced obesity-accelerated triple negative breast cancer (Chapter 2). Briefly, in this model, 6-week-old, wild-type B6 female animals are randomized to HFD or normal chow diet. After 9 weeks on HFD, female B6 mice have significantly higher body weight than lean control, which is attributed to the accumulation of fat mass. At 15 weeks of age, E0771 murine mammary cancer cells are implanted into the 4th mammary fat pad. The resulting tumors are significantly larger by volume and weight in obese animals compared to lean, which can be attributed to increased cancer cell proliferation in obesity. Previous studies from our group which used this model were focused on understanding obesity specific changes to the adipose tissue in the tumor microenvironment that promote tumor growth (Ackerman 2020). The focus of this thesis is to utilize this model of obesity-accelerated TNBC to better understand the behavior of cancer cells in obesity that may potentiate accelerated tumor progression.

3.2 Transcriptomic analysis of bulk tumors in obesity-accelerated breast cancer

We performed RNA sequencing of E0771 tumors isolated from lean or obese animals to assess differences in gene expression between tumors located in these different environments. Our aim was to identify early differences in gene expression that were likely to drive and sustain accelerated tumor growth in obesity; thus, we chose to study tumors both before and after the experimental groups had significantly diverged in tumor volume. We defined midpoint as day 14 after orthotopic implantation, a time point when the tumors were palpable in both lean and obese animals, but the groups had not yet significantly diverged in volume. Endpoint, or day 21 after implantation, was when the tumors in the obese group had reached humane endpoint and had significantly diverged in volume from the tumors in lean mice. We isolated bulk tumors, purified RNA, and performed ribosomal-RNA depleted, paired-end RNA sequencing (n=4 or 5 per group) (Figure 3.2.1).

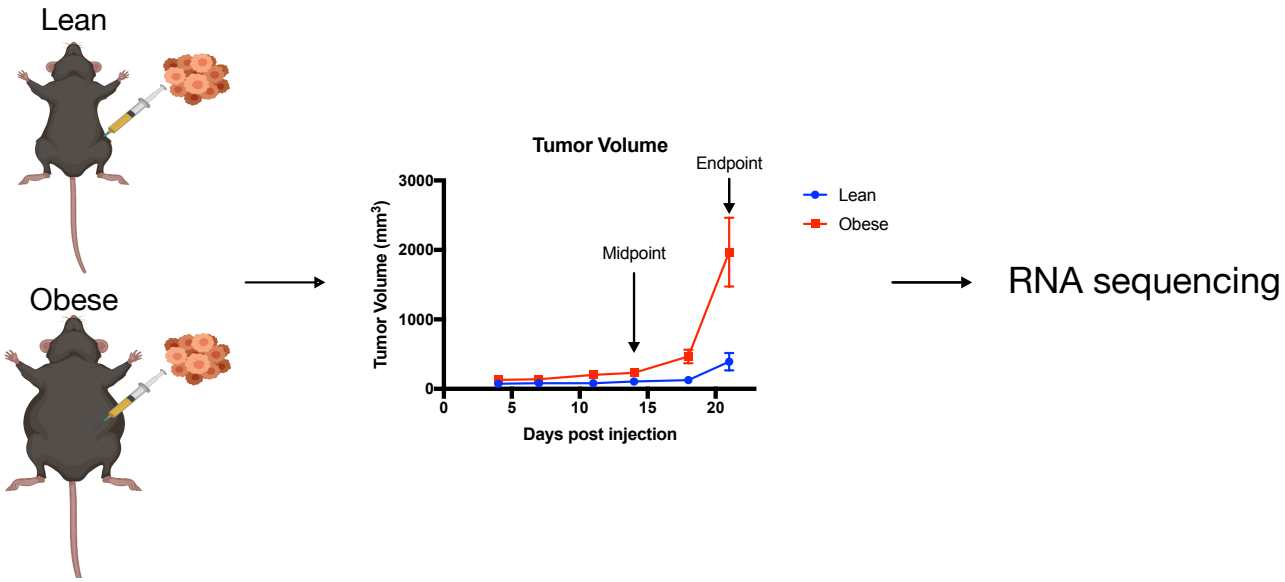

Figure 3.2.1 Schematic representation of the RNA sequencing experimental plan.

E0771 cancer cells were implanted into lean or obese animals, and the tumors were monitored over time with calipers. At midpoint or endpoint, we dissected tumors and performed RNA sequencing.

This analysis achieved a sequencing read depth of 42-50 million reads per sample, 74 to 90 percent of which mapped to the reference mouse genome. First, we used principal component analysis (PCA) to assess the similarity among samples in the experiment. In this type of analysis, the greatest sources of variation are collapsed into two principal components, and the separation of the samples along these two axes represents the overall similarity among the samples. In this experiment, the samples that comprise any one group were scattered across the plot, and the groups overlapped. This suggests that there is a high degree of heterogeneity within the experimental groups (Figure 3.2.2).

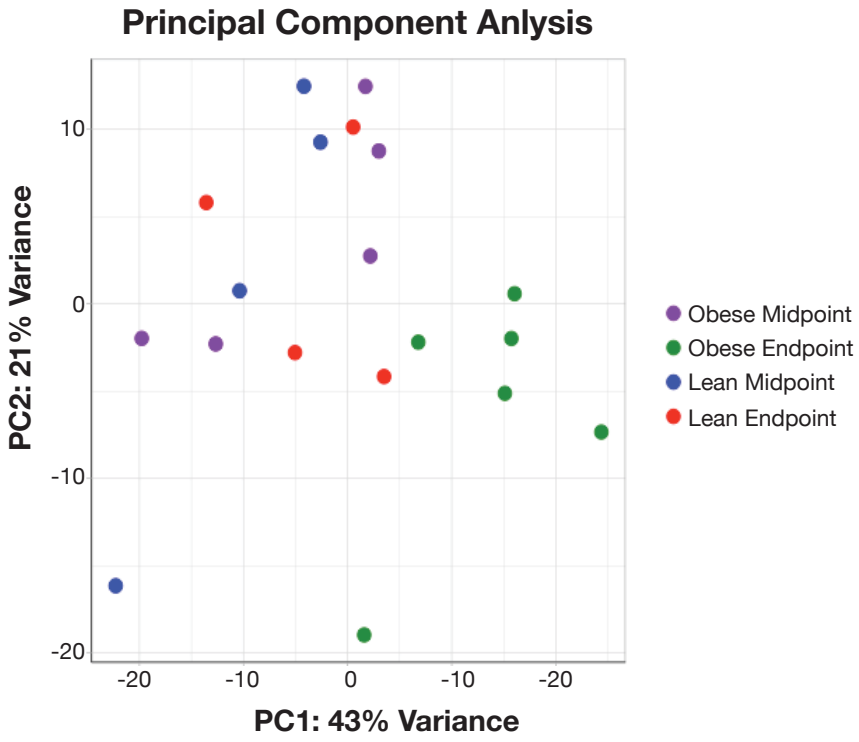

Figure 3.2.2 Principal component analysis of RNA sequencing analyzing tumors from lean or obese animals at midpoint or endpoint.

We utilized Gene Set Enrichment Analysis (GSEA) to identify differentially regulated pathways in this dataset. When lean midpoint tumors were set as the reference level, 11 of the 12 most differentially regulated terms among any of the other groups were related to immune cell function and inflammation, with the most significant terms related to leukocyte chemotaxis and migration (Fig 3.2.3 A). Many of the genes that were specifically dysregulated within these terms were cytokines and chemokines known to be expressed by immune cells, for example *Il-1* and *Ccl3*. Other differentially regulated genes in this dataset are known to modulate the immune response, such as *Cxcl1* and *Il-23* (Fig 3.2.3 B,C).

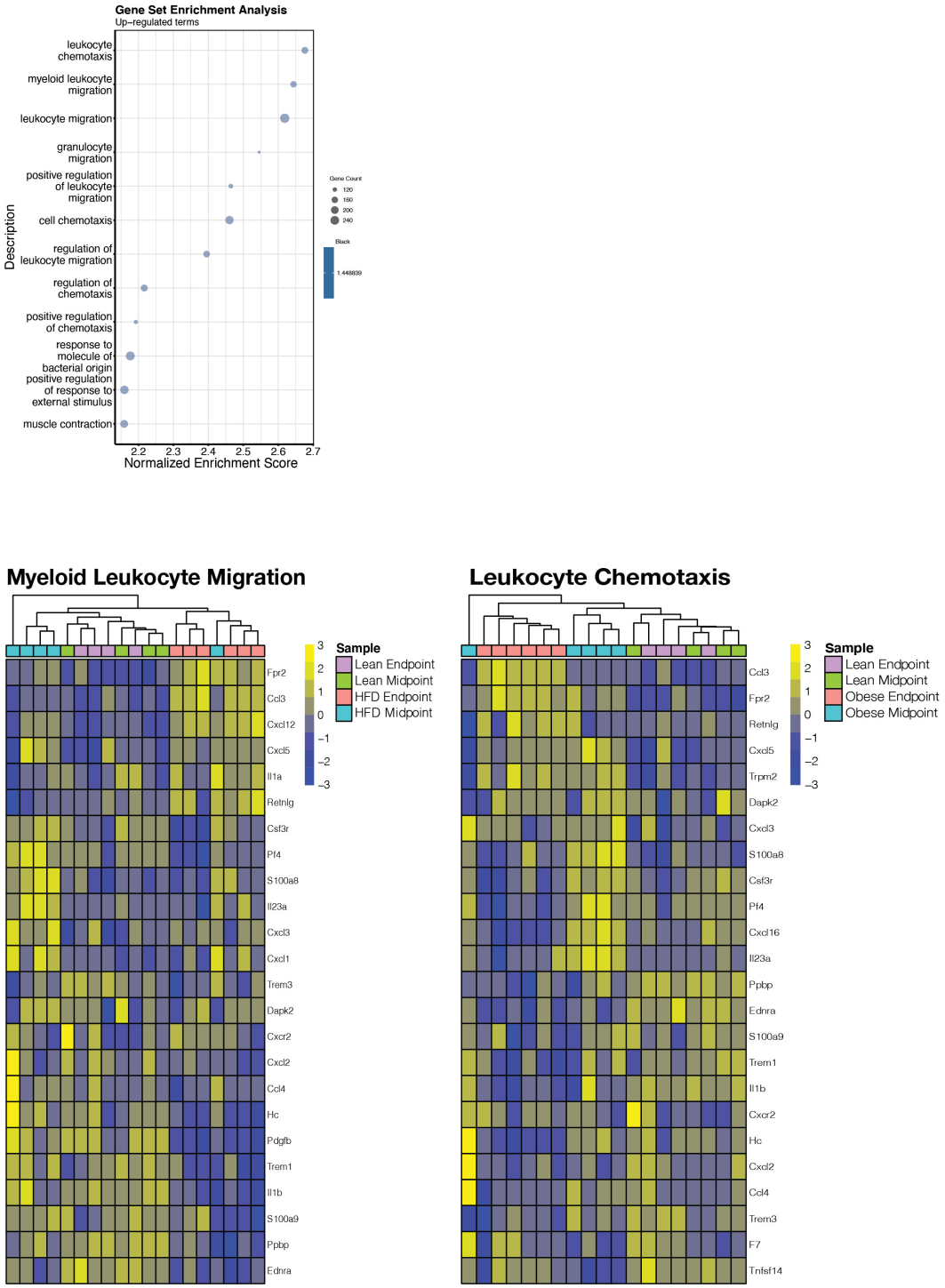

Figure 3.2.3 Gene set enrichment analysis of bulk RNA sequencing of tumors from lean or obese animals.

A. GSEA depicting the 12 most highly regulated pathways compared to chow, midpoint tumors. B. Heatmap depicting the terms in myeloid leukocyte migration. C. Heatmap depicting the terms in leukocyte chemotaxis.

3.3 Using bioinformatics to probe the immune cell profile of tumors isolated from lean and obese tumors

The GSEA data suggest that shifts in tumor infiltrating immune cell populations or phenotypes may contribute to many of the differences in gene expression we observe between tumors isolated from lean or obese animals. We performed flow cytometry at tumor endpoint to establish whether immune cells were present at comparable levels in the bulk tumors isolated from lean or obese animals in E0771 orthotopic tumors. We confirmed that more than eighty-five percent of the live cells isolated from this model were CD45 positive, and therefore likely hematopoietic in origin (Figure 3.3.1). Since these tumors were cellularly heterogeneous, and our approach involved RNA sequencing of the entire, homogenized tumor, we could not confidently determine whether the transcripts that were differentially expressed among the groups originated in cancer cells, infiltrating immune cells, or a different cell type.

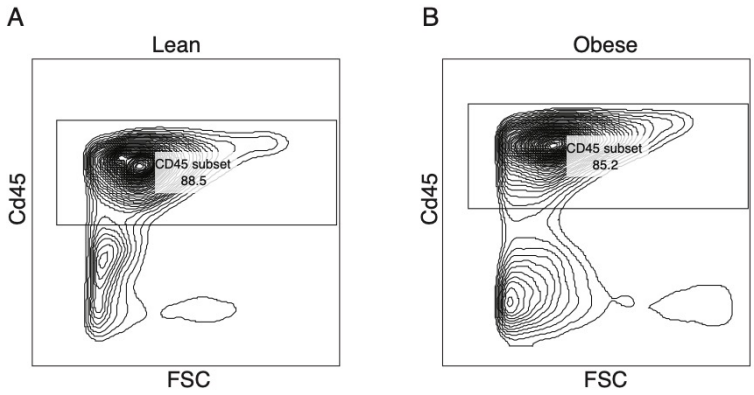

Figure 3.3.1 Flow cytometric data depicting the percent CD45 cells of live cells in homogenized tumors.

A. Representative plot of cells isolated from a lean tumor. B. Representative plot of cells isolated from an obese tumor.

We utilized Cibersort (Newman et al. 2019), a publicly available analytical tool from Stanford University, to infer whether infiltrating immune cell populations or phenotypes may be altered in tumors isolated from obese compared to lean animals. Cibersort estimates the relative contribution of different immune types to a bulk population by comparing a user's RNA sequencing data to known transcriptional profiles mined from published studies (Fig 3.3.2 A). When we used Cibersort to analyze the gene expression data generated from this RNA sequencing study, the program estimated that the most highly represented population of immune cells in E0771 tumors from lean or obese animals was monocytes, followed by CD4 positive T cells (Fig 3.3.2 B). This is consistent with preliminary flow cytometry data performed by previous members of our laboratory. The Cibersort analysis, however, did not identify significant differences in these highly represented immune compartments between tumors isolated from lean or obese animals.

Overall, mast cell related gene expression was less abundant than monocyte and CD4 positive T-cell related gene expression; however, there was a phenotypic switch in mast cell related gene expression between lean and obese animals at both midpoint and endpoint. Tumors

from lean animals had gene expression patterns more consistent with inactive, resting mast cells whereas tumors from obese animals had a phenotype more consistent with activated mast cells (Fig 3.3.2 B). This finding was particularly interesting to us because mast cell infiltration has been shown to promote angiogenesis in breast cancer and is associated with worse outcomes in human solid tumors (Hu, Wang, and Cheng 2018; Cimpean et al. 2017). Furthermore, mast cell infiltration has been shown to promote tumor progression in the MMTV-PyMT mouse model of spontaneous murine breast cancer (Majorini et al. 2020).

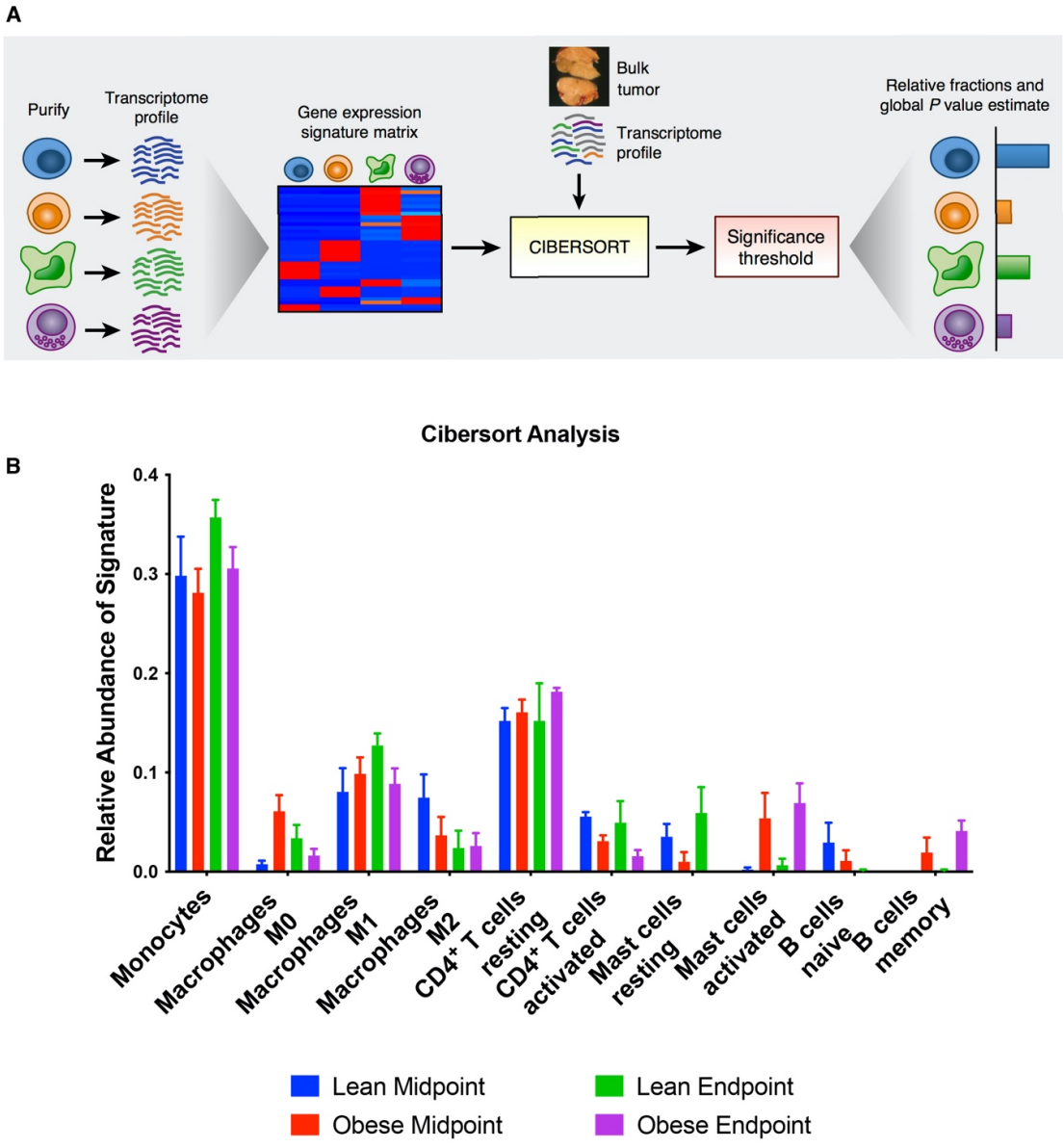

Figure 3.3.2 Cibersort analysis from tumors isolated from lean or obese tumors.

A. Schematic depicting the Cibersort workflow (Newman et al. 2019). B. The relative abundance of transcriptional signatures of different immune populations generated from RNA sequencing comparing lean and obese tumors (n=4 or 5 tumors per group). Data are presented as mean +/- standard error of the mean (SEM).

This analysis of immune cell gene expression signatures suggests a phenotypic switch in tumor-associated mast cells in obesity. Though compelling, this finding was generated based on inferences made from heterogeneous transcriptional data. To validate these correlative findings in our tumor model, we stained formalin fixed tumor sections with toluidine blue dye to highlight mast cells located within the parenchyma of tumors isolated from lean or obese animals at endpoint. Toluidine blue is a commonly used metachromatic dye specific for histidine and heparin located in mast cell granules (Sridharan and Shankar 2012). Importantly, it allows for the distinction between resting mast cells and active, degranulated mast cells by careful observation of the appearance and distribution of granules at high magnification (40X). Resting mast cells have a deep purple appearance, and the granules are confined to a clearly defined cell (Fig 3.3.3 A, red arrows). Active, degranulated mast cells have a light purple appearance with sparse granules dispersed both within the mast cell and in the surrounding interstitial space (Fig 3.3.3 A, yellow arrow). Importantly, histological analysis with toluidine blue revealed that mast cells are rare, but present within E0771 orthotopic tumors isolated from lean or obese animals. We quantified mast cells in a blinded manner, and there were no significant differences in the number of mast cells present in tumors from lean or obese animals (Fig 3.3.3 B). Furthermore, there were no significant differences in the activation state of mast cells located within tumors from lean or obese animals (Fig 3.3.3 C).

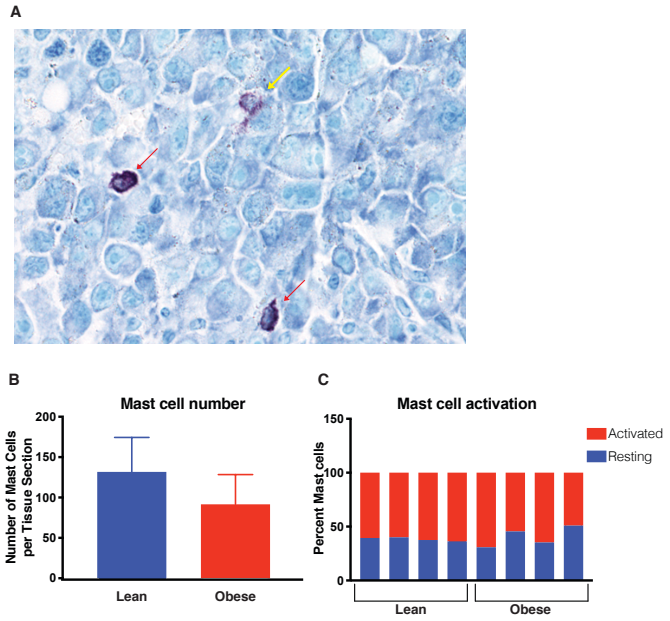

Figure 3.3.3 Histological analysis of intratumoral mast cells in lean or obese tumors.

A. Toluidine blue staining of a representative tumor section (40X). The red arrows indicate resting mast cells. The yellow arrow indicates an active, degranulated mast cell. B. Quantification of mast cell activation in lean or obese animals (n=4 tumors per group). C. Quantification of activated or resting mast cells as a proportion of total mast cells. Data are presented as mean +/- standard error of the mean (SEM).

3.4 Analyzing differentially expressed transcripts in bulk tumors isolated from lean or obese tumors

Next, we performed analyses to broadly compare differences in gene expression between lean and obese tumors at midpoint. We utilized volcano plots to identify genes that exhibited significant differences in expression with the highest magnitude of change. In this analysis, we identified granzymes D, E, F, and G as highly upregulated in tumors from obese animals. Granzymes are proteases that are classically located in the granules of immune cells, so this finding is consistent with our earlier observations that immune cell related gene expression may contribute meaningfully to this dataset (Figure 3.4.1 A). We also utilized smear plots to identify genes that are both highly expressed and highly dysregulated. In this analysis, ornithine decarboxylase 1(Odc1), the rate limiting step in polyamine synthesis, was among the highest expressed, significantly upregulated genes in tumors isolated from obese animals (Figure 3.4.1 B). Importantly, previous studies from our group have identified Odc1 as a gene that is significantly upregulated in the adipocytes located in the breast tumor microenvironment in obese animals.

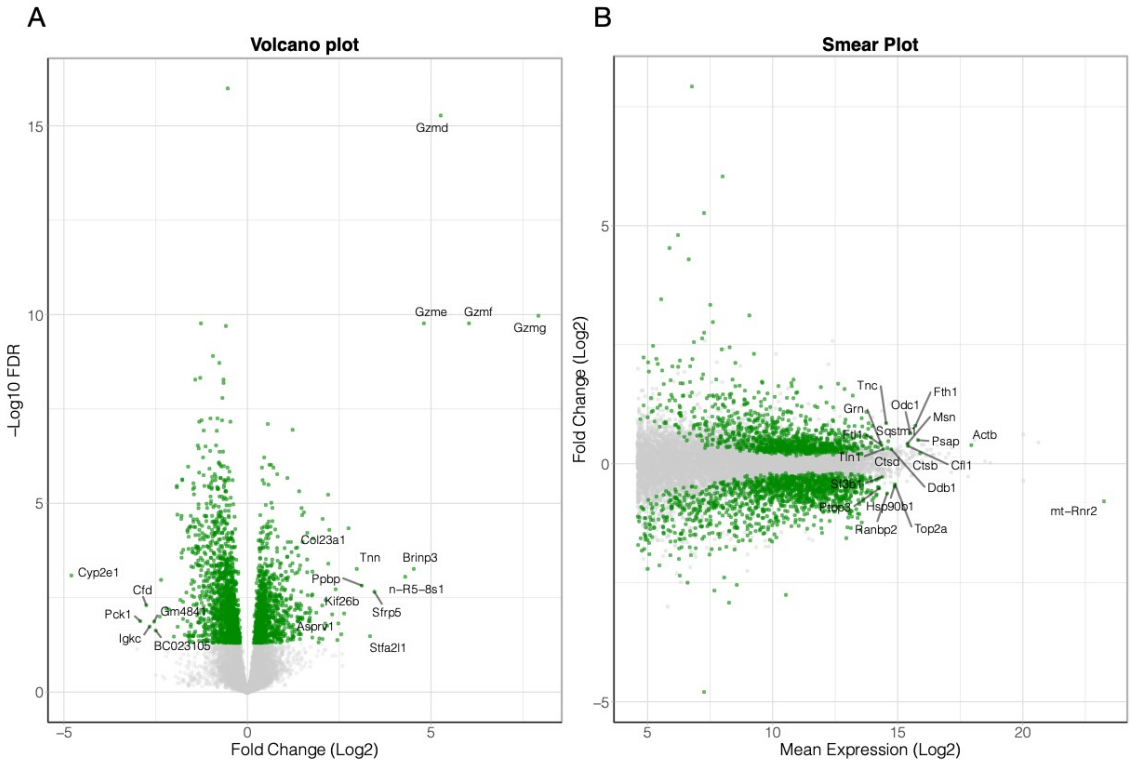

Figure 3.4.1 Analysis of specific transcripts identified in bulk tumors isolated from obese compared to lean animals at midpoint.

A. Volcano plot describing the relationship between statistical significance and fold change. B. Smear plot describing the relationship between fold change and overall expression. Statistically significant differences (adjusted $p<0.05$) are highlighted in green.

Next, we performed pairwise analyses to compare differentially regulated transcripts between tumors isolated from tumors from lean or obese animals at midpoint or at endpoint. We

chose to prioritize genes which had a base mean above 100 since we reasoned that the most important genes for driving accelerated tumor growth would be highly expressed. We also identified genes which had a fold change above 2 or below 0.5 in obese tumors compared to lean tumors as well as an adjusted p value less than 0.05. The top 50 genes that met these criteria are listed in Tables 3.4.1 and 3.4.2. Furthermore, we reasoned that the transcriptional program driving these changes would be sustained throughout the experiment, so we prioritized differences that were consistent between midpoint and endpoint (Table 3.4.3). Finally, we performed an independent orthotopic experiment to validate our RNA sequencing candidates via qPCR. Of the candidates which were commonly regulated at both midpoint and endpoint in the RNA sequencing experiment, only two validated in the second, independent cohort: Bone morphogenetic protein 7 (Bmp7) and Cysteine dioxygenase type 1 (Cdo1) (Highlighted in red in Table 3.4.3) (Figure 3.4.2).

Table 3.4.1 Significantly regulated genes between lean and obese tumors at midpoint.

Genes are ranked by ascending adjusted p.value.

Gene	Base Mean	Fold Change	padj
Gzmd	152.92	38.45	5.46E-16
Gzmg	109.20	242.96	1.09E-10
Gzmf	255.61	65.59	1.74E-10
Ccdc18	548.86	0.33	1.09E-06
Gpr84	110.74	4.58	6.00E-06
Fpr1	475.00	2.90	1.76E-05
Zfp960	234.41	0.34	2.17E-05
Apoc2	104.20	4.13	2.64E-05
Zfp97	355.55	0.29	2.65E-05
Arhgap5	7877.00	0.34	4.19E-05
Zfp930	1132.24	0.34	4.26E-05
Col23a1	153.68	6.74	4.67E-05
Zfp994	1010.94	0.32	5.23E-05
Zfp976	399.94	0.32	5.88E-05
Mmp9	1200.81	3.09	6.17E-05
Cep290	945.35	0.33	7.83E-05
Lpcat2	692.11	2.83	1.06E-04
Zfp820	283.28	0.30	1.74E-04
Spint1	363.70	3.09	3.12E-04
Dio2	153.21	0.35	4.83E-04
Tnn	195.19	7.86	5.53E-04
Cd300e	214.37	3.41	6.55E-04
Cd14	1741.81	3.09	6.85E-04
Cyp2e1	153.08	0.04	8.26E-04
n-R5-8s1	100.03	19.63	9.04E-04
Ppbp	536.10	8.66	1.53E-03
Il1a	249.45	5.29	1.92E-03
Tmem26	336.31	3.40	2.66E-03
Mcemp1	410.33	3.12	2.76E-03
Spo11	102.65	0.30	4.15E-03
Cfd	1479.84	0.15	5.08E-03
Dkk3	103.57	3.29	7.15E-03
Grem1	149.39	3.67	8.01E-03

Mmp13	3889.89	3.05	8.03E-03
Col12a1	7503.97	2.97	8.27E-03
Kif26b	144.98	6.21	8.41E-03
Trem1	609.02	4.95	8.90E-03
Bmp7	266.99	0.19	1.02E-02
Slpi	769.67	3.25	1.10E-02
Clec4d	2029.75	2.83	1.17E-02
Mmp12	6291.74	3.21	1.24E-02
Acod1	1718.63	3.24	1.35E-02
Pck1	305.60	0.13	1.35E-02
Mmp8	363.57	4.34	1.55E-02
Igkc	204.03	0.16	1.86E-02
Ifitm1	760.98	3.30	2.03E-02
Asprv1	115.85	5.87	3.00E-02
Tmem56	104.11	0.35	3.32E-02
Stfa2l1	181.70	10.11	3.37E-02
Cdo1	146.33	0.33	3.41E-02

Table 3.4.2 Top 50 significantly regulated genes between lean and obese tumors at endpoint.

Genes are ranked by ascending adjusted p.value.

Gene	Base Mean	Fold Change	p.adj
Hbb-bs	6627.84	13.29	7.34E-10
Hbb-bs	6627.84	13.29	7.34E-10
Hba-a2	473.54	7.12	2.10E-08
Gzmd	152.92	9.72	3.53E-08
Hbb-bt	715.66	11.30	1.21E-07
Slc40a1	1406.54	4.41	1.80E-07
Clec4n	5464.27	3.40	7.84E-07
Mcub	891.67	3.18	8.40E-07
Irf4	243.62	0.31	8.68E-07
Rps10	4862.56	2.97	1.52E-06
Rpl41	47218.36	3.06	1.54E-06
Rps10-ps1	6152.44	3.23	1.58E-06
Gzmg	109.20	17.81	2.74E-06
Hba-a1	822.07	6.06	2.78E-06
Cyp2e1	153.08	0.02	3.29E-06
Phxr4	156.33	0.18	3.29E-06
Cops9	2315.33	3.40	3.47E-06
Rpl9-ps4	476.22	2.94	3.70E-06
Atp5e	3178.11	3.12	5.00E-06
Gzmc	559.83	3.05	5.65E-06
Retnlg	216.79	19.90	6.64E-06
Gng10	184.44	3.02	1.69E-05
Chchd1	2126.60	2.85	2.65E-05
Hmox1	9126.85	3.32	3.99E-05
S100a8	4812.65	14.51	4.39E-05
Cebpd	1052.54	2.93	4.56E-05
Insrr	136.35	0.30	5.14E-05
Retnla	807.79	0.06	7.09E-05
Hist4h4	14653.73	3.56	1.36E-04
Fam196a	102.13	0.33	1.49E-04
Egfros	191.45	0.30	1.68E-04
Cd14	1741.81	2.95	2.34E-04

Spo11	102.65	0.25	2.48E-04
Omg	175.38	0.34	2.67E-04
Itk	226.24	0.32	4.21E-04
Fam196b	251.09	0.27	4.52E-04
Krt18	144.72	0.33	5.76E-04
Spic	327.56	3.40	8.89E-04
Ifit1bl2	169.04	2.90	9.13E-04
Clec4d	2029.75	3.22	9.46E-04
Stfa2l1	181.70	18.79	1.02E-03
Gzmf	255.61	6.79	1.19E-03
Wfdc17	3800.89	3.46	1.29E-03
Chil3	948.18	3.46	1.37E-03
Col10a1	100.61	0.30	1.41E-03
Rmrp	102833.63	3.13	1.62E-03
Clec4e	2775.69	3.60	1.67E-03
Fcgbp	122.03	0.09	1.73E-03
Tmem56	104.11	0.28	1.93E-03
S100a9	5385.56	14.71	1.93E-03

Table 3.4.3 Commonly regulated genes between obese and lean tumors at midpoint and endpoint.

Genes from Tables 3.4.1 and 3.4.2 that validated in a second cohort are highlighted in red.

Gene	Direction in obese vs. lean	qPCR validation in an independent cohort
Gzmd	up	no
Gzmg	up	no
Gzmf	up	no
Cd14	up	no
Cyp2e1	down	no
Ppbp	up	no
Spo11	down	no
Cfd	down	no
Trem1	up	no
Bmp7	**down**	**yes**
Slpi	up	no
Clec4d	up	no
Pck1	down	no
Mmp8	up	no
Igkc	down	no
Ifitm1	up	no
Asprv1	up	no
Tmem56	down	no
Stfa2l1	up	no
Cdo1	**down**	**yes**
Cxcr2	up	no
Retnlg	up	no
S100a8	up	no
Lep	up	no
S100a9	up	no

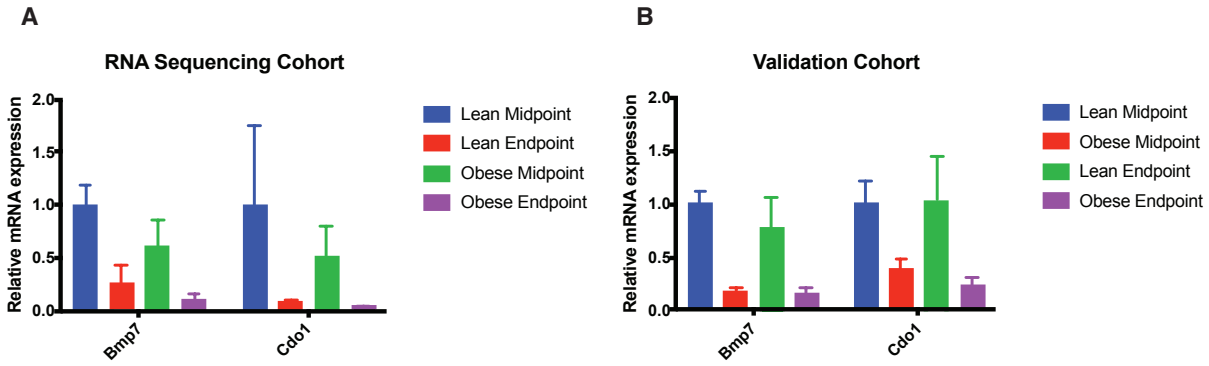

Figure 3.4.2 . qPCR of validated candidates.

A: qPCR of candidates identified in the RNA sequencing cohort. B: qPCR of bulk tumors isolated from a second orthotopic experiment (n=4 or 5 tumors per group). Data are presented as mean +/- standard error of the mean (SEM)

Bmp7 is a member of the transforming growth factor beta (Tgf-β) superfamily of proteins. It acts to inhibit Tgf-β1 signaling and is widely expressed by many cell types, including immune cells and adipocytes, which are non-malignant, but tumor associated cell types in our orthotopic model. Interestingly, Bmp7 signaling has described roles in inhibiting Tgf-β1 related epithelial to mesenchymal transition (EMT) in breast cancer cell lines, and treatment with ectopic Bmp7 promotes breast cancer cell viability (Ying, Sun, and He 2015; Alarmo et al. 2009). This suggests that suppression of Bmp7 expression in obese tumors may contribute to increased progression in our tumor model.

Cdo1 is involved in the first step of cysteine metabolism and is a major regulator of intracellular cysteine levels. In human breast cancer, Cdo1 is frequently silenced by DNA methylation, and restoration of Cdo1 expression in breast cancer cell lines leads to elevated reactive oxygen species and reduced cellular viability (Jeschke et al. 2013). Importantly, Cdo1 is highly expressed by adipocytes, a major non-cancer cell type present in the bulk tumor.

Bmp7 and Cdo1 are both interesting candidates that are significantly and reproducibly dysregulated in obese tumors. The previously described functions of these genes in breast cancer suggest compelling mechanisms by which they may contribute to accelerated tumor growth in obesity. However, both Bmp7 and Cdo1 are expressed by multiple cell types in the heterogeneous tumor, and the design of these RNA sequencing and bulk tumor studies limit our ability to discern which cell type or types may be most important for the differences we observe in gene expression.

3.5 Summary

We utilized a murine diet-induced model of obesity accelerated triple-negative breast cancer to examine the differences in gene expression between tumors in lean and obese animals. The goal was to identify early changes in the cancer cells that drive tumor progression. We began our studies with bulk transcriptomic analysis of tumors from lean and obese animals, but further examination revealed that these are cellularly heterogenous tumors, with a substantial degree of immune and adipose infiltration. With our bulk approach, the majority of genes and pathways that were differentially regulated with obesity were related to immune signaling,

suggesting that changes to the immune cell infiltration or phenotype may play an important role in obesity-accelerated breast cancer. Our goal is to understand the behavior of lean and obese cancer cells, and ultimately, these findings highlight the need to address our question with cell type specific techniques. The following chapters will describe the cancer cell-type specific approaches we used to understand how neoplastic cancer cells behave differently in the obese environment.

CHAPTER 4 Transcriptomic analysis of cancer cells isolated from orthotopic E0771 tumors from lean or obese animals

4.1 Introduction

Our comparative analysis of the bulk transcriptomes of tumors from lean or obese animals identified compelling candidates that may be dysregulated in the setting of obesity and may drive obesity-related tumor growth. Furthermore, this analysis revealed potentially interesting relationships between non-malignant, tumor associated cell types and tumor progression in obesity. However, our approach involved homogenization and RNA sequencing of the bulk, cellularly heterogenous tumor, and as a result, we were unable to precisely identify the cell types responsible for the differences we observed in gene expression among the experimental groups. The main goal of this work is to understand the mechanisms by which breast cancer cells respond to the obese environment. The studies described in the previous chapter highlighted the need to develop novel strategies to isolate tumor cells from the heterogeneous bulk tumor prior to analysis. Therefore, we chose to employ a florescence-based labeling approach to address this need.

4.2 Establishing a model of mCherry positive E0771 orthotopic tumors in vivo

We engineered E0771 cancer cells to stably express mCherry fluorescent protein. After orthotopic implantation, the tumors produced by this method were digested and dissociated. Then, mCherry positive cancer cells were isolated using fluorescence activated cell sorting (FACS) before transcriptional analysis by qPCR or RNA sequencing (Figure 4.2.1). This method ensured that we specifically probed the cancer cells despite a heterogeneous microenvironment.

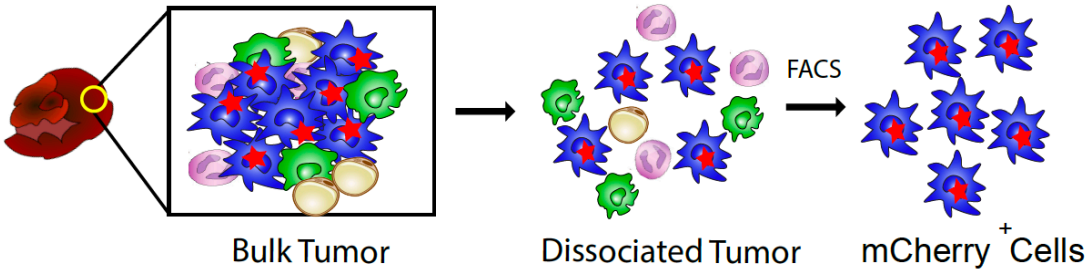

Figure 4.2.1 Schematic representation of florescence-based cancer cell isolation.

We used a lentiviral approach to transduce E0771 cells with a construct expressing mCherry fluorescent protein (Figure 4.2.2). After infection, we used FACS to isolate the highest mCherry expressing cells and cultured those *in vitro* to establish a stable mCherry E0771 cell line, which we named mE0771. We first verified that mE0771 cells were able to establish tumors in both lean and obese animals *in vivo* and that those tumors maintained obesity-accelerated growth similar to the parental E0771 cell line. mE0771 overall grew less large by our predetermined endpoint, but they did show significant acceleration in tumor volume in obesity, similar to the parental E0771 cell line. (Figure 4.2.3 A and Figure 4.2.3 B). After dissection, we

digested and dissociated the mE0771 tumors for flow cytometric analysis to establish that we could isolate live, mCherry positive cancer cells from the homogenized tumor (Figure 4.2.3 C).

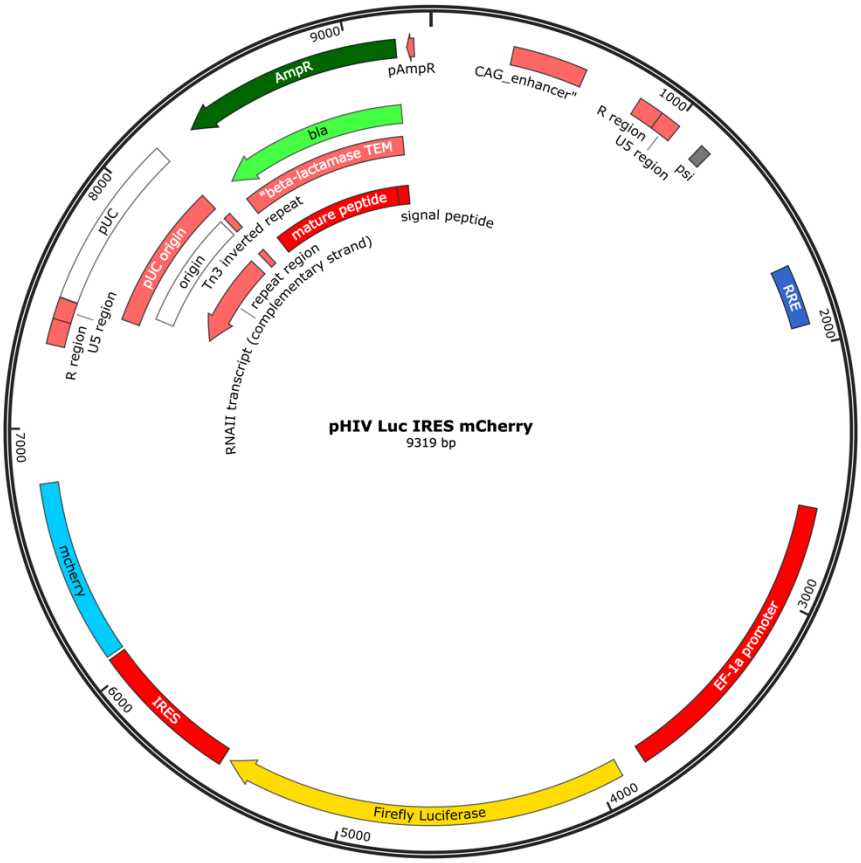

Figure 4.2.2 Plasmid map of lentiviral mCherry construct.

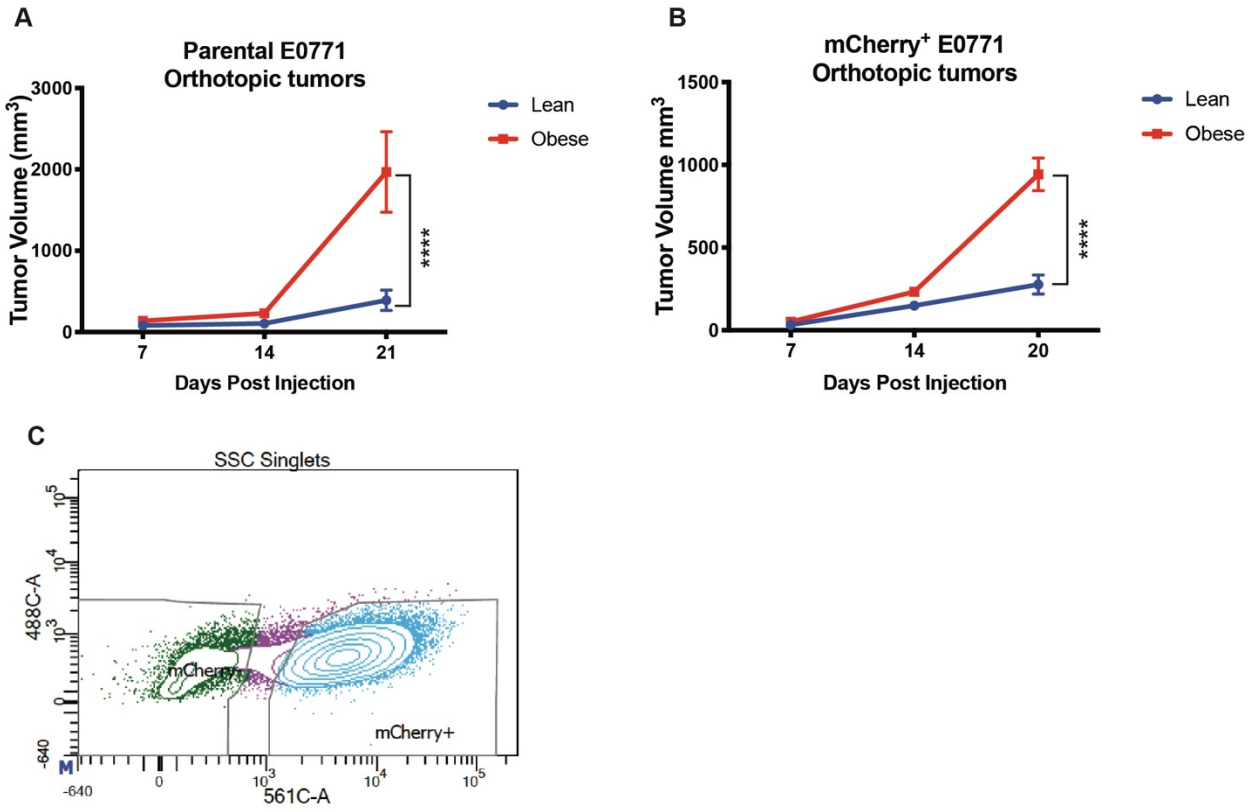

Figure 4.2.3 Establishing an mCherry positive E0771 orthotopic tumor model

A. Tumor volume of parental E0771 tumors over time in lean or obese animals (n=7 or 9 tumors per group). B. Tumor volume of mE0771 tumors over time in lean or obese animals (n=7 or 11 animals per group). C. Density plot depicting the mCherry positive and negative populations of an mE0771 orthotopic tumor. Data are presented as mean tumor volume +/- standard error of the mean (SEM). **** $p<0.0001$.

4.3 Validating the efficacy of FACS to isolate cancer cells in a heterogeneous tumor

Next, we aimed to confirm that the process of digesting and dissociating the tumors from this model was effective in depleting non-malignant, but tumor associated cell types, like immune cells and adipocytes. We verified that our method successfully enriched cancer cells by using qPCR to assess a panel of well-established immune and adipose marker genes at three stages: the bulk tumor, the digested single-cell suspension, and the FACS isolated mCherry positive or negative cell populations.

The first steps of tumor dissociation involve mechanical and enzymatic digestion followed by centrifugation to isolate the cellular fraction. Lipid-laden, mature adipocytes are less dense than the aqueous medium and should be separated and discarded during these steps. We expected that if this were the case, adipocyte-specific gene expression should be depleted during digestion. Consistent with this, adipocyte related gene expression was highest in bulk tumor and was minimal in the digested sample as well as both mCherry positive and negative sorted samples (Figure 4.3.1 A).

Immune cells are present in both the bulk tumor and the digested, single cell suspension. However, given that immune cells originate from the host and do not express mCherry fluorescent protein, they should be sorted into the mCherry negative population during FACS. Consistent with this, immune related genes were slightly enriched in the digested samples compared to bulk tumor, depleted in the mCherry positive population, and highest in the mCherry negative population (Figure 4.3.1 B). These results were consistent among tumors from lean and obese animals and confirm that tumor dissociation and digestion is effective at depleting non-malignant, but tumor associated cell types from bulk tumor samples.

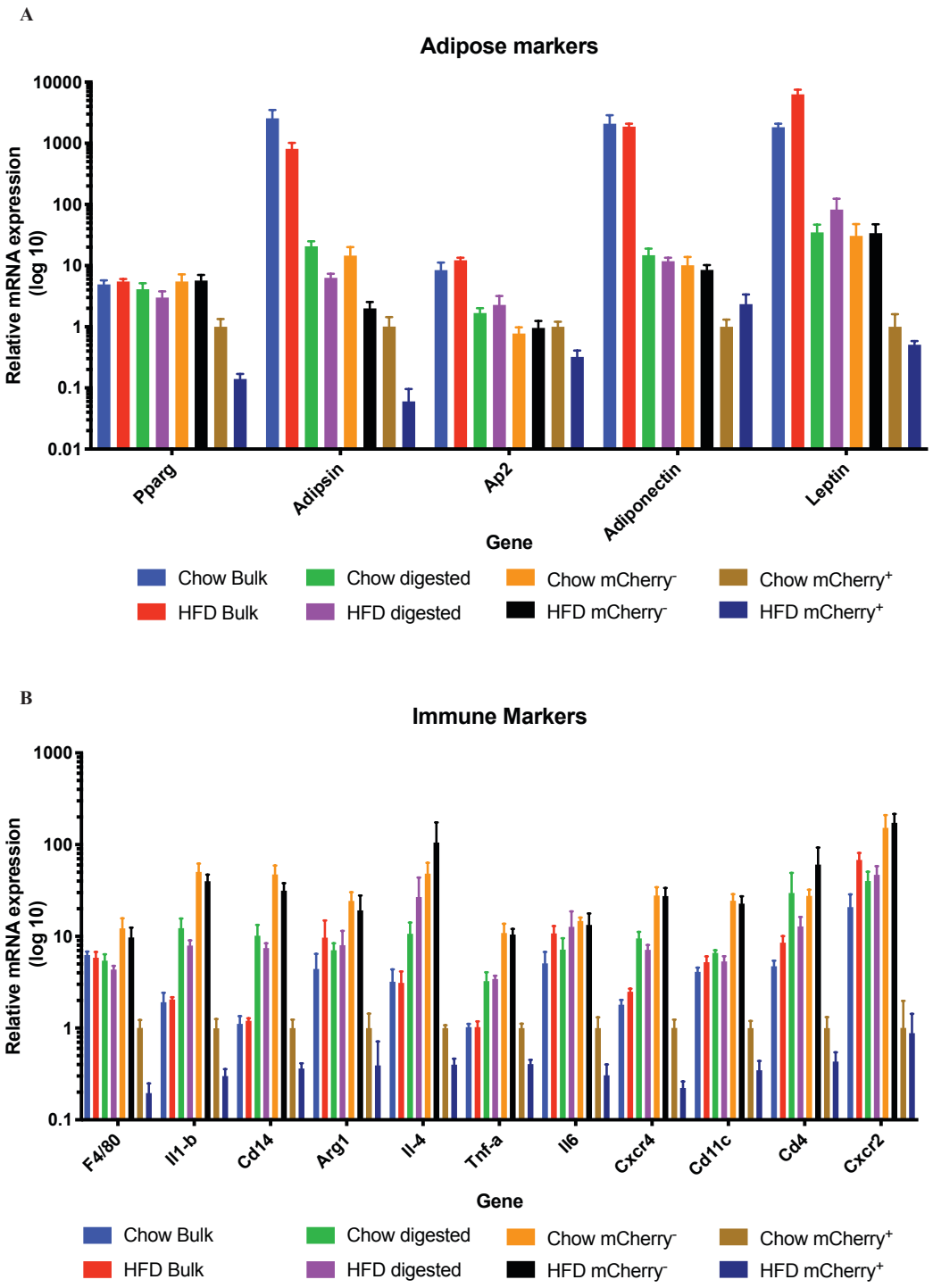

Figure 4.3.1 Assessing the efficacy of tumor dissociation and cell sorting.

A. Bar plot depicting relative mRNA expression of adipose markers by qPCR (n=5 tumors per group). B. Bar plot depicting relative mRNA expression of immune markers by qPCR (n=5 tumors per group). Data are presented as mean +/- standard error of the mean (SEM).

4.4 Transcriptomic analysis of mCherry positive cells isolated from lean or obese tumors

Once we established that our technique was effective at isolating mCherry positive cancer cells from the bulk tumor and depleting other cell types, we performed RNA sequencing to compare the gene expression of mCherry positive cells isolated from lean or obese tumors. Similar to the RNA sequencing strategy described in Chapter 3, our aim was to identify early gene expression changes that may accelerate tumor growth; therefore, we chose to isolate cells from tumors at midpoint (day 14 after implantation) and endpoint (day 21 after implantation).

Principal component analysis (PCA) was used to examine gene expression data among all of the samples. PCA uses an orthogonal transformation of gene expression data to collapse the major sources of variation into two principal components, which are graphed along two axes. This analysis can be used to visually represent the overall similarity in gene expression among samples within and between experimental groups. The midpoint and endpoint samples, regardless of obesity, appear to separate along PC1 in this type of analysis. When considering pairwise analyses of the effect of obesity within each timepoint, we noticed an interesting trend: despite the drastic differences in tumor volumes between obese and lean tumors at endpoint, these groups overlap in the PCA plot. This suggests that there are few differences in the overall gene expression patterns of the cancer cells isolated at this timepoint (Figure 4.4.1). At midpoint, there was some overlap between the lean and obese groups, but the separation of the groups represents more overall differences in this pairwise analysis than at endpoint. This data suggests that the differences in tumor volume at endpoint may be directed by earlier differences in the gene expression between tumors in lean or obese animals. Consequently, we decided to focus our attention on the differences between the lean and obese groups at midpoint.

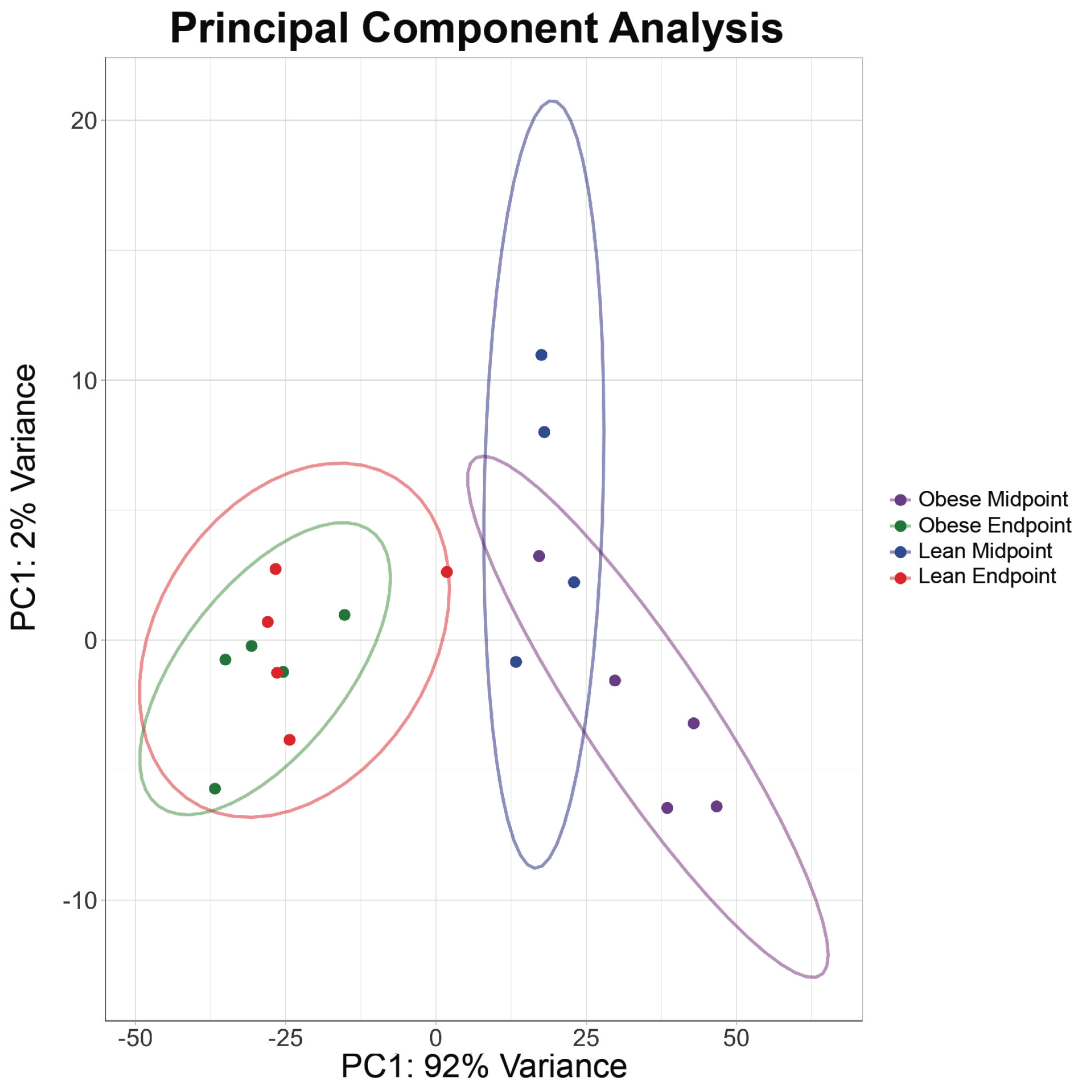

Figure 4.4.1 Principal component analysis from RNA sequencing of mCherry positive cancer cells isolated from tumors from lean or obese animals.

We performed gene set enrichment analysis to identify pathways that were modulated in cancer cells by obesity at midpoint. Interestingly, many of the terms that were overrepresented in the cancer cells from obese tumors compared to lean were related to inflammation and immunity (Figure 4.4.2 A). This, taken with our bulk tumor RNA sequencing analysis (Chapter 3), suggests that cancer cells may differentially interact with components of the immune system in obesity. Another significantly up-regulated term in the gene set enrichment analysis was response to lipid (Figure 4.4.2 A, starred). When we plotted all of the genes listed in this term on a heatmap, there appears to be clustering in gene expression between lean and obese cancer cells at midpoint. This analysis suggests that obesity may affect the expression of genes related to lipid response at an early timepoint (Figure 4.4.2 B). Other groups have demonstrated that circulating and local lipids can meaningfully contribute to tumor progression in breast cancer as well as other cancer models (Balaban et al. 2017; Zhang et al. 2018; Gallagher et al. 2017;

Alikhani et al. 2013). However, this relationship has not yet been therapeutically targeted and remains an interesting mechanistic link between obesity and cancer progression.

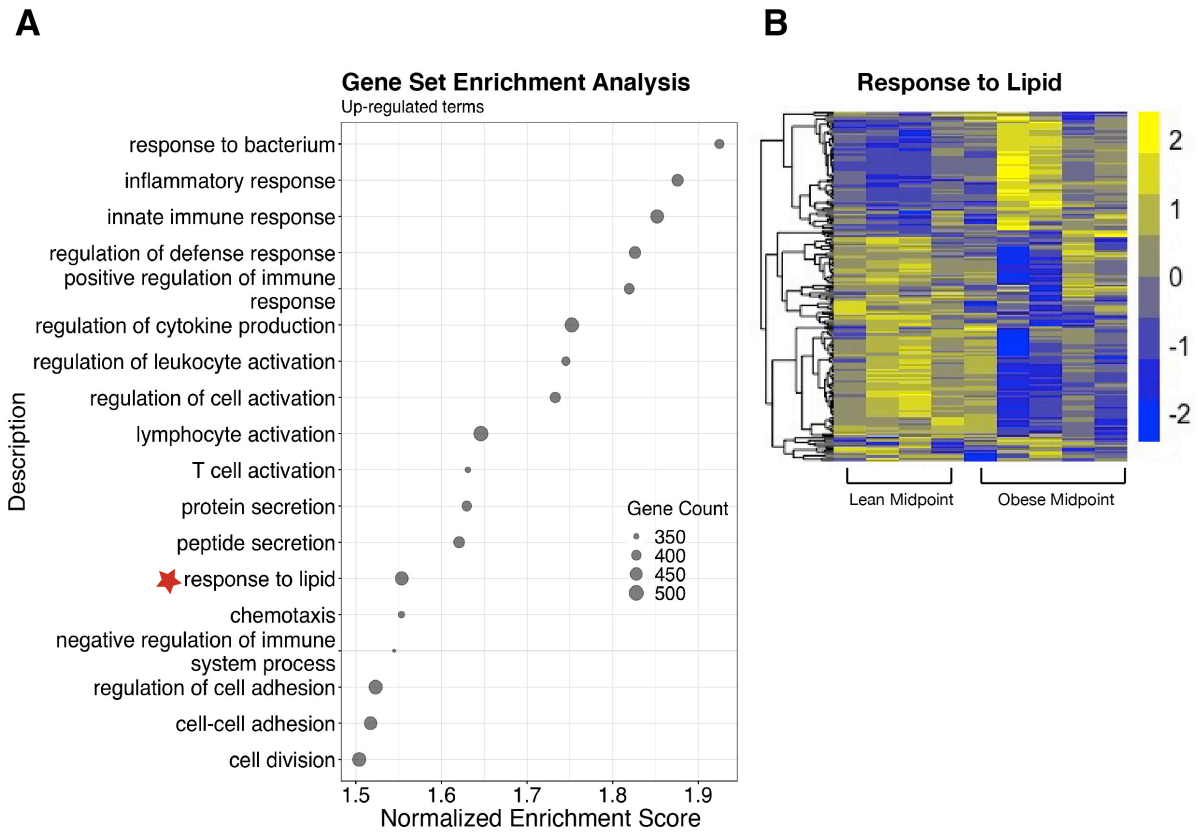

Figure 4.4.2 Gene Set Enrichment Analysis (GSEA) comparing obese and lean cancer cells at midpoint

A. The top 18 terms most upregulated in obese cancer cells compared to lean at midpoint. B. Heatmap depicting the gene expression dispersion of terms related to lipid response.

When we examined the most highly regulated genes in cancer cells isolated from obese animals compared to lean, we prioritized genes that had a base mean read count above 100, a fold change greater than 20% in either direction, and an adjusted p value below 0.05. More than 1000 genes met these criteria. We then ranked these candidate genes by fold change and focused on the top fifty upregulated and top fifty downregulated candidate genes (Tables 4.4.1. and 4.4.2).

The most highly upregulated, non-histone, protein-coding gene in this data set was acyl-CoA synthetase bubblegum family member 1 (Acsbg1). Importantly, neither Cdo1 nor Bmp7, which were identified as candidates in our bulk studies, were among the top regulated genes in this cancer-cell specific analysis. This suggests that Cdo1 and Bmp7 may be differentially regulated by obesity in cell types other than cancer cells.

Table 4.4.1 Top 50 upregulated genes expressed by obese cancer cells compared to lean cancer cells isolated at midpoint.

Genes are ranked by descending fold change.

Gene	Base Mean	Fold Change	padj
Hist1h2ak	6528.13	3.00	6.36E-03
Rpph1	396917.45	2.96	7.47E-03
Hist1h4n	1697.70	2.95	2.92E-02
Hist2h2ac	1339.30	2.86	5.41E-03
Hist4h4	2030.15	2.83	3.89E-03
Acsbg1	497.76	2.83	2.97E-03
Hist1h2ab	722.45	2.78	8.77E-03
Hist1h3c	2864.28	2.76	6.99E-03
Hist1h4h	3688.95	2.74	9.40E-03
Ncor2	3383.36	2.71	9.78E-03
Rmrp	3213.46	2.70	3.78E-03
Hist1h2an	462.17	2.70	1.51E-02
Hist1h4a	3078.75	2.66	6.83E-03
Hist1h4b	413.11	2.65	1.19E-02
Rny1	134.27	2.64	3.00E-02
Atn1	3146.95	2.61	1.13E-02
Hist2h4	5456.01	2.59	2.30E-03
Hist1h4k	1344.08	2.55	1.87E-02
Hist1h2bl	996.75	2.53	5.48E-03
Cacng7	163.80	2.51	1.70E-02
Hist1h3a	1547.27	2.51	7.37E-03
Hist1h2ac	782.38	2.50	1.23E-02
Hist1h4j	628.55	2.43	2.41E-02
Ier5l	998.44	2.43	7.57E-03
Bicra	383.95	2.42	2.61E-02
Hist1h2bp	164.99	2.37	3.55E-03
Hist1h4c	4257.78	2.36	1.44E-02
Hist1h4d	24375.32	2.36	8.77E-03
Hist3h2bb-ps	226.52	2.35	8.62E-03
Hist1h3e	4043.00	2.32	1.39E-02
Rps2-ps10	203.29	2.32	6.57E-03
Eva1b	976.01	2.32	7.72E-03

Ppp1r13l	181.85	2.30	4.14E-03
Hist1h2ai	1552.73	2.30	7.79E-03
Hist1h4f	4018.57	2.25	1.19E-02
Gm22270	156.54	2.24	9.82E-03
Ccdc85b	437.28	2.24	6.57E-03
Reep6	1576.66	2.21	6.03E-03
Apc2	1528.53	2.21	3.74E-03
Prr7	115.29	2.18	4.40E-02
Zfp628	477.42	2.18	1.36E-02
Klf16	1697.66	2.17	4.70E-03
Myl9	358.97	2.17	5.40E-03
Galk1	4805.61	2.16	4.71E-03
Ankrd13b	1847.69	2.16	2.24E-03
Pcx	705.40	2.15	5.76E-03
Rnf26	895.40	2.14	4.17E-03
Prr12	1425.24	2.14	1.48E-02
Hist1h3b	3903.55	2.14	1.37E-02
Hspg2	30033.24	2.13	2.74E-02

Table 4.4.2 50 most downregulated genes expressed by obese cancer cells compared to lean at midpoint

Genes are ranked by ascending fold change.

Gene	Base Mean	Fold Change	padj
Mmp12	675.65	0.15	3.54E-03
Cd53	554.58	0.16	1.18E-04
Clec4a2	135.08	0.18	1.50E-03
Tlr13	271.54	0.19	1.50E-04
Ifit1bl1	216.46	0.19	5.50E-03
Pid1	110.11	0.19	3.72E-04
Ly86	179.78	0.20	5.32E-04
Ms4a6d	816.17	0.21	7.37E-04
6720427I07Rik	1033.65	0.21	1.34E-03
Msr1	350.53	0.21	1.59E-03
Selenop	733.44	0.21	8.07E-03
Spic	270.69	0.21	2.63E-02
Clec12a	131.60	0.22	4.53E-03
Cxcl9	1402.28	0.22	1.90E-02
Cd86	112.73	0.23	1.34E-03
Cd84	222.88	0.23	2.97E-03
Rnf130	186.35	0.23	2.40E-03
Ctsc	1514.70	0.24	2.40E-03
Tgtp2	394.20	0.24	2.95E-02
Frmd4b	268.33	0.24	1.34E-03
Ms4a4c	802.02	0.25	2.50E-03
Slfn1	212.05	0.25	3.16E-03
Slamf7	363.74	0.26	8.97E-03
Slco1a5	294.14	0.26	3.00E-03
Rgs2	116.32	0.26	1.47E-03
Igsf6	179.76	0.26	1.66E-02
Ap1s2	162.10	0.26	3.07E-03
Mospd1	112.48	0.26	2.79E-03
Slc40a1	102.76	0.26	4.12E-02
Tmem26	102.37	0.27	5.71E-03
Tlr7	153.81	0.27	6.57E-03
Cd300ld	365.64	0.27	4.03E-03

Gm10800	421.45	0.27	3.67E-02
Mmp1a	192.73	0.27	4.56E-03
Eif3s6-ps1	413.44	0.27	3.40E-03
Cytip	151.23	0.28	2.56E-03
Ogfrl1	160.97	0.28	3.89E-03
Marcks	380.26	0.28	4.88E-03
Mmp13	736.54	0.28	1.32E-02
Ccr5	424.97	0.28	2.40E-03
Clec4a3	285.22	0.28	5.39E-03
Havcr2	126.05	0.28	8.28E-04
Ptprc	335.18	0.28	4.22E-03
Xist	366.32	0.28	3.26E-03
Aoah	108.02	0.29	4.61E-03
Rnf144b	124.59	0.29	1.46E-03
Srgn	948.09	0.29	2.67E-03
Entpd1	317.62	0.29	1.46E-03
Ms4a6b	325.18	0.29	2.68E-03
Casp1	2547.76	0.29	3.20E-03

Acsbg1 was more than 2.8-fold upregulated in cancer cells isolated from tumors in obesity, with an adjusted p value <0.0001. It was also 2.3-fold upregulated at endpoint, although this difference did not reach statistical significance (adjusted p value = 0.10). When we examined our bulk RNA sequencing results (Chapter 3), Acsbg1 was significantly upregulated in obese tumors at both midpoint and endpoint to similar levels as the mCherry positive cells. In bulk, obese tumors at midpoint, Acsbg1 was 2.6-fold higher than lean with an adjusted p value of 0.0068. At endpoint, it was 1.67-fold upregulated in obese tumors with an adjusted p value of 0.04. This confirmed that Acsbg1 upregulation in obese cancer cells was not a result of a differential response to the process of tumor digestion and dissociation.

Acsbg1 is an acyl-CoA synthetase, a class of enzymes that is essential for long-chain fatty acid metabolism (Tang, Tsai-Morris, and Dufau 2001; Pei et al. 2003). Acyl-CoA synthetase enzymes catalyze the conversion of fatty acids to fatty acyl-CoAs through a two-step, ATP dependent reaction. Fatty acyl-CoAs can then move into the mitochondria, where they are oxidized to produce acetyl coAs, which enter the TCA cycle to ultimately generate ATP. The number of ATP molecules generated per fatty acyl coA depends on the carbon length of the fatty acyl molecule. Fatty acyl coAs can also participate in anabolic processes like membrane lipid synthesis, to support the expansion of biomass (Figure 4.4.3) (Grevengoed, Klett, and Coleman 2014). Both of these processes are essential for cancer cell viability and tumor progression and suggest interesting mechanisms by which obesity-regulated Acsbg1 may potentiate breast cancer growth and progression. Importantly, none of the other acyl-CoA synthetase enzymes were differentially regulated with obesity at midpoint or endpoint, suggesting that Acsbg1 may play a unique role in obese cancer cells.

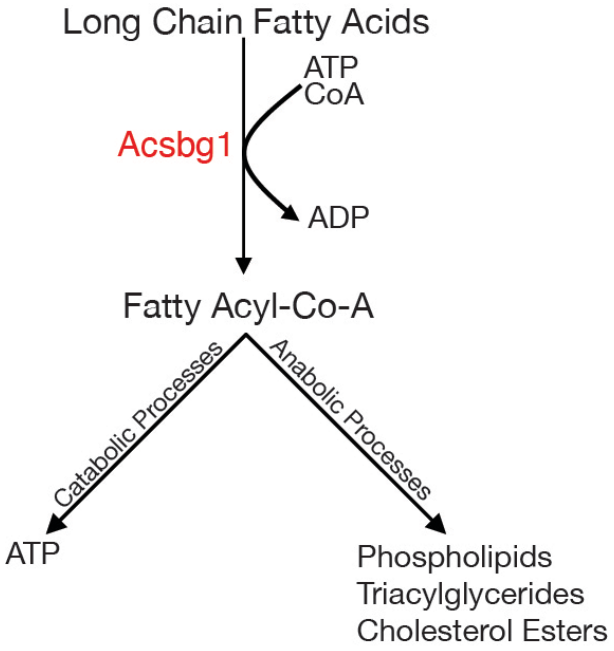

Figure 4.4.3 Schematic depicting the function of Ascbg1 and fates of Fatty Acyl Co A species in the cell.

We validated Acsbg1 upregulation in obese cancer cells in an independent cohort by qPCR (Figure 4.4.4 A). Furthermore, we confirmed that the expression of Acsbg1 is enhanced at the protein level by Western Blot of bulk tumors (Figure 4.4.4 B). Additionally, we performed IHC to confirm Acsbg1 expression *in situ* and observed expansive expression of Acsbg1 in tumors from obese animals and sparse expression in tumors from lean animals (Figure 4.4.4 C and D). We hypothesize that the upregulation of this enzyme, which plays a critical role in long chain fatty acid metabolism, may allow cancer cells to more effectively utilize long chain fatty acids for energy production and to support the expansion of biomass, thereby potentiating tumor progression in obesity.

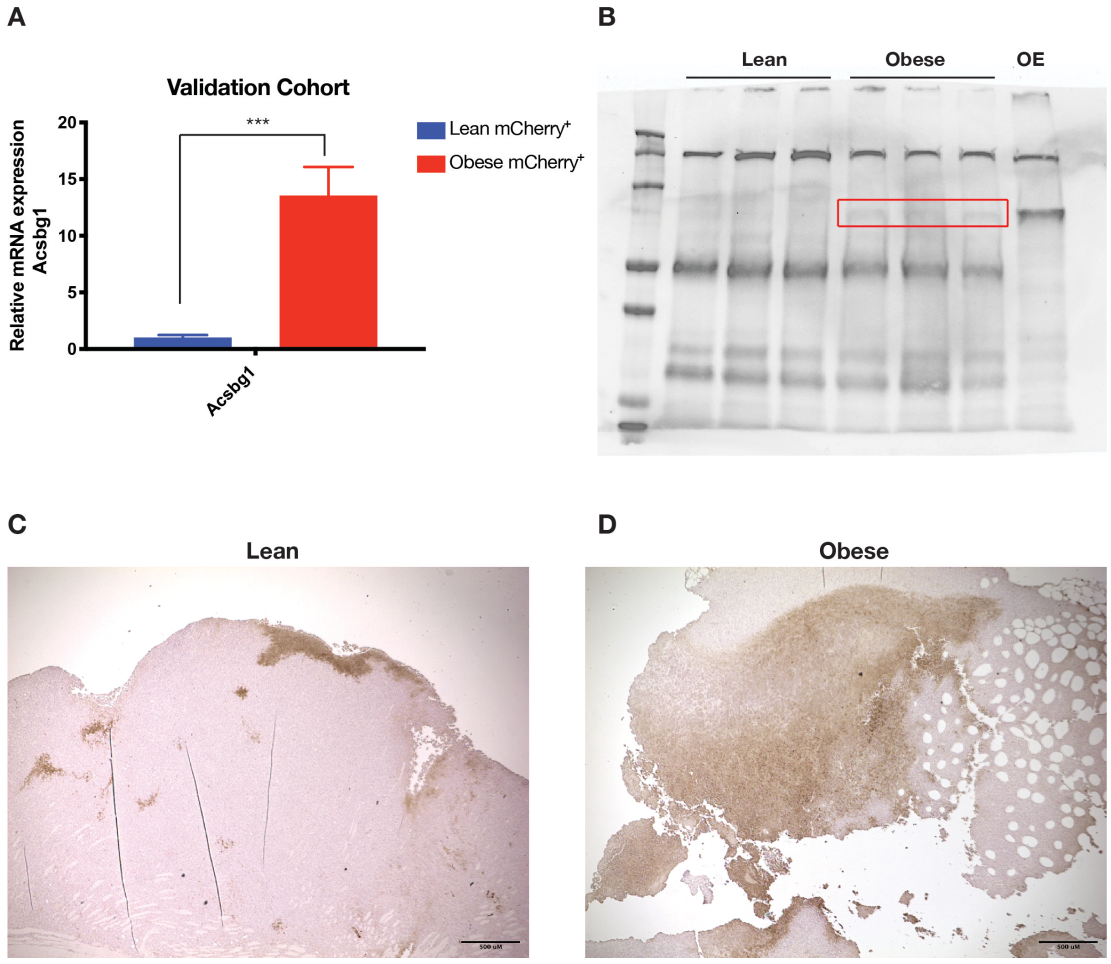

Figure 4.4.4 Confirmation of Acsbg1 expression in lean and obese tumors.

A. qPCR measuring gene expression of Acsbg1 in mCherry positive cells isolated from lean or obese animals. n=6 or 7 tumors per group. B. Western blot for Acsbg1 in bulk tumors from lean or obese animals or a cell line which expresses transgenic Ascbg1 (OE) C. Immunohistochemistry for Acsbg1 in a tumor from a lean animal at 2.5x. D. Immunohistochemistry for Acsbg1 in tumor from an obese animal at 2.5x. Data are presented as mean +/- standard error of the mean (SEM). Scale bars represent 100uM. *** $p<0.001$.

4.5 Summary

In this chapter, we developed a cancer cell specific approach to analyze the differences in gene expression between tumors in lean or obese tumors. We created a stable E0771 cell line that expresses mCherry fluorescent protein and employed FACS to separate cancer cells from other tumor-associated cell types before transcriptomic analysis. Our goal was to identify early changes that may be involved in the underlying mechanisms that drive accelerated tumor progression in obesity, so we collected cells at both midpoint and endpoint. Surprisingly, there were few transcriptional differences between cancer cells isolated from obese or lean animals at endpoint, and therefore, we focused on the differences at midpoint. We identified Acsbg1, which was significantly and reproducibly upregulated in obese cancer cells, and we hypothesize that increased long chain acyl-CoA synthetase activity may contribute to accelerated tumor progression in obesity. The following chapter will focus on our work to investigate the roles of Acsbg1 in potentiating breast cancer tumor progression.

CHAPTER 5 The role of Acsbg1 in obesity accelerated breast cancer

5.1 Introduction

In chapter 4, we developed a fluorescence-based labeling approach to isolate cancer cells from cellularly heterogeneous tumors in a murine model of obesity-accelerated triple negative breast cancer. We then performed transcriptomic profiling of the purified cancer cells to identify transcripts which were differentially regulated in obese compared to lean animals. The goal of this analysis was to identify candidate genes and pathways that may drive obesity-accelerated breast cancer progression. We identified an acyl-CoA synthetase, Acyl-CoA synthetase Bubblegum Family member 1 (Acsbg1), as being robustly upregulated in obese cancer cells early in the disease process.

Acsbg1 is a long-chain acyl-CoA synthetase (Acsl), a class of enzymes essential for long chain fatty-acid metabolism. Acyl-CoA synthetase enzymes comprise twenty-six members which are differentially regulated and display distinct patterns of tissue expression, preferred substrates, and subcellular localization (Ellis et al. 2010). Acsls activate long chain fatty acid species by catalyzing a two-step, ATP dependent reaction that results in the ligation of CoA to a fatty acid to produce a fatty acyl-CoA (Mashek, Li, and Coleman 2007; Lopes-Marques et al. 2018; Steinberg et al. 2000). Long chain fatty acyl-CoA species can then go on to participate in a number of cellular processes. For example, fatty acyl-CoAs can enter the mitochondria through the carnitine shuttle, where they undergo beta-oxidation to generate acetyl CoA to fuel the TCA cycle. Ultimately, this leads to the generation of ATP through oxidative phosphorylation. In addition to energy production, fatty acyl-CoAs can be directed to anabolic processes, like the synthesis of phospholipids, triacylglycerols and cholesterol, as well as post-translational acylation and transcriptional regulation (Grevengoed, Klett, and Coleman 2014) (Figure 5.1.1).

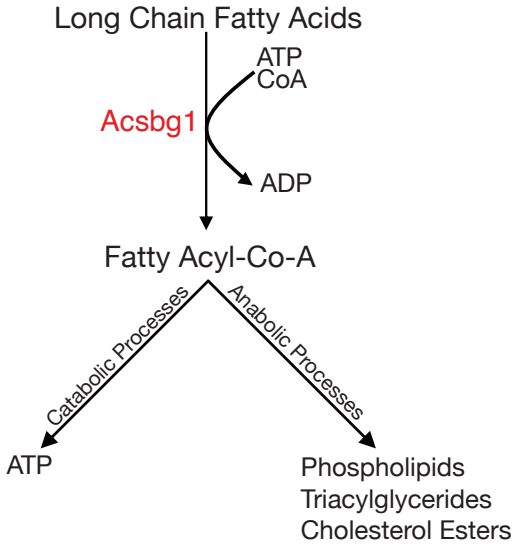

Figure 5.1.1 Schematic depicting the activation of long chain fatty acids by Acsbg1 and potential fates of fatty acyl-CoA species.

Acsbg was first described in Drosophila melanogaster, and flies with mutations in Acsbg have elevations in very-long chain fatty acids and display evidence of neurodegeneration (Steinberg et al. 2000). The mammalian homolog, Acsbg1, was identified in both human and mouse and is highly expressed in brain and steroidogenic tissues. Acsbg1 activates long and very long chain fatty acids in neuronal cells, and *in vitro,* Acsbg1 deletion leads to decreased fatty acid beta oxidation (Pei et al. 2003). Similar to drosophila mutants, whole body Acsbg1 knock-out mice have increased levels of some long chain fatty acids in testes, ovaries, and brain, and mutations in Acsbg1 have been implicated in the pathogenesis of the neurodegenerative disease, X-linked adrenoleukodystrophy (X-ALD) (Sheng et al. 2009).

Acsbg1 expression has been linked to human breast cancer in a study that examined the gene expression of breast cancers compared to normal mammary tissue in a small cohort of 84 women (Makoukji et al. 2016). However, the mechanistic role of Acsbg1 in promoting tumorigenesis or cancer progression has not been studied. Interestingly, other long chain acyl-CoA synthetase enzymes have described roles in promoting tumorigenesis in several cancer types, including breast cancer. Acyl-CoA Synthetase 4 (Acsl4), for example, has been associated with colon, prostate, breast, and liver cancers (Cao et al. 2001; Maloberti et al. 2010; Monaco et al. 2010; Young et al. 2007; Sung et al. 2003). High expression of Acsl4 has been shown to promote colon cancer progression by inhibiting apoptosis, and in hepatocellular carcinoma, Acsl4 overexpression led to increased cell proliferation (Young et al. 2007; Cao et al. 2001). Furthermore, the administration of triacsin C, a potent inhibitor of Acsl enzymes, induces cancer cell death *in vitro* and limits tumor progression in human xenograft models of lung cancer (Mashima et al. 2005; Tomoda et al. 1991). These studies support a potential role of long chain acyl-CoA synthetase activity in promoting tumor progression. Therefore, we hypothesize that the obesity-specific upregulation of Acsbg1 in breast cancer cells identified in Chapter 4 may represent one mechanism by which breast cancer is accelerated in obesity. The work presented in this chapter is aimed at understanding whether Acsbg1 upregulation in obesity contributes to obesity-accelerated tumor progression. Furthermore, we employ metabolomic and lipidomic approaches to assess the cellular function of Acsbg1 in tumors from obese mice.

5.2 Generating a stable mE0771 cell line overexpressing Acsbg1.

Acsbg1 was robustly upregulated in E0771 breast cancer cells isolated from obese compared to lean animals (Chapter 4). We hypothesize that Acsbg1 upregulation may contribute to enhanced tumor growth in obesity by facilitating the activation of long chain fatty acids for energy production and by producing phospholipids and other essential lipid-containing species to support the accumulation of biomass. To test whether enhanced Acsbg1 expression can potentiate tumor growth in obesity *in vivo*, we used a lentiviral approach to produce mE0771 cells which stably overexpress Acsbg1 or LacZ control. We transduced mE0771 cells with a construct obtained from a commercially available lentiviral gain-of-function expression library (X. Yang et al. 2011). The Acsbg1 gene was cloned into the pLX304-Blasticidin V5 vector, resulting in V5-tagged Acsbg1 protein. We selected infected cells with blasticidin to produce a stable population of Acsbg1 overexpressing cells, then confirmed Acsbg1 overexpression by Western blot (Figure 5.2.1 A).

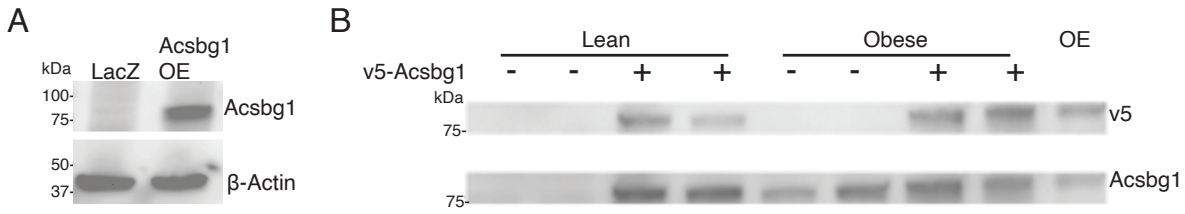

Figure 5.2.1 Western blot of E0771 cells stably expressing LacZ control or Acsbg1.

A. Immunoblot of E0771 cells that stably overexpress Acsbg1 *in vitro.* B. Immunoblot of V5 or Acsbg1 in lean or obese tumors from a pilot experiment. OE represents cultured Acsbg1 overexpressing mE0771 cells.

We then used mE0771 LacZ or Acsbg1 overexpressing cells in a pilot orthotopic experiment, similar to those described in Chapter 4, in which we implanted 50,000 cells per animal into lean or obese female B6 mice. We confirmed that Acsbg1 protein is overexpressed via immunoblot of bulk, homogenized tumors at endpoint. We distinguished the endogenous Acsbg1 from the exogenous protein by using antibodies specific for either the V5 tag or the Acsbg1 protein (Figure 5.2.1 B). As we have observed in Chapter 4, obesity induces Acsbg1 expression in control cells, and we can detect V5-tagged Acsbg1 in both lean and obese tumors from stable Acsbg1 cells. Importantly, there is no V5 signal in the LacZ control tumors.

Next, we implanted control or Acsbg1 overexpressing (Acsbg1 OE) cells into a second cohort of lean or obese animals. Importantly, the obese animals weighed significantly more than lean, with no difference in weight between the animals that received control or Acsbg1 OE cells (Figure 5.2.2 A) Tumors were larger in obese animals compared to lean, and cells that overexpress Acsbg1 formed tumors that were significantly larger than the control cells in obesity (Figure 5.2.2 B). There was no significant difference in tumor volume between the Acsbg1 OE and control tumors in lean animals, indicating that the role of Acsbg1 in potentiating tumor growth is specific to obesity.

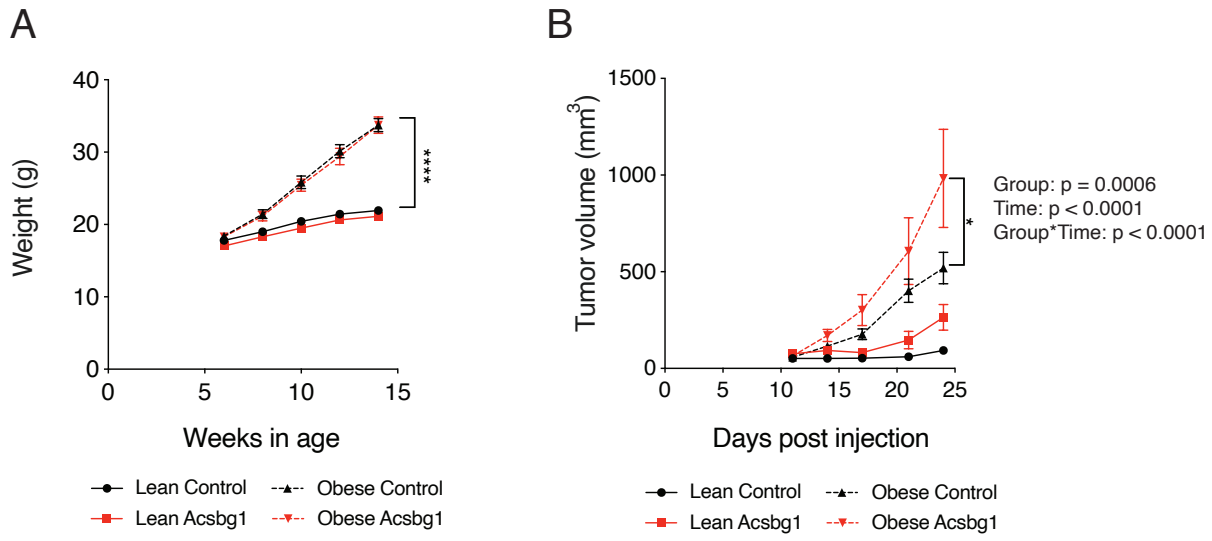

Figure 5.2.2 mE0771 progression is accelerated in obesity with Acsbg1 overexpression.

A. Body weights of animals fed a chow or high fat diet prior to injection (n=9-12 per group). B. Longitudinal tumor volume of control or Acsbg1 overexpressing tumors in lean or obese animals, measured with external calipers (n=9-12 per group). Data are presented as mean +/- standard error of the mean (SEM). **** $p<0.0001$. For panel B, group, time, and group by time p-values are denoted in the figure. *$p<0.05$ by post-hoc analysis at the final time point.

5.3 Acyl-CoA synthetase activity is required for obesity-accelerated breast cancer

The data we generated with Acsbg1 gain-of-function in mE0771 cells suggest that overexpression of this enzyme may be sufficient to enhance obesity-accelerated tumor growth. We were next interested in assessing whether Acsbg1 upregulation is required for obesity-accelerated tumor growth. We used a lentiviral approach to produce a stable mE0771 cell line that expresses a short hairpin targeting Acsbg1 (Acsbg1 KD). After lentiviral transduction, we used puromycin to select for a stable population of cells which express the Acsbg1-specific short hairpin. Importantly, Acsbg1 is not expressed by mE0771 cells *in vitro*, so we confirmed the efficacy of the short hairpin via qPCR of tumors produced by these cells *in vivo* (Figure 5.3.1 A).

We implanted Acsbg1 KD or control cells into lean or obese animals and followed tumor growth longitudinally. Importantly, the obese animals were significantly heavier than the lean, with no differences in body weight among the obese groups (Fig. 5.3.1 B) There was no significant difference in tumor volume between tumors that express a scrambled control or those expressing a short hairpin targeting Acsbg1 in lean or obese animals (Figure 5.3.1 C). This suggests that Acsbg1 expression alone is not required for obesity-dependent acceleration of tumor growth in this model. However, Acsbg1 is a member of a large class of enzymes with redundant roles, so we hypothesized that one or several other Acsl enzymes might compensate for the loss of Acsbg1 activity in Acsbg1 deficient cells. Interestingly, the expression of Acsl1, Acsl 3 and Acsl 4 all trended upward when Acsbg1 was knocked down in mCherry sorted cells (Figure 5.3.1 D). Of note, these enzymes were not upregulated by obesity in the mE0771 cells that we analyzed in our RNA sequencing experiments (Chapter 4).

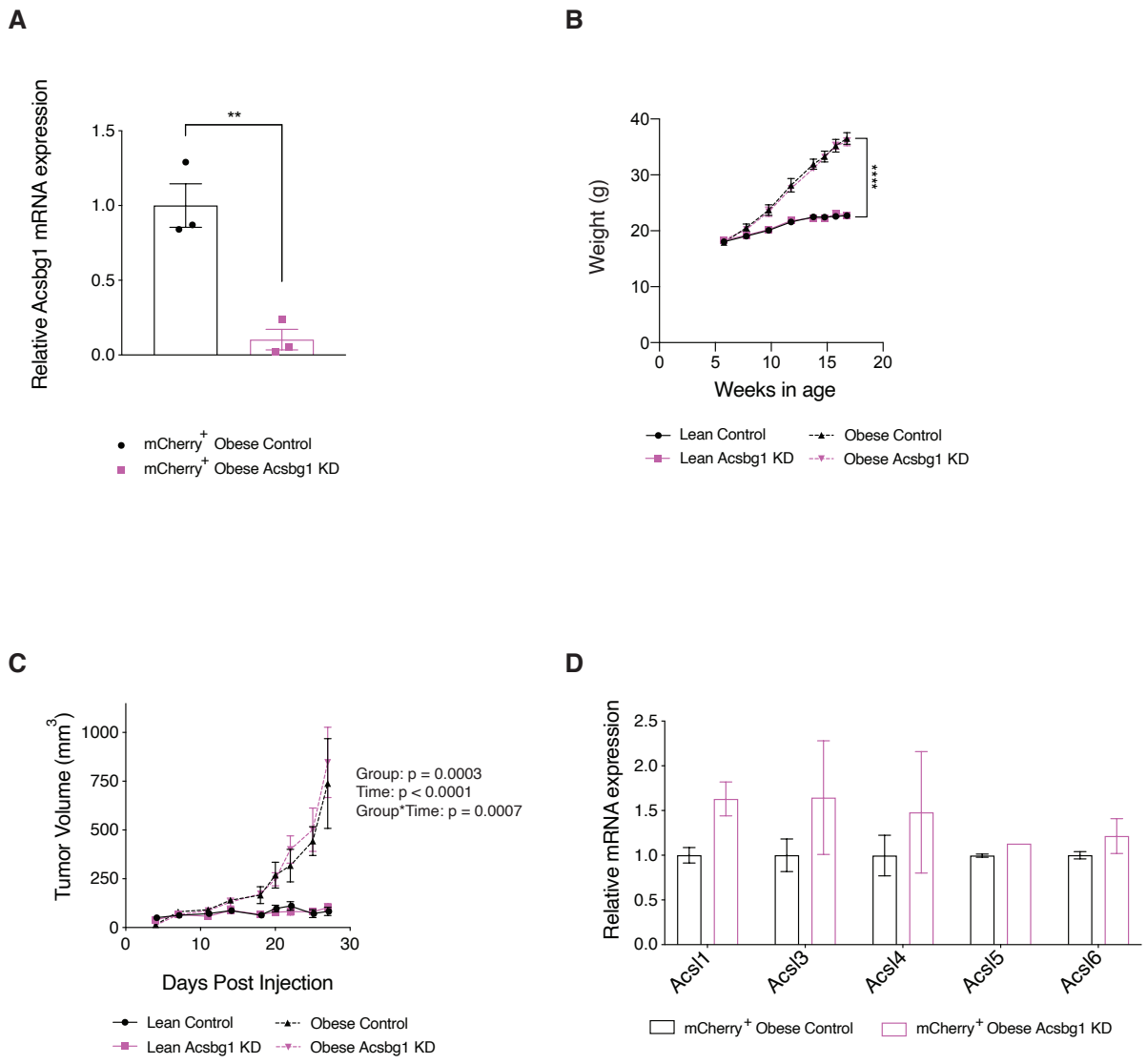

Figure 5.3.1 Acsbg1 knockdown does not attenuate obesity-driven tumor growth.

A. Acsbg1 expression by RT-qPCR of control or Acsbg1 KD tumors (n=3 tumors per group). B. Body weights of B6 animals on chow or HFD. (n=8-10 animals per group). C. Tumor volumes of control or Acsbg1 KD tumors in lean or obese animals (n=8-10 animals per group). D. RT-qPCR comparing the relative expression of long chain fatty acyl coA isoforms in mCherry positive cells isolated from control or Acsbg1 deficient tumors in obese animals. Data shown here represent mean +/- standard error of the mean (SEM). ** $p<0.01$, ****$p<0.0001$. For panel C, group, time, and group by time p-values are denoted in the figure.

We therefore employed a pharmacologic approach to test whether Acsbg1 activity may be compensated for by other acyl-CoA synthetase enzymes. We repeated the previous

experiment, but in addition to implanting control or Acsbg1 KD cells, we also treated animals with vehicle or triacsin C, a potent inhibitor of acyl-CoA synthetase activity (Figure 5.3.2 A) (Mashima et al. 2005; Tomoda et al. 1991). We administered triacsin C three times per week to achieve a dose of 2 mg/kg/week beginning on day 7 after implantation, when the tumors were palpable but not significantly different in volume. This treatment did not cause weight loss or other signs of toxicity (Figure 5.3.2 B). Neither Acsbg1 knockdown nor triacsin C treatment alone was sufficient to attenuate obesity-driven tumor growth. However, when tumors were deficient in Acsbg1 and animals were also treated with triacsin C, obesity-driven tumor progression was significantly attenuated (Figure 5.3.2 C). This suggests that other acyl-CoA synthetase enzymes can compensate for Acsbg1 activity when it is inhibited. Together, these findings support that acyl-CoA synthetase activity, preferentially through Acsbg1 but compensated for by other enzyme homologues, is required for obesity-driven tumor progression.

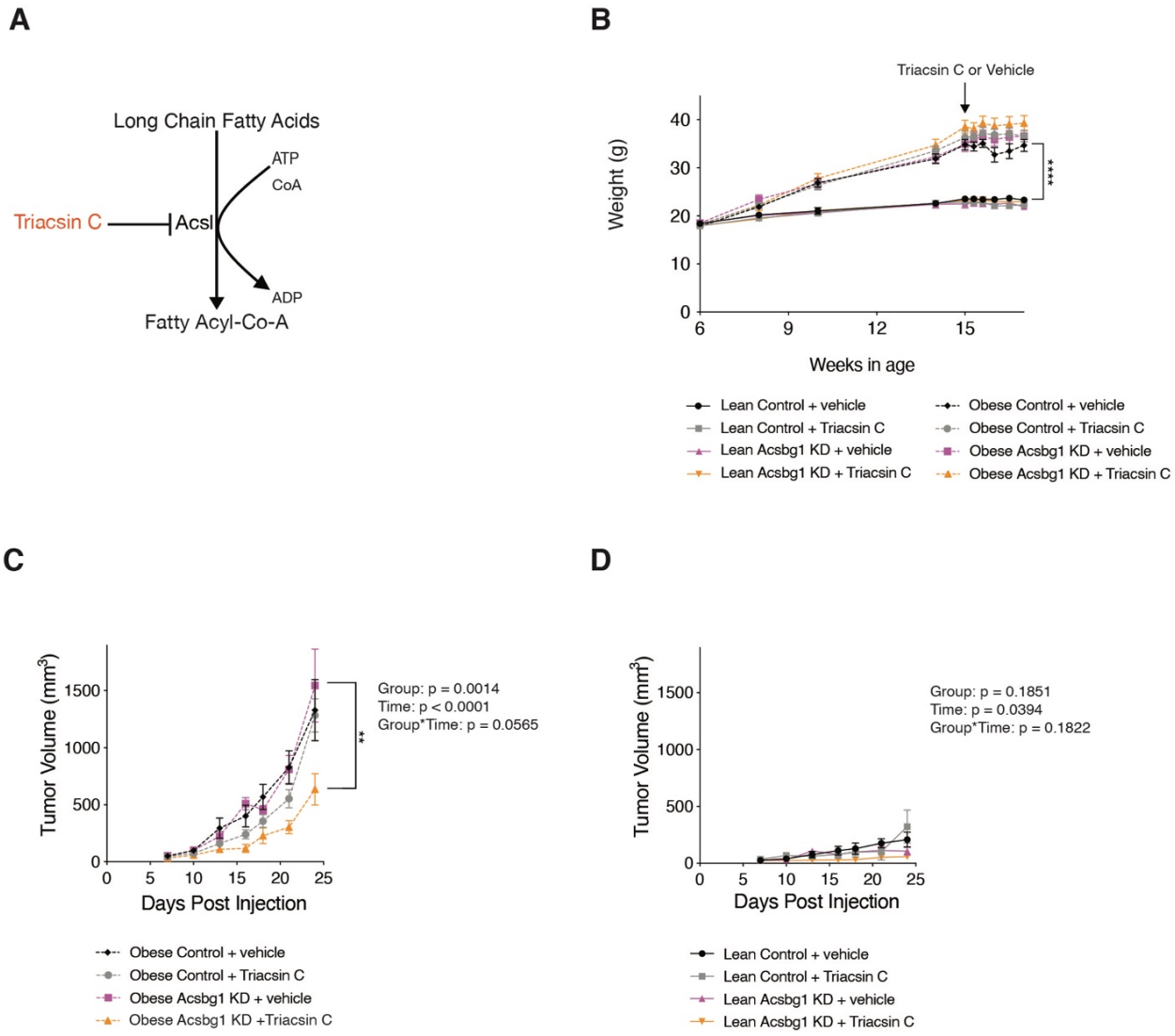

Figure 5.3.2 Acsbg1 knockdown with acyl-CoA synthetase inhibition attenuates obesity-driven tumor progression.

A. Schematic depicting the function of triacsin C. B. Body weights of animals fed chow or HFD (n=3-7 per group). C. Longitudinal tumor progression in obese animals with control or Ascsbg1 KD tumors, treated with vehicle or triacsin C (n=3-4 per group). D. Tumor progression in lean animals with control or Ascsbg1 KD tumors, treated with vehicle or triacsin C (n=4-7 per group). Data shown here represent mean +/- standard error of the mean (SEM). ** $p<0.01$, **** $p<0.0001$ For panels C and D, group, time, and group by time p-values are denoted in the figure. **$p<0.01$ by post-hoc analysis at the final time point

5.4 Obese Acsbg1 overexpressing tumors have altered metabolism.

Our *in vivo* data revealed that mE0771 cells which overexpress Acsbg1 form significantly larger tumors in obese animals. We hypothesized that Acsbg1 overexpression may potentiate

tumor growth by enhancing the ability of cancer cells to charge fatty acid species to act as substrates for beta oxidation. This would ultimately increase flux through the citric acid cycle to produce ATP through oxidative phosphorylation. We therefore assessed whether Acsbg1 overexpressing cells confer an energetic advantage *in vitro*. We started by using the Cell Titer Glo kit to determine the relative amounts of ATP produced by control or Acsbg1 OE mE0771 cells. In this system, cellular ATP is used as a substrate for luciferase enzymatic activity. Since ATP is required for bioluminescence, light measured by a plate reader is directly proportional to the amount of ATP contained in a cellular sample. Importantly, Cell Titer Glo is often used as an indicator of cell number, so it was essential to first determine whether Acsbg1 OE cells confer a proliferation advantage over control cells under basal conditions *in vitro*. We plated equal numbers of control or Acsbg1 OE cells and counted live cells by trypan blue exclusion at 24, 48, and 72 hours after plating. Acsbg1 OE cells did not promote increased proliferation under basal cell culture conditions (Figure 5.4.1 A). Despite no difference in cell number, after 24 hours, Acsbg1 overexpressing cells had increased ATP content as measured by luminescence (Figure 5.4.1 B).

Cells can generate ATP through mitochondrial oxidative phosphorylation or glycolysis. To determine the pathway through which ATP is produced by Acsbg1 OE cells, we utilized plate based respirometry to continuously measure the oxygen consumption rate (OCR) and extracellular acidification rate (ECAR) of control or Acsbg1 OE cells (Nadanaciva et al. 2012; Mookerjee et al. 2015). Specifically, OCR measures oxygen-dependent mitochondrial respiration, and the mitochondrial stress test is designed to assess the components of mitochondrial respiration by sequentially inhibiting complexes of the electron transport chain. The first step of the mitochondrial stress test is oligomycin treatment, which inhibits ATP synthetase. The decrease in OCR observed after oligomycin treatment represents cellular ATP production. Carbonyl cyanide-4 phenylhydrazone (FCCP) collapses the proton gradient across the mitochondrial membranes, allowing uninhibited electron flow through the electron transport chain. This results in enhanced OCR that reflects maximum mitochondrial respiration. Finally, rotenone and antimycin A are co-administered to inhibit complexes I and III to completely inhibit the electron transport chain. Any remaining oxygen consumption after the administration of rotenone and antimycin A represents non-mitochondrial respiration (Agilent Technologies, 2019).

We performed mitochondrial stress tests on Acsbg1 control and overexpressing cells *in vitro* and found that Acsbg1 overexpressing cells had increased ATP production, basal respiration, and maximal respiration (Figure 5.4.1, C-F) compared to control. This indicates that Acsbg1 overexpression increases flux through the electron transport chain, supporting our hypothesis that Acsbg1 activity ultimately produces energy by promoting mitochondrial respiration. We also performed glycolysis stress tests, which measure changes to ECAR in response to treatment with compounds designed to assess glycolytic activity. First, glucose is administered to activate glycolysis, which leads to an increase in ECAR. Next, oligomycin is administered to inhibit mitochondrial ATP production, shifting all energy production to glycolysis and enhancing ECAR. This represents maximal glycolytic capacity. Finally, a glucose analog, 2-deoxyglucose (2-DG) is administered to block glycolysis by competitively inhibiting hexokinase. Any extracellular acidification measured after the administration of 2-DG represents non-glycolytic acidification (Agilent Technologies, 2017). There was no difference in glycolysis or glycolytic capacity between Acsbg1 OE and control cells, further supporting the notion that

the differences in ATP that were measured under basal conditions were dependent on mitochondrial respiration and independent of glycolysis (Figure 5.4.1 G).

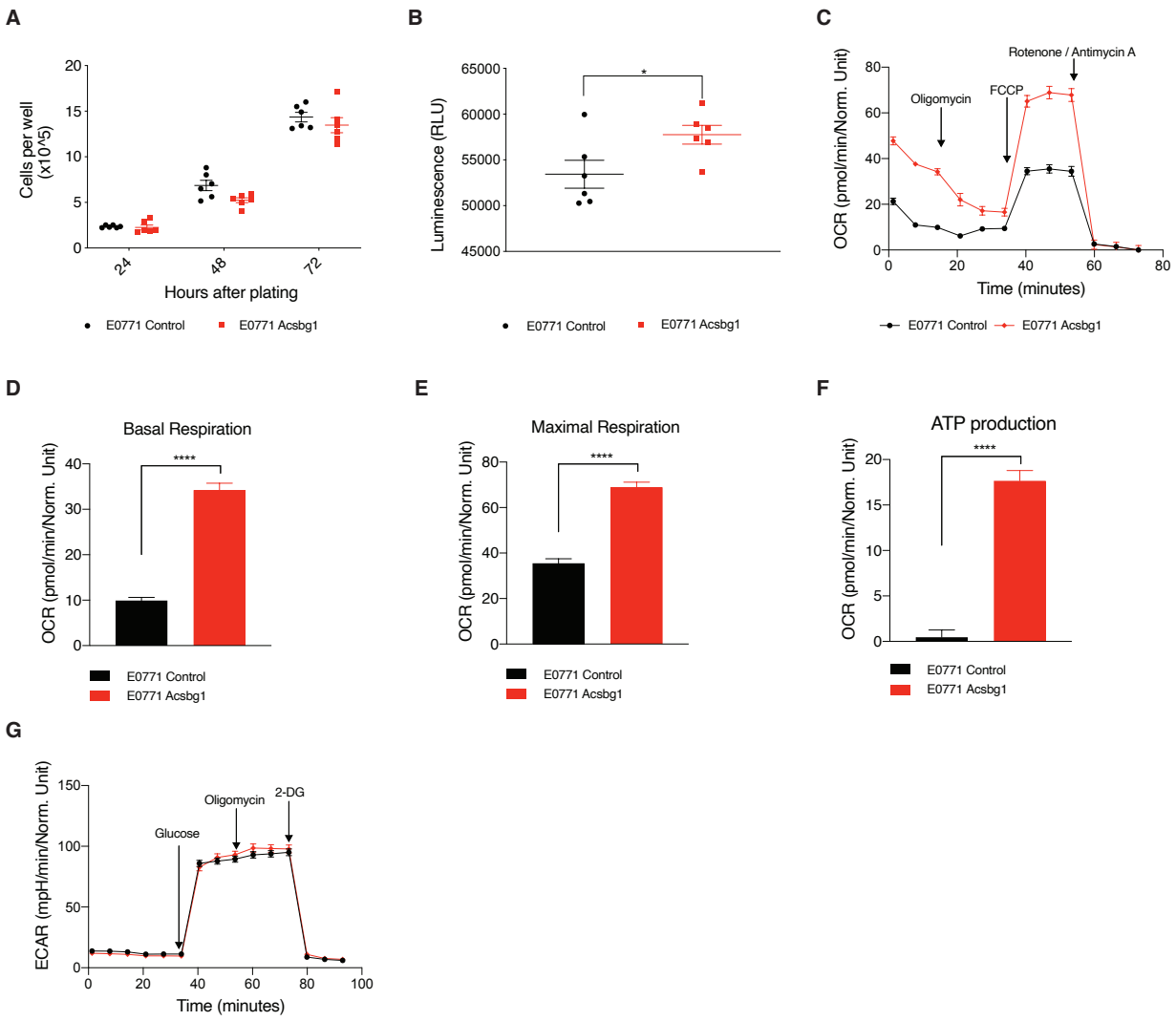

Figure 5.4.1 *In vitro*, Acabg1 overexpressing cells have increased ATP compared to control cells via oxidative phosphorylation, not glycolysis.

A. Cell number per well under basal *in vitro* conditions. B. Luminescence measured using the Cell Titer Glo kit. C. Mitochondrial stress testing of control or Acsbg1 overexpressing cells (n=10 wells per condition) D. quantification of basal respiration from C. E. Quantification of maximal respiration from C. F. Quantification of ATP production from C. G. Glycolysis stress testing of control or Acsbg1 overexpressing cells. *p<0.05, **** p<0.0001.

To comprehensively explore Acsbg1-dependant regulation of breast cancer metabolism, we next performed targeted, polar metabolomic analysis of control or Acsbg1 overexpressing tumors from lean or obese animals. We homogenized bulk tumors and extracted polar metabolites for analysis by liquid-chromatography mass spectroscopy (LC-MS) (Garcia-Bermudez et al. 2018). 180 unique polar metabolites were detected using this technique.

We performed principal component analysis of the metabolites identified in this experiment. As expected, tumors from lean or obese animals clustered separately, indicating that obesity can remodel the metabolome of these tumors. Of note, Acsbg1 OE tumors clustered separately from the control tumors in obesity but overlapped in the lean groups. We performed pathway enrichment analysis of the differentially abundant metabolites using MBROLE (López-Ibáñez, Pazos, and Chagoyen 2016). Interestingly, the pathways which were differentially regulated with Acsbg1 overexpression in obesity, which included purine metabolism and the urea cycle, were distinct from the pathways regulated by obesity alone or by Acsbg1 overexpression in lean animals. These results, along with our previous finding that Acsbg1 modulation has no effect on tumor volume in lean animals, strongly supports our hypothesis that Acsbg1 has an obesity-specific role in promoting tumor progression (Figure 5.2.2 B and Figure 5.4.2 A-C).

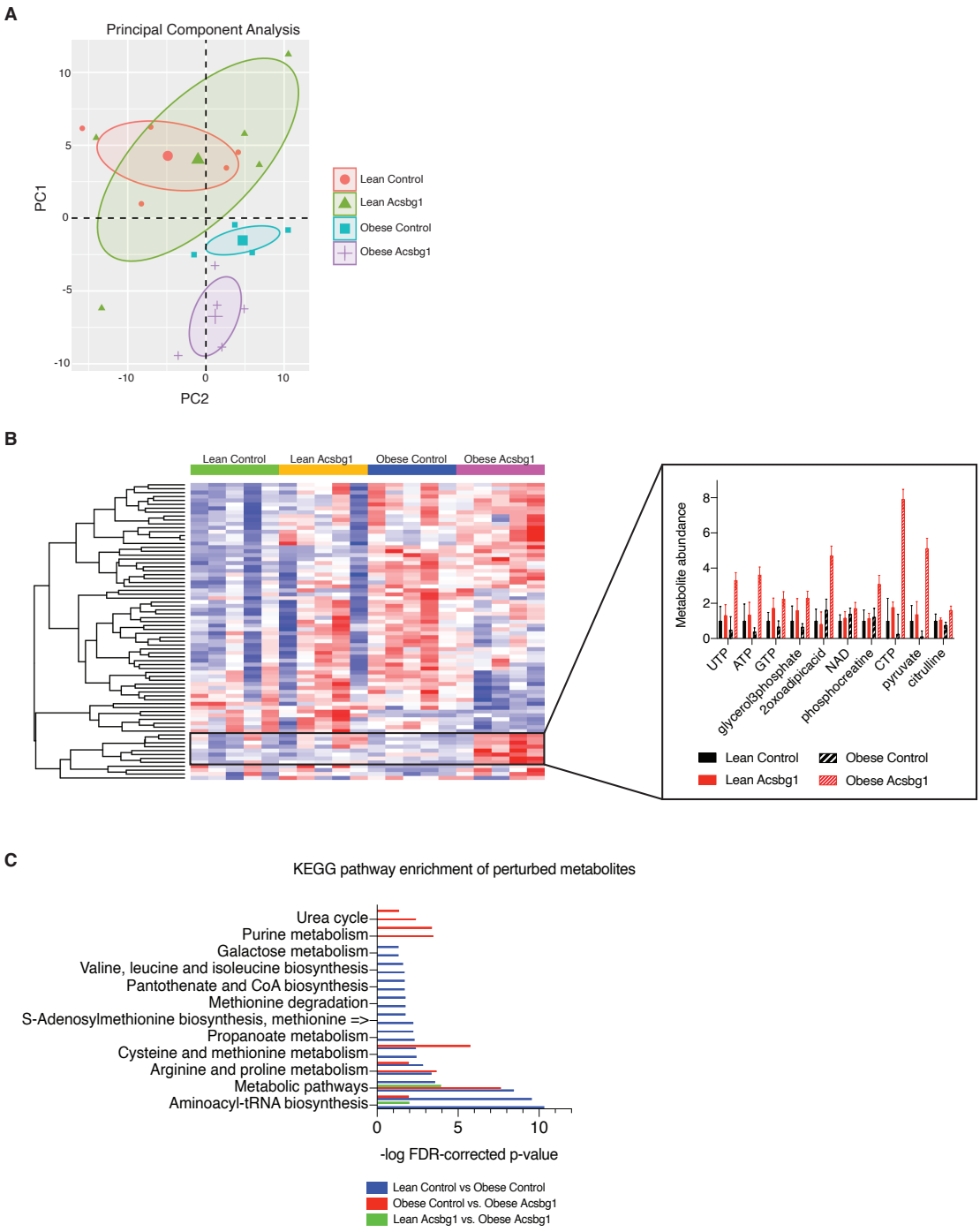

Figure 5.4.2 Acsbg1 overexpression reprograms the cellular metabolome in an obesity-specific manner.

A. Principal component analysis comparing the metabolomes of control or Acsbg1 overexpressing tumors from lean or obese animals. B. Heatmap depicting the abundance of metabolites in Acsbg1 overexpressing or control tumors in lean or obese animals ($p<0.05$). C. Pathway enrichment analysis of significantly dysregulated metabolites from pairwise comparisons as labeled using MBROLE (p-value < 0.05).

We examined the specific metabolites which were significantly modulated in obese Acsbg1 overexpressing tumors compared to control. In support of our previous *in vitro* findings, ATP was more abundant in Acsbg1 OE tumors from obese animals compared to control. This confirms that Acsbg1 overexpression leads to enhanced energy production *in vivo*. Furthermore, all of the nucleotide triphosphates as well as phosphocreatine were more abundant in the Acsbg1 OE tumors, suggesting that Acsbg1 overexpression has an important effect on high-energy phosphate pools (Fig. 5.4.2 B). Notably, glycerol-3-phosphate (G3P), an essential intermediate in phospholipid synthesis, was significantly more abundant in Acsbg1 overexpressing tumors in obese animals (Figure 5.4.2 B) (Yamashita et al. 2014). This suggests that Acsbg1 may play a role in lipid metabolism, which will be examined later in the chapter.

We were particularly interested in understanding the potential role of phosphocreatine in the mechanism by which Acsbg1 promotes obesity-accelerated breast cancer. In muscle, a creatine kinase/phosphocreatine circuit has been described, whereby creatine is interconverted with phosphocreatine in juxtaposition with ATP/ADP interconversion, a reaction mediated by creatine kinase. This process can produce ATP in times of metabolic stress, like hypoxia, when energy demand outpaces the ability of cells to generate ATP through the canonical means (Bessman 1985; Kazak et al. 2015). Previous studies by our group have identified a crucial role of adipose tissue derived creatine in driving obesity-accelerated cancer growth in the E0771 orthotopic tumor model. Furthermore, we have previously shown that blocking creatine import by knocking down the creatine transporter, Solute Carrier Family 6 member 8 (Slc6a8), in E0771 cells can abrogate obesity-driven tumor growth (Ackerman 2020). Importantly, Slc6a8 expression is upregulated in Acsbg1 overexpressing tumors compared to control in obese animals (Figure 5.4.3 A). These findings led us to hypothesize that Acsbg1-dependent tumor progression may require exogenous creatine.

To test whether Acsbg1-dependent tumor progression in obesity requires exogenous creatine, we further modified Acsbg1-OE cells to also express a short hairpin that targets the creatine transporter, Slc6a8. We implanted these cells into lean or obese animals. All of the obese animals were significantly heavier than the lean, with no differences among the obese groups (Figure 5.4.3 B). As we have previously demonstrated, cells overexpressing Acsbg1 produced tumors that were larger than controls, and blocking creatine transport through Slc6a8 attenuated Acsbg1-dependent growth in obesity (Fig 5.4.3 C). These data suggest a role for exogenous creatine in Acsbg1 dependent tumor progression.

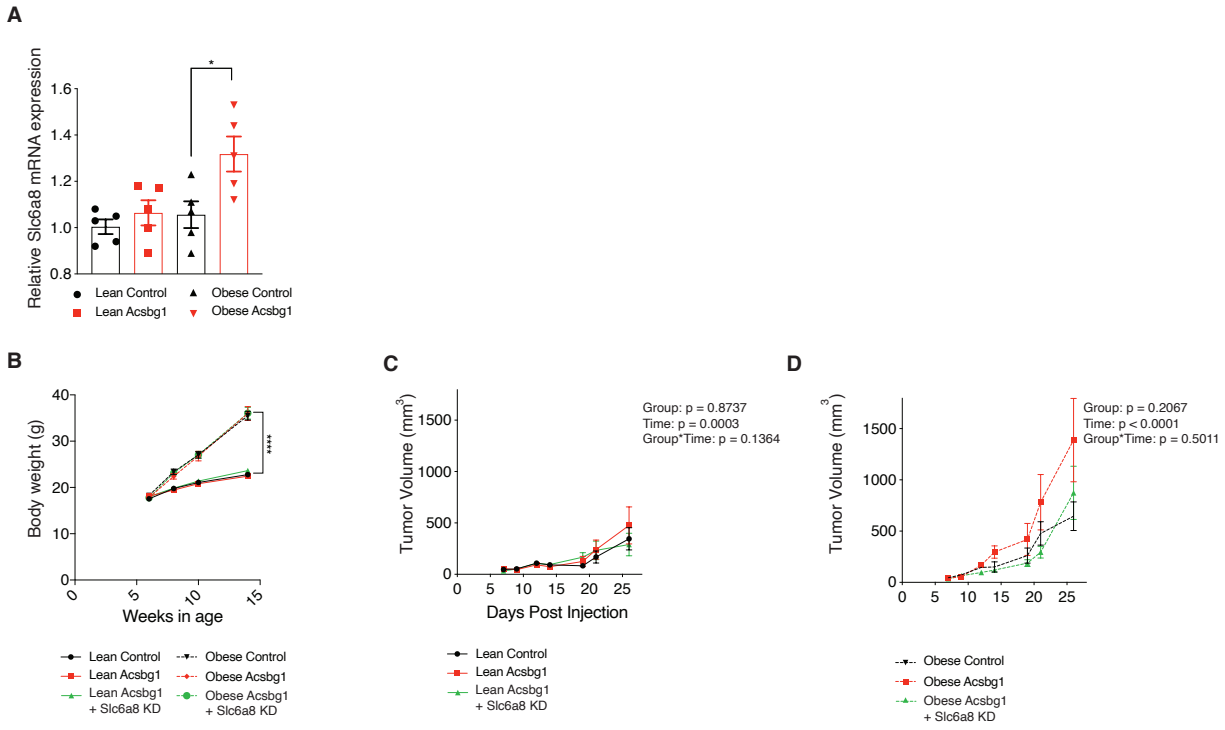

Figure 5.4.3 The import of exogenous creatine may promote Acsbg1 dependent tumor growth.

A. Relative mRNA expression of Slc6a8 in lean or obese control or Acsbg1 overexpressing tumors (n=5 tumors per group). B. Body weights of animals fed a chow or high fat diet prior to injection (n=5-9 animals per group). C. Tumor volume of lean animals measured with external calipers (n=8-9 animals per group). D. Tumor volume of obese animals measured with external calipers (n=5-7 animals per group). Data are presented as mean +/- standard error of the mean (SEM) For panels C and D, group, time, and group by time p-values are denoted in the figure. *p<0.05, ****p <0.0001.

These findings suggest a mechanism in which cancer cells in the obese microenvironment upregulate Acsbg1, which promotes ATP production through oxidative phosphorylation as well as enhanced import of creatine from the microenvironment through Slc6A8. Increased intracellular concentrations of both ATP and creatine support the production of phosphocreatine, which may promote tumor progression by ensuring a means to maintain anabolic processes (Figure 5.4.4).

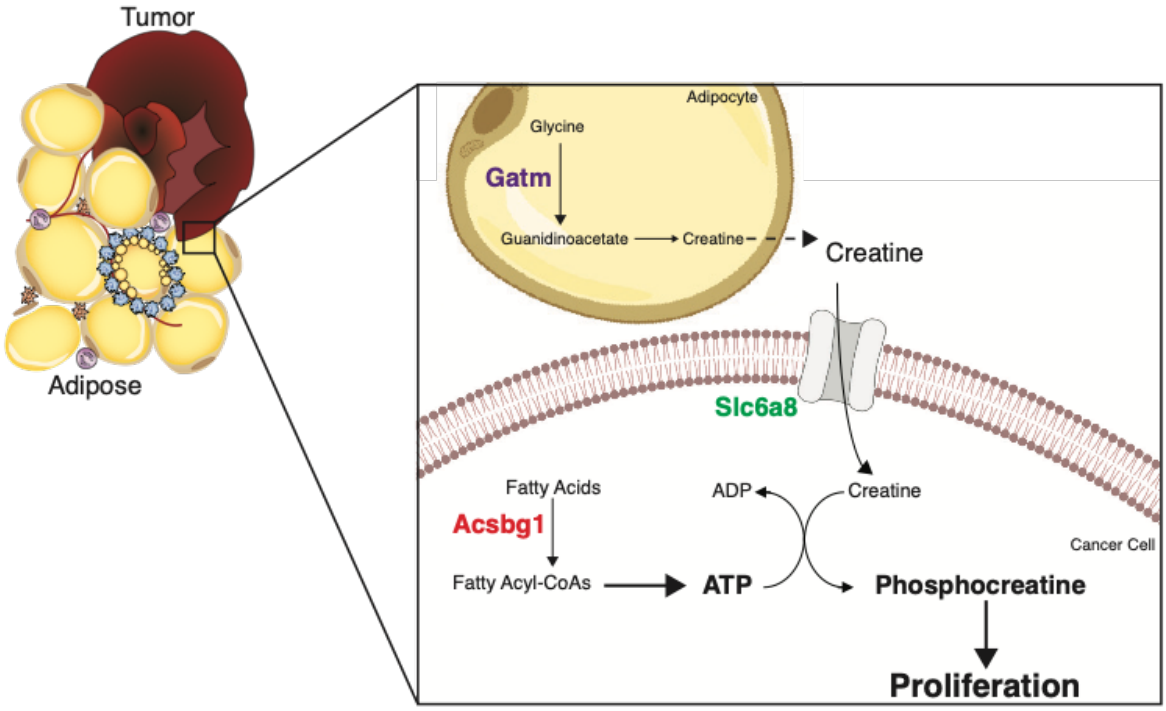

Figure 5.4.4 Schematic of a proposed mechanism by which exogenous, adipocyte-derived creatine may support Acsbg1 dependent tumor growth.

5.5 Analyzing the effects of Acsbg1 overexpression on lipid metabolism in tumors from lean and obese animals.

Based on the previously reported function of Acsbg1 as a long-chain fatty acyl-CoA synthetase, we hypothesize that the increase in ATP production through oxidative phosphorylation we described in the previous section may be dependent on enhanced lipid metabolism. To test this hypothesis, we analyzed tumors derived from Acsbg1 overexpressing or control mE0771 cells that were orthotopically implanted into lean or obese animals. We isolated RNA from these samples and used RT-qPCR to assess the relative expression of a panel of enzymes involved in lipid metabolism, including lipid oxidation. Many genes involved in lipid oxidation were significantly upregulated with Acsbg1 overexpression in obesity (Figure 5.5.1). These data reveal that elevated Acsbg1 fatty acyl-CoA activity may promote lipid oxidation, in part by upregulating the mRNAs of enzymes required to process fatty-acyl-CoA species for energy production.

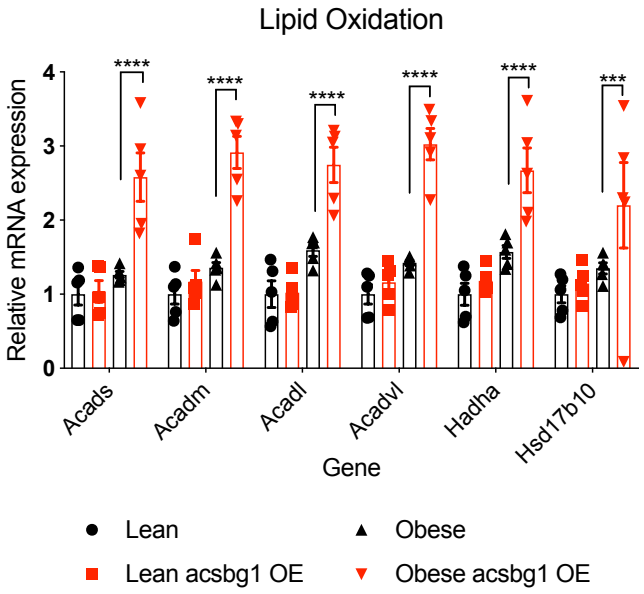

Figure 5.5.1 qPCR of genes related to lipid oxidation.

Data are displated as mean relative mRNA expression (n=5 tumors per group) Data represent mean relative expression +/- standard error of the mean (SEM). ***p<0.001, ****p<0.0001.

In addition to assessing the effects of Acsbg1 on energy production, we were interested in identifying possible substrates and products of Acsbg1 as well as the fates of Acsbg1-charged fatty acyl species. We performed unbiased lipidomic profiling on bulk tumors isolated from control or Acsbg1 overexpressing tumors from lean or obese animals using LC-MS. We filtered our results to only include lipid species which had a background signal less than 20% of the pooled mean signal. 3,344 distinct lipid species were detected by LC-MS that met this criterion. We then filtered these data to identify species with a coefficient of variance below 30% for each group. This reduced our list of candidates to 844 species. The most abundant classes of lipids detected were plasma membrane species, like phosphatidylcholines and phosphatidylethanolamines. Cholesterol esters and sphingomyelin species were detected at low levels. Importantly, acyl-CoA species, which are the direct products of acyl-CoA synthetase enzymes like Acsbg1, cannot be detected by this method (Table 5.5.1).

Table 5.5.1 List of lipid classes detected by LC-MS.

Class	#Lipids detected
Phosphatidylcholine	254
Phosphatidylethanoamine	153
Lysophosphatidylcholine	63
Triacylglycerols	56
Diacylglycerols	51
Acyl Carnitines	40
Phosphatidylglycerols	40
Sphingomyelin	37
Phosphoitidylnositols	36
Phosphotidylserines	27
Ceramides	24
Lysophosphatidylethanol	12
Monoacylglycerols	10
phSM	10
Cholesterol Esters	9
Hex1Ceremides	8
Hex2Ceremides	5
Hex3Ceremides	3
SPH	2
Coenzyme	2
Anandamide	1
Phosphatidylmethanol	1

We then used principal component analysis to assess the overall lipidomic landscape of the samples. As expected, samples isolated from lean animals of both groups were distinct from the obese samples. When we analyzed the significantly modulated lipids by heatmap, most lipid species were downregulated by obesity and few were modulated by Acsbg1 expression (Figure 5.5.2).

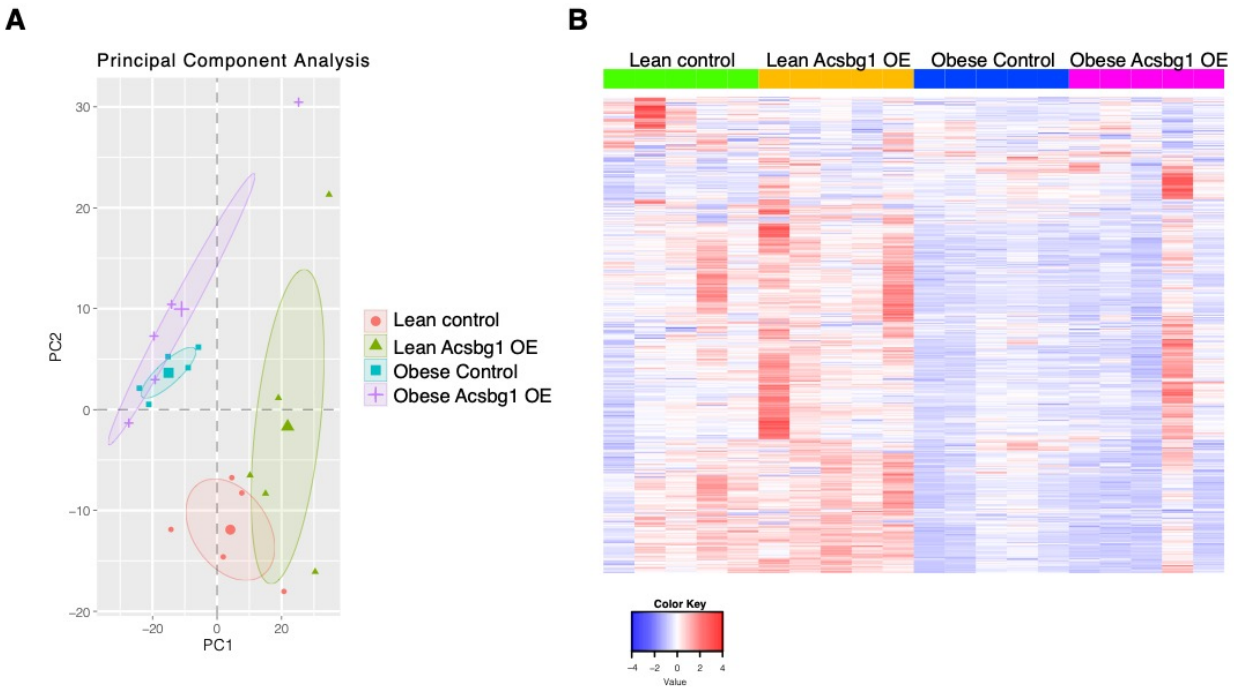

Figure 5.5.2 Lipid species differentially regulated in obese Acsbg1 overexpressing tumors compared to control.

A. Principal component analysis of the lipids identified by unbiased lipidomics in control or Acsbg1 OE tumors in lean or obese animals. B. Heatmap of significantly modulated lipids.

We next analyzed the degree of saturation of the lipid species that were significantly regulated by Acsbg1 overexpression in obesity compared to control tumors. The polyunsaturated fatty acid species were most highly modulated, being both up and downregulated by Acsbg1 overexpression (Figure 5.5.3).

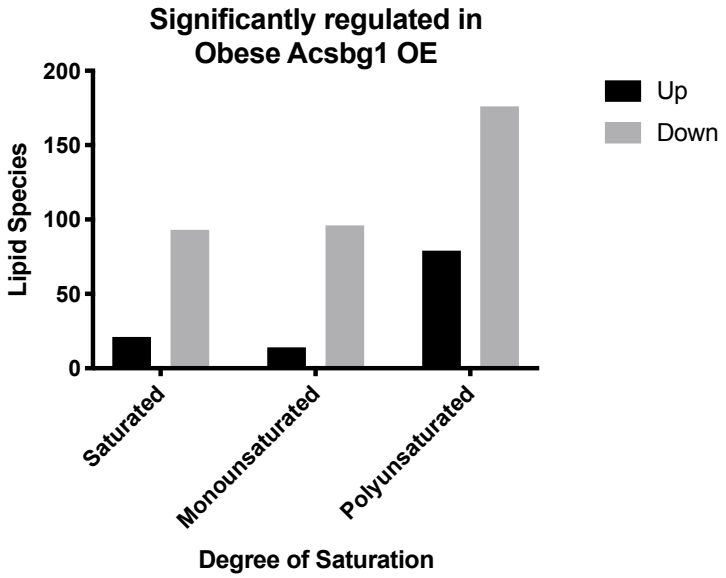

Figure 5.5.3 Polyunsaturated fatty acid species were most differentially modulated in Acsbg1 OE tumors compared to control in obesity .

Data represent the number of species in each category which were significantly different ($p<0.5$) in Acsbg1 overexpressing tumors compared to control in obese animals. The direction of change is indicated by the color of the bar.

Since there were relatively few overall changes in lipid abundance based on Acsbg1 expression, we moved from a global approach to a more targeted approach by examining specific lipid classes and species that were modulated by Acsbg1 in obesity. Acyl-CoA species are the immediate downstream product of acyl-CoA synthetase enzymes, like Acsbg1. However, these species were not detected in any of the samples by our mass spectrometry method. This likely represents a technical limitation of the lipid isolation and detection methods of this study rather than a biological finding. We hypothesize that one important fate of these acyl-CoA species charged by Acsbg1 is transport into the mitochondria through the carnitine shuttle. Carnitine palmitoyltransferase I (Cpt1) converts acyl-CoAs to acyl-carnitine species as they are transported through the outer and inner mitochondrial membranes (Qu et al. 2016). Acyl-carnitine species were detected in this analysis, so we used these to infer the types of lipid species that may be regulated by Acsbg1 activity.

The acyl-carnitine species that were significantly upregulated by Acsbg1 expression were 20:4 and 22:4 species (Figure 5.5.4). The major 20:4 unsaturated lipid species found in nature is arachidonic acid, an omega-6 polyunsaturated fatty acid. The major 22:4 polyunsaturated species found in nature is docosatetraenoic acid, commonly called adrenic acid, another omega-6 polyunsaturated fatty acid. Both arachidonic and adrenic acid are downstream of linoleic acid metabolism: linoleic acid can be desaturated to form arachidonic acid, which is then elongated to produce adrenic acid. Importantly, dietary linoleic acid, an essential fatty acid, represents more than 28% of the lipid in the standard obesogenic, high fat diet fed to these animals (Research Diets D12492). Linoleic acid is the most commonly consumed polyunsaturated fatty acid in human diets (Whelan and Fritsche 2013). It is the major fatty acid species in soybean oil, a common additive in fried and processed foods. The estimated consumption per capita of soybean

oil in the United States increased more than 1000 fold during the 20th century, leading to a concomitant increase in linoleic acid consumption. (Blasbalg et al. 2011).

Since 20:4 and 22:4 acyl-carnitines are present in higher abundance in Acsbg1 overexpressing tumors, we hypothesize that obesity-sensitive E0771 may upregulate Acsbg1 to enhance the metabolism of lipids that originate from the diet. This may also contribute to the apparent obesity specific function of Acsbg1. Ongoing studies are aimed at examining the role of dietary fatty acids in the mechanism of Ascbg1-associated tumor progression (Chapter 6).

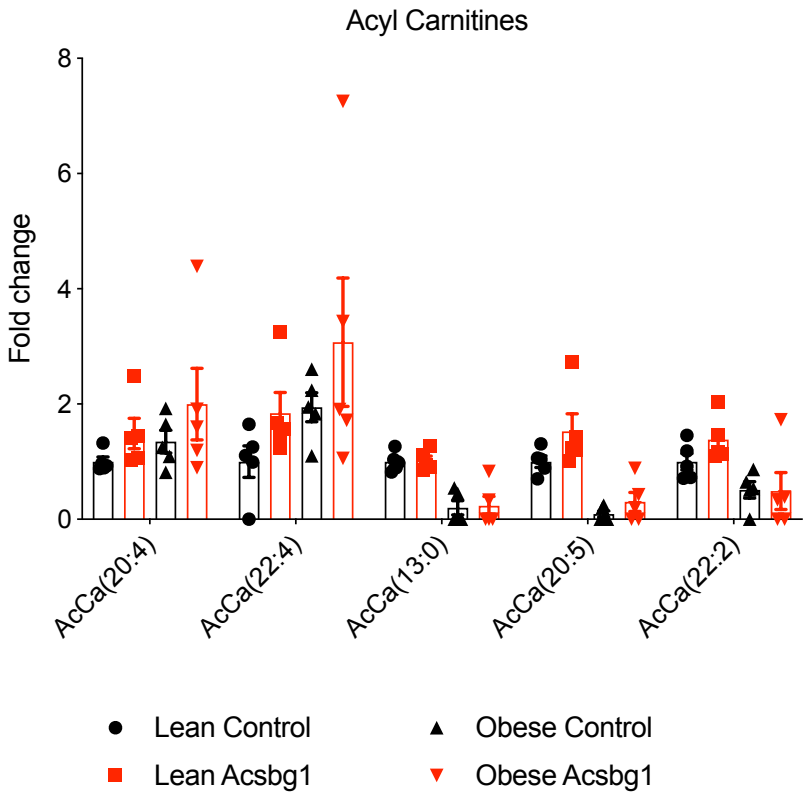

Figure 5.5.4 Acyl-carnitine species differentially regulated by Acsbg1 in obesity

In addition to identifying potential substrates of Acsbg1 in this breast cancer model, we were interested in understanding the downstream fates of the fatty acids which were differentially charged by Acsbg1. Besides entering the mitochondria for energy production via beta-oxidation, fatty acyl-CoA species can also become incorporated into other lipid containing molecules that are essential to support increased biomass. We probed our unbiased lipidomics analysis for lipid-containing molecules that may be downstream of Acsbg1 activity by specifically examining those which exhibited differential abundance in Acsbg1 overexpressing tumors compared to control. Interestingly, a number of cholesterol esters were upregulated in both lean and obese tumors that overexpressed Acsbg1. These include cholesterol esters of 22:2, 22:3, 24:1, and 24:2 species (Figure 5.5.5).

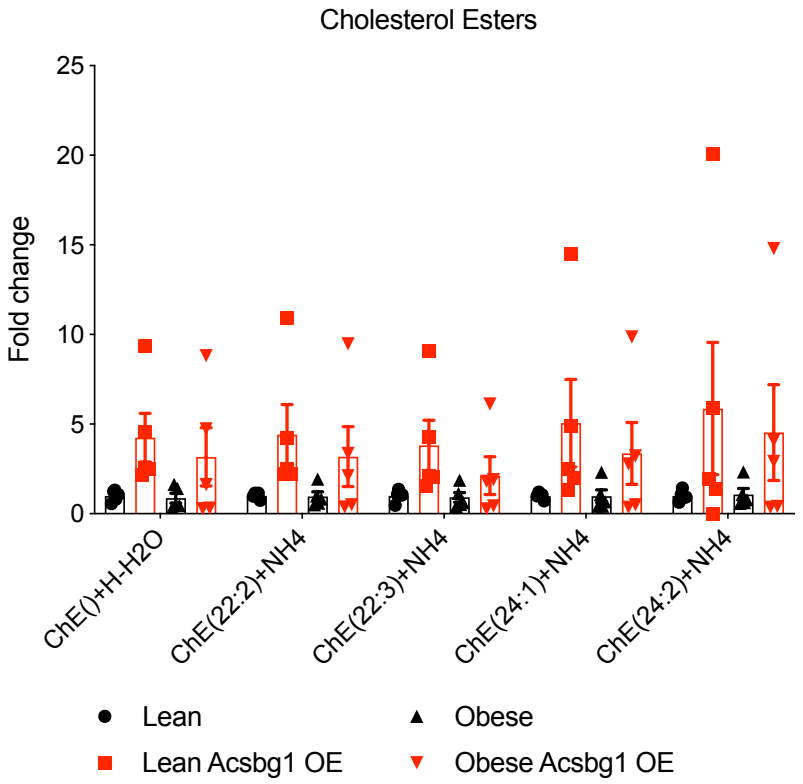

Figure 5.5.5 Cholesterol ester species that are differentially regulated in Acsbg1 overexpressing tumors in obesity.

In keeping with our hypothesis that Acsbg1 preferentially charges 22:4 and 20:4 fatty acids, most of the mono, di, and triacylglyceride species which were more abundant in Acsbg1 overexpressing tumors contained 22:4 and 20:4 fatty acid tails (Figure 5.5.6 and Figure 5.5.7).

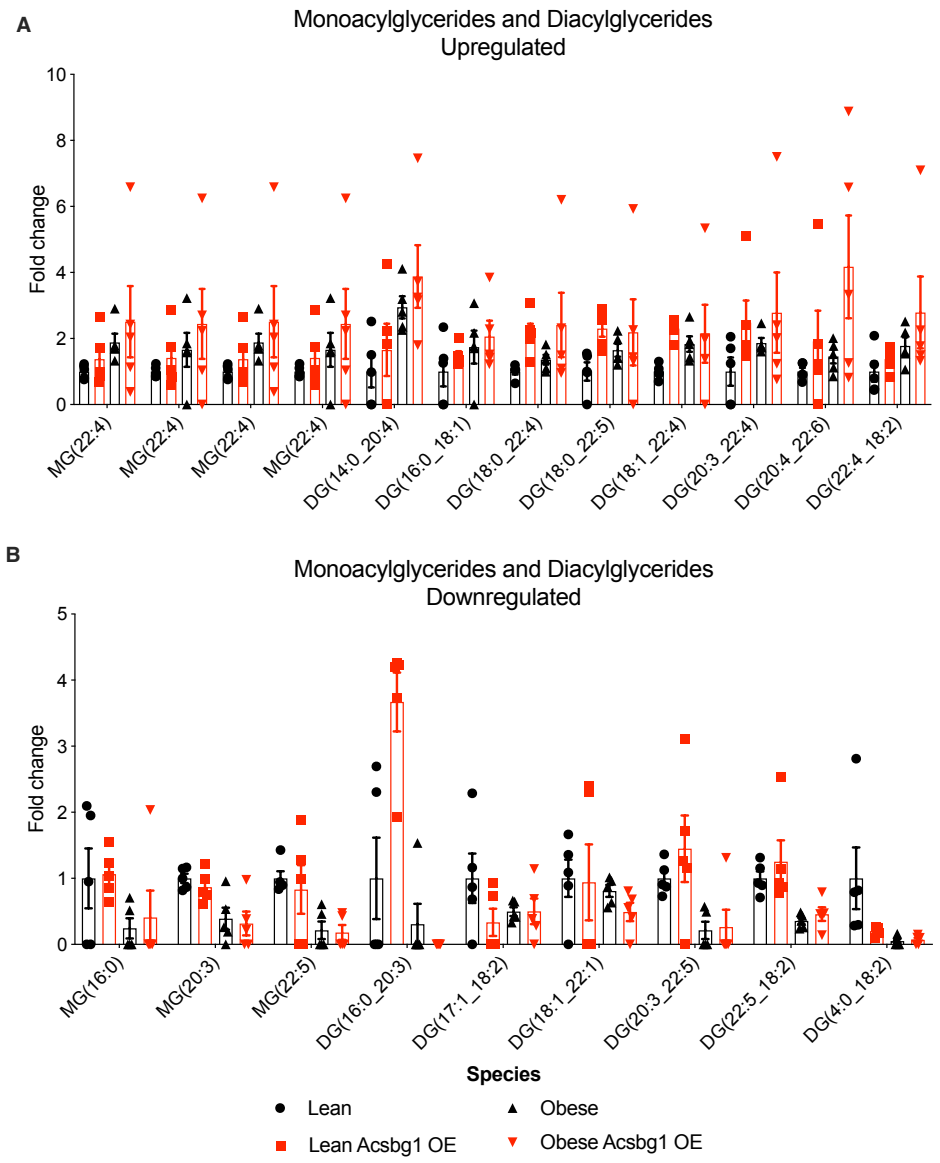

Figure 5.5.6 Monoacylglyeride and diacylglyceride species that are differentially regulated in Acabg1 overexpressing tumors in obesity.

A. Fold change of monoacylglyceride and diacylglyceride species that are higher in abundance in Acsbg1 overexpressing tumors in obesity. B Fold change of monoacylglyceride and diacylglyceride species that are lower in abundance in Acsbg1 overexpressing tumors in obesity.

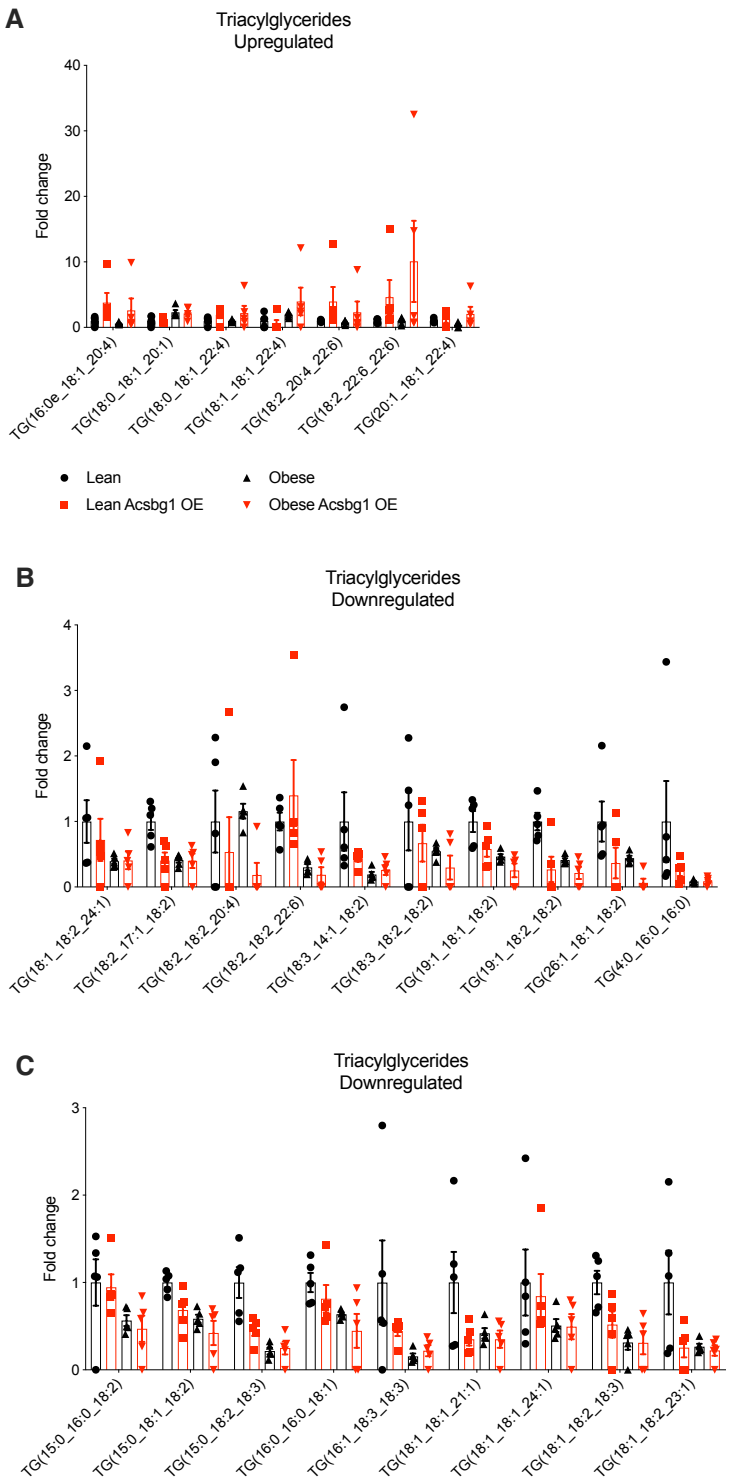

Figure 5.5.7 Triacylglyceride species that are differentially regulated in Acsbg1 overexpressing tumors in obesity.

A. Fold change of triacylglyceride species that are higher in abundance in Acsbg1 overexpressing tumors in obesity. B and C. Fold change of triacylglyceride species that are lower in abundance in Acsbg1 overexpressing tumors in obesity.

Furthermore, we examined the most abundant lipid species that contribute to phospholipid synthesis: phosphatidylcholine, phosphatidylglycerol, and phosphatidylethanolamine species. Consistent with our previous findings, many of the differentially abundant species contain 22:4 and 20:4 fatty acids (Figure 5.5.8). Together, these findings suggest that Acsbg1 may preferentially charge fatty acids of 22:4 and 20:4 species to support the production of essential molecules for lipid storage and membrane synthesis.

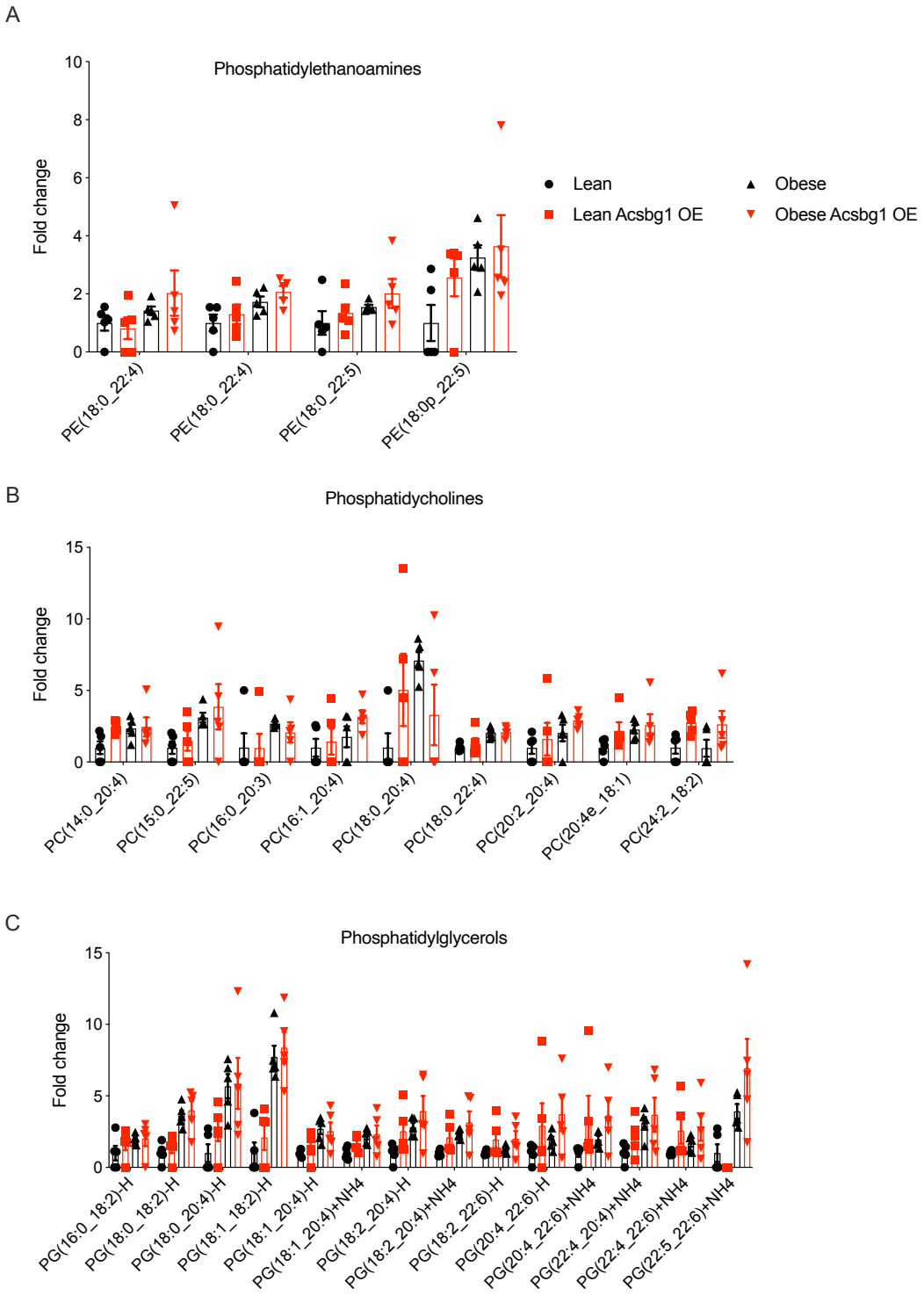

Figure 5.5.8 Phospholipid species which are upregulated in Acsbg1 OE tumors in obesity.

A. Fold change of phosphatidylethanolamine species that are upregulated in Acsbg1 OE cells in obesity. B. Fold change of phosphatidylcholine species that are upregulated in Acsbg1 OE cells in obesity. C. Fold change of phosphatidylglycerol species that are upregulated in Acsbg1 OE cells in obesity

Finally, we sought to establish whether Acsbg1 may be relevant for obesity-associated breast cancer in humans. We analyzed a published cohort of more than 400 human breast cancer samples with paired gene expression and clinicopathologic data. (Toro et al., 2016). The purpose of this study was to identify gene expression signatures that are associated with obesity in human breast cancer. We identified a significant association between Acsbg1 expression and worse tumor grade. Additionally, among overweight and obese women, Acsbg1 expression was significantly associated with a triple-negative, basal tumor subtype, which portends a worse prognosis compared to luminal A cancers (Figure 5.5.8 A and B).

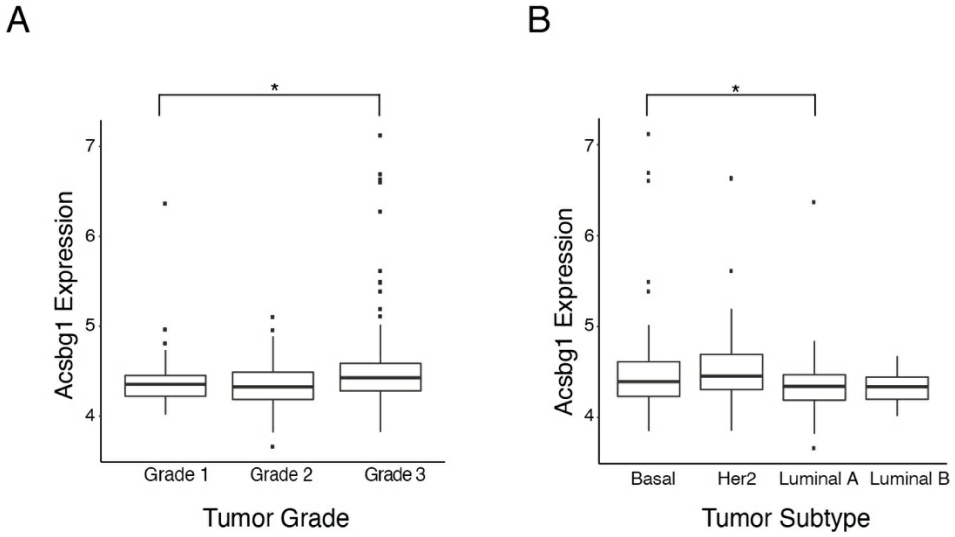

Figure 5.5.9 Acsbg1 expression is associated with worse tumor grade and tumor subtype in human breast cancers

A. Acsbg1 expression in human breast tumors by tumor grade (grade 1, n=88; grade 2, n=156; grade 3, n=178). B. Acsbg1 expression in human breast tumors by tumor subtype in overweight or obese women (Luminal A, n=141; Luminal B, n=26; Her2, n=33; Basal, n=68). *$p<0.05$

5.6 Summary

In chapter 4, we used RNA sequencing to identify Acsbg1, an enzyme which was significantly upregulated in cancer cells isolated from obese compared to lean tumors at an early time point in the disease progression. Acsbg1 is an enzyme with an important role in long-chain fatty acid metabolism, and we hypothesized that Acsbg1 may uniquely allow cancer cells to utilize long chain fatty acids to promote ATP production and support increased biomass through the production of lipid containing molecules.

To test this hypothesis, we produced stable cell lines which overexpress or knockdown Acsbg1 and performed orthotopic experiments in a model of obesity-accelerated breast cancer. We found that enhanced Acsbg1 expression increased tumor volume in an obesity specific manner. The inhibition of Acsbg1 by a short hairpin was not sufficient to attenuate obesity-

driven tumor growth. However, Acsbg1 inhibition along with broad Acsl inhibition with a pharmacologic inhibitor, triacsin C, was effective in reducing obesity accelerated tumor growth. This indicates that Acsl activity, preferentially through Acsbg1, but compensated by other family members, is required for obesity-accelerated tumor progression,

We went on to assess the effects of Acsbg1 overexpression on cellular metabolism and found that high Acsbg1 expression led to increased intracellular ATP, higher basal and maximal respiration, and increased mitochondrial ATP production. Furthermore, Acsbg1 overexpressing tumors in obesity had increased phosphocreatine abundance, and Acsbg1-dependent tumor progression is supported by exogenous creatine transport through the creatine transporter, Slc6a8. This suggests a role for the creatine-phosphocreatine shuttle in the mechanism of Acsbg1 accelerated tumor growth.

We used unbiased lipidomic analysis to investigate the types of lipids modulated by enhanced Acsbg1 activity. 22:4 and 20:4 fatty acids, which likely represent arachidonic and adrenic acids respectively, were incorporated into acyl-carnitine species which were overrepresented in Acsbg1 overexpressing tumors in obesity. This suggests that arachidonic and adrenic acids may be the preferred substrates for Acsbg1. Furthermore, 22:4 and 20:4 lipid side chains were more abundant in cholesterol esters, phospholipids, and triacylglyceride species isolated from these tumors. This supports the hypothesis that in addition to undergoing beta oxidation for ATP production, fatty acids charged by Acsbg1 may also go on to become incorporated into lipid containing molecules required to support biomass accumulation.

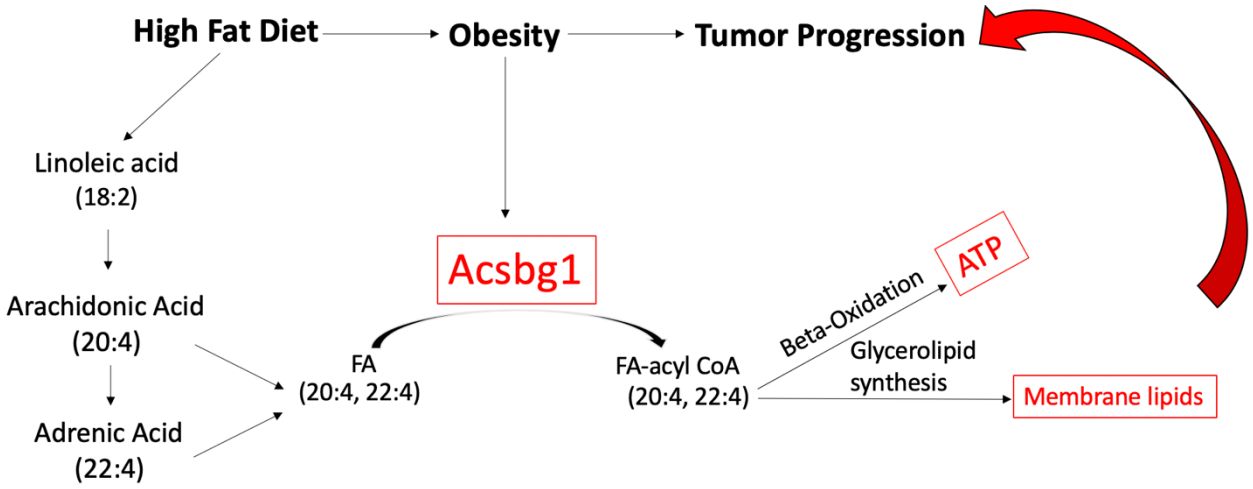

Figure 5.6.1 Schematic of the proposed role of Acsbg1 in obesity-accelerated tumor growth.

Finally, we analyzed a published dataset of paired gene expression and clinicopathologic data from a cohort of more than 400 human breast cancer samples and found that Acsbg1 expression is associated with worse tumor grade. Furthermore, in overweight and obese individuals, Acsbg1 expression is associated with more aggressive tumor subtype, suggesting that Acsbg1 may play a role in the pathogenesis of human breast cancer.

The findings presented in this chapter describe a novel role for Acsbg1 in promoting obesity-accelerated tumor progression in a model of obesity-driven breast cancer. Acsbg1 is

specifically upregulated in cancer cells in obesity and drives enhanced oxidative phosphorylation, likely through fatty acid oxidation. Furthermore, we hypothesize that Acsbg1 upregulation allows cancer cells to take unique advantage of arachidonic and adrenic fatty acids, which are downstream products of the metabolism of linoleic acid, a major component of obesogenic diets. The following chapters will discuss our ongoing and future directions as well as the overall implications of this work as it fits into our understanding of human disease.

CHAPTER 6 Discussion

The goal of this thesis was to better understand the mechanisms that drive adverse breast cancer outcomes in obesity, with a particular focus on elucidating the pathways that may link the adipose rich tumor microenvironment in obesity with accelerated tumor growth. Since obesity is a multi-factorial disease which cannot be fully recapitulated *in vitro*, we chose to use diet-induced models of obesity in immunocompetent female animals to study this connection. We used the triple negative E0771 orthotopic model of murine breast cancer and started this project by characterizing morphological differences in tumors that arise in lean or obese animals. E0771 tumors were significantly larger in obese animals compared to lean. This difference in size can likely be attributed to enhanced proliferation, since obese tumors had increased EdU incorporation relative to lean. Importantly, there was no difference between lean or obese tumors in assays of apoptosis, like cleaved caspase 3 immunohistochemistry. This suggests that inhibition of apoptosis is not a major contributing factor in promoting obesity-related growth. In addition to being highly proliferative, obese tumors were more hypoxic than lean. Finally, obese tumors contained larger and more abundant lipid droplets than lean tumors.

After carefully phenotyping the tumors, we began our molecular studies by performing RNA sequencing on tumors isolated from lean or obese animals. This bulk approach was complicated by the presence of tumor-associated, but non-cancerous cell types within the bulk tumor, such as immune cells and adipocytes. The most highly regulated pathways were immune related, and the specific genes that were most differentially expressed between tumors in lean and obese animals were genes which are highly expressed by immune cells and adipocytes. Ultimately, it was impossible with this approach to determine whether the differences in gene expression we identified were related to cancer cells or other tumor-associated cell types. This highlighted the need to develop a method to enrich for cancer cells before analysis. We chose to employ a florescence-based method to achieve cancer cell specific analysis. We developed a stable cell line that expresses mCherry fluorescent protein for use in orthotopic experiments, allowing us to use FACS to isolate cancer cells from the bulk tumor before analysis.

After validating that this approach was effective in separating cancer cells from non-cancer cell types in the bulk tumor, we performed RNA sequencing of mCherry positive cancer cells isolated from tumors from both lean and obese animals. Importantly, we chose to collect samples from endpoint, when the tumors were drastically different in volume, as well as from midpoint, when the tumors had not yet diverged in size, with the goal of identifying early changes that were drivers of the obesity-accelerated phenotype. We identified Acsbg1, a long-chain fatty acyl-CoA synthetase, as significantly upregulated in obese cancer compared to lean cancer cells at both midpoint and endpoint. We performed gain and loss of function experiments to assess the contribution of Acsbg1 to obesity-driven breast cancer and determined that Acsbg1 overexpression is sufficient to potentiate obesity-driven breast cancer. While Acsbg1 knockdown alone did not impede obesity related cancer progression, a combinatorial approach which utilized both Acsbg1 knockdown and a pharmacologic inhibitor of acyl-CoA synthetase enzymes led to significantly attenuated tumor growth. This suggests that other acyl-CoA synthetase enzymes may compensate for loss of Acsbg1 function and that the role of these enzymes is essential for obesity-driven tumor growth. Importantly, modulating Acsbg1 expression had no effect on tumor growth in lean animals, demonstrating that Acsbg1 has an obesity-specific role in tumor growth.

We performed metabolomic analysis to further probe the mechanisms by which Acsbg1 overexpression may contribute to tumor progression in an obesity-specific manner. We found

that Acsbg1 overexpression led to increased ATP content compared to control tumors from obese animals. *In vitro*, we also measured an increase in ATP content by Cell Titer Glo and plate-based respirometry. This increase in ATP was accompanied by increased basal and maximal mitochondrial respiration. The previously described function of Acsbg1 is to charge long-chain fatty acids to active, fatty acyl-CoA species. We hypothesize that overexpression of Acsbg1 leads to increased transport of long-chain fatty acyl-CoA species into the mitochondria, where they undergo beta oxidation to produce acetyl-CoA that enters the citric acid cycle. Our ongoing *in vitro* experiments are aimed at testing this by blocking fatty acyl-CoA transport into the mitochondria through the carnitine shuttle. We are taking a pharmacologic approach by treating Acbsg1 overexpressing cells with etomoxir, an inhibitor of CPT1, the rate limiting step in this process. Additionally, we are employing a genetic approach to knockdown CPT1 in Acsbg1 overexpressing cells. We will then use these double-modified cells in an orthotopic experiment in lean and obese animals. We expect that reducing lipid transport into the mitochondria in Acsbg1 overexpressing cells will diminish Acsbg1-dependent tumor progression, demonstrating that mitochondrial lipid oxidation is essential for the function of Acsbg1 in obesity.

We used untargeted lipidomics to identify the types of lipid species which were differentially abundant in Acsbg1 overexpressing tumors compared to control in lean and obese animals. We found that in obesity, the fatty acid containing molecules which were upregulated with Acsbg1 overexpression were those that most likely contained arachidonic and adrenic acid side chains. Arachidonic and adrenic acids are sequential products of linoleic acid metabolism, a major lipid component in the obesogenic diet. This raises the possibility that Acsbg1 overexpression leads to increased tumor growth in obesity by allowing cancer cells to better utilize the specific fatty acid species which are in high abundance when animals are fed this lipid-rich diet formulation. We hypothesize that this major dietary component may play a causal role in promoting Acsbg1 dependent tumor growth, and ongoing experiments are focused on testing this hypothesis by inducing obesity with diets that are calorically matched but differ in lipid composition. We have worked to develop a high-fat diet formulation which is matched to the standard high fat diet in total lipid content by percentage, but with linoleic acid levels matched to the chow or low-fat control diets. If Acsbg1 works specifically by charging products of linoleic acid metabolism, we expect obese animals fed low linoleic acid diets to have attenuated tumor progression, despite Acsbg1 overexpression. To confirm this mechanism, we are also working *in vitro* to treat Acsbg1 overexpressing cancer cells with labeled linoleic, arachidonic, and adrenic acids and plan to use LC-MS to determine the fates of those lipid species in Acsbg1 overexpressing cells. We expect to see significantly enhanced cell proliferation and increased labeling of arachidonic and adrenic fatty acid containing phospholipids and other lipid-containing molecules in Acsbg1 overexpressing cells compared to control.

In this study, we also identified a role for exogenous creatine in Acsbg1-dependent tumor growth in obesity. Not only was the creatine transporter upregulated with Acsbg1 overexpression in obese tumors, but phosphocreatine was significantly more abundant in obese, Acsbg1 overexpressing tumors. When we knocked down the creatine transporter in cells that overexpress Acsbg1, tumor growth was attenuated in obesity. We hypothesize that the interconversion of creatine and phosphocreatine plays an essential role in maintaining high-energy phosphate levels to support the demands of rapid proliferation. We are currently working to confirm the role of phosphocreatine in promoting Acsbg1-dependent tumor growth by using cyclo-creatine *in vivo*

to inhibit creatine kinase, the essential enzyme responsible for interconverting creatine and phosphocreatine. We expect that cyclo-creatine treatment will significantly inhibit Acsbg1-dependent tumor progression *in vivo.*

Improved methods of early detection as well as significant advances in treatment have led to marked improvements in breast cancer prognosis. However, breast cancer remains a major cause of mortality in the United States and around the world. Obesity is a significant risk factor for worse breast cancer outcomes, and therapeutic strategies aimed at breaking the connection between obesity and breast cancer may lead to effective treatments to improve outcomes in this high-risk patient population. Here, we comprehensively described a murine model of obesity-accelerated breast cancer as well as the transcriptional changes in the cancer cells associated with obesity at both early and late time points in the disease progression. Using this strategy, we identified a novel role for Acsbg1 in promoting tumor growth in an obesity-specific fashion. We performed metabolic and lipidomic studies to further probe the mechanism by which this enzyme promotes tumor growth in obesity. Finally, we found a significant association between Acsbg1 expression and worse tumor grade in human breast tumors; and among overweight and obese patients, Acsbg1 was associated with a more aggressive tumor subtype. Further work will be directed at defining the downstream mediators of Acsbg1 dependent growth, developing human-derived models of obesity-driven tumor progression, and evaluating the role of Acsbg1 in other types of obesity-associated cancers, like pancreatic, colorectal, and hepatocellular carcinomas.

CHAPTER 7 Future directions

7.1 Introduction

The overarching goal of the work described in previous chapters was to better understand the mechanisms that drive obesity-accelerated tumor progression in an orthotopic murine model of breast cancer. We chose to employ transcriptomic approaches to identify a candidate enzyme, Acsbg1, and went on to perform gain and loss of function experiments to assess its role in obesity-driven E0771 growth *in vivo*. We also performed metabolomic and lipidomic analyses to better understand the function of Acsbg1 and its contribution to obesity accelerated cancer. In addition to the approaches described in previous chapters, there are several other, complementary strategies that one might employ to better understand the connection between obesity and breast cancer. This chapter will describe some of the future directions that could expand upon the findings presented thus far.

7.2 Proteomic profiling of obesity-driven breast cancer

This project involved unbiased transcriptional profiling of an orthotopic model of breast cancer to identify candidate genes that may be involved in driving cancer progression in obesity. A complementary strategy would be to perform unbiased profiling of the proteome of cancer cells from tumors in lean or obese animals. Similar to our transcriptomic approach, analyzing the proteome of cancer cells in a heterogeneous tumor would require a cell-specific labeling technique. Our group has utilized bio-orthogonal noncanonical amino acid tagging (BONCAT) in other contexts to enable cell type specific proteomic analysis, and this approach can be applied in cancer cells *in vivo*.

The principle of the BONCAT method is based on the specificity of the methionyl tRNA synthetase (metRS). MetRS specifically charges methionine to its cognate tRNA for incorporation into a growing polypeptide. Importantly, the wildtype metRS will not recognize and charge the azide-containing methionine analog, azidonorleucine (ANL). However, with a single amino acid mutation, L274G, in the sequence encoding metRS, the modified protein will recognize and charge ANL to the methionyl tRNA. This leads to the formation of azide-containing polypeptides with ANL in place of methionine. In a heterogenous sample, like bulk tumor, the only proteins that will contain azide-tagged side chains will be those produced by the L274G metRS modified cell type. These proteins can then be isolated using a copper catalyzed click-chemistry reaction with alkyne containing beads and analyzed by LC-MS. (Link et al. 2006; Erdmann et al. 2015; Ngo et al. 2009; Mahdavi et al. 2016; Liu et al. 2017)

We plan to produce E0771 cancer cells which express the metRS L274G protein and use these cells to perform an orthotopic experiment in lean and obese animals, similar to those described in chapters 3 and 4. We will then treat tumor-bearing animals with ANL through feeding or intraperitoneal injection, and only the modified cancer cells will be able to incorporate ANL into nascent proteins. We will isolate those azide-tagged proteins from a bulk sample using click chemistry with alkyne conjugated beads and analyze those azide-containing proteins using LC-MS. This will allow us to achieve cancer cell specific proteomic labeling *in vivo* (Figure 7.2.1A).

Previous studies from our group have clearly demonstrated that the presence of a tumor is sufficient to shift the gene expression profiles of the surrounding adipose; however, it is not clear

which signals from the cancer cells mediate this crosstalk. The BONCAT technique described above is particularly powerful because it will allow us to identify not only the intracellular proteome, but also polypeptides produced in cancer cells that were secreted into the microenvironment to signal to adjacent cell types in a paracrine manner. Furthermore, this technique would allow us to identify cancer-derived peptides in the blood or distant organs, which may elucidate the role of cancer-derived proteins in establishing a metastatic niche, for example (Figure 7.2.1 B).

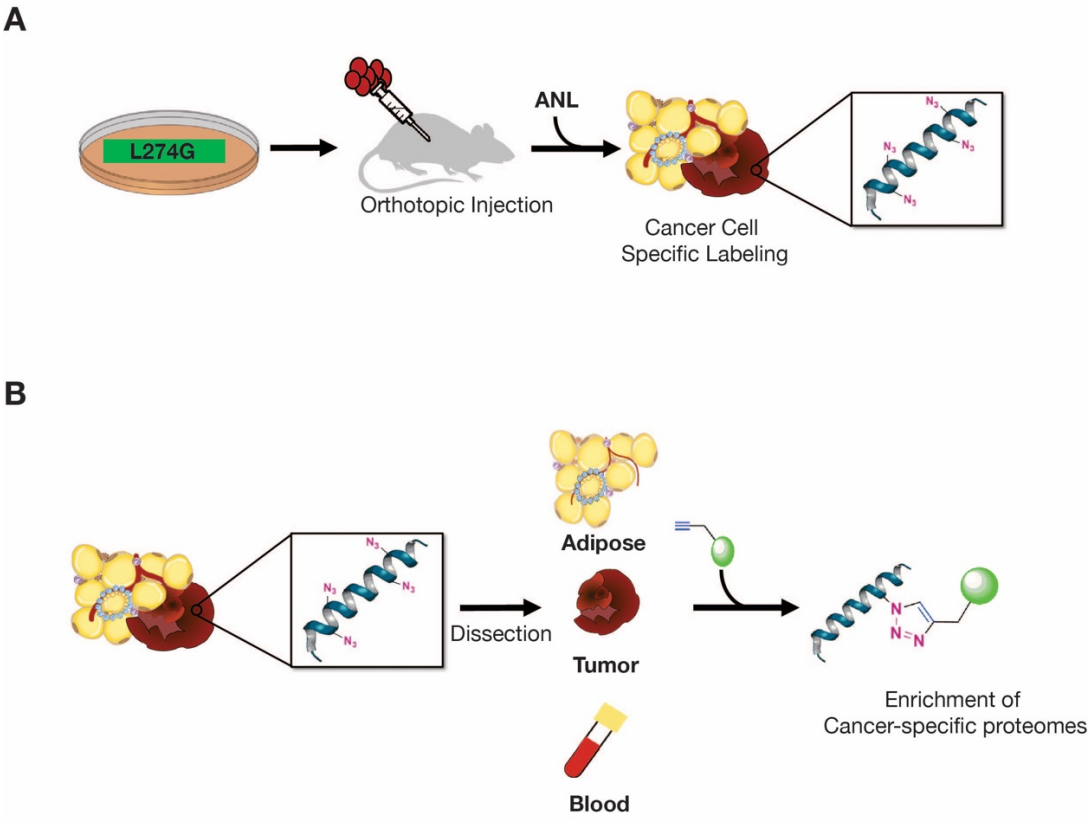

Figure 7.2.1 Schematics of L274G metRS BONCAT method.

A. L274G metRS expressing E0771 cells will be produced and used in an orthotopic experiment *in vivo* to achieve cancer cell specific proteomic labeling. B. Cancer-derived secreted proteins can be isolated from the tumor, the microenvironment, and distant sites.

We have initiated the early stages of this project by utilizing a lentiviral approach to produce a stable mE0771 cell line which expresses the L274G metRS protein, and we have confirmed *in vitro* that we can achieve specific labeling with ANL containing medium. Our next steps are to develop an *in vivo* protocol to robustly label cancer cells in an orthotopic mouse model *in vivo*, then to use LC-MS to identify and compare the proteomes of cancer cells in lean and obese animals.

7.3 Cell barcoding

Another approach is to exploit the inherent heterogeneity of the E0771 cell line to identify genetic variations that predispose cells to be sensitive or resistant to obesity. Importantly, E0771 is not a clonal cell line, and we have established more than 30 distinct cell lines derived from the parental E0771. We have performed basic phenotyping *in vitro* and have established that the clonal cell lines have a range of growth rates and responses to adipocyte conditioned medium. (Figure 7.3.1 A) Additionally, we have tested a small subset of the clonal cell lines *in vivo* and found that there are a range of responses to obesity *in vivo*. Clonal line 19, for example, did not exhibit obesity-accelerated tumor growth. Paradoxically, clonal line 4 had slower growth in obese animals (Figure 7.3.1 B). This finding demonstrates that some, but not all of the cells derived from the E0771 parental cell line are sensitive to accelerated growth in obesity. If we are able to identify and compare those cells lines which are more or less responsive to obesity, we may be able to identify the genetic differences that underlie these responses. We envisage a forward genetics approach whereby we utilize genetic barcodes to label each clonal cell line. We can then pool the lines and perform orthotopic experiments in lean and obese animals. At endpoint, we will isolate tumors from lean and obese animals and use DNA sequencing to identify the barcodes, and thus the specific clonal lines, which are more or less abundant in tumors isolated from obese animals. Finally, we will compare the genomes of these resistant and sensitive lines to identify mutations in genes that may drive a response to obesity (Figure 7.3.2). We can also use transcriptomic, metabolomic, and proteomic approaches to compare resistant and sensitive cell lines.

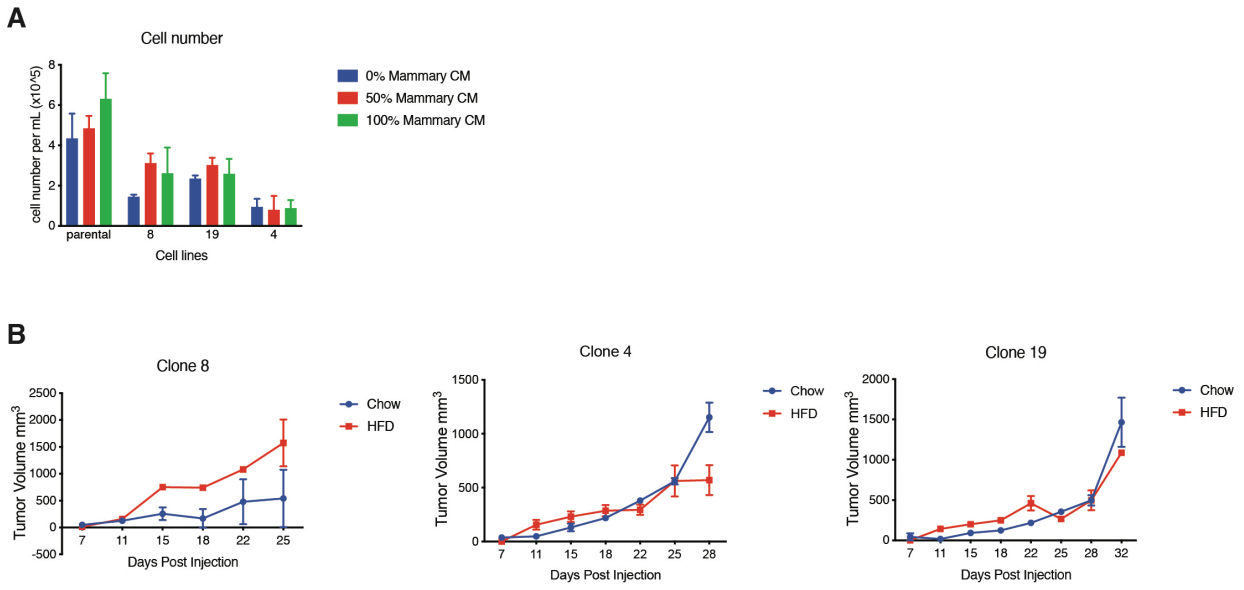

Figure 7.3.1 E0771 clones have a range of responses *in vitro* and a pilot *in vivo* experiment.

A. Cell number of selected cell lines after 24 hours of treatment with the indicated amount of mammary adipocyte conditioned medium. B. Longitudinal tumor volume of selected clonal cell lines in lean or obese animals (n=2 animals per group).

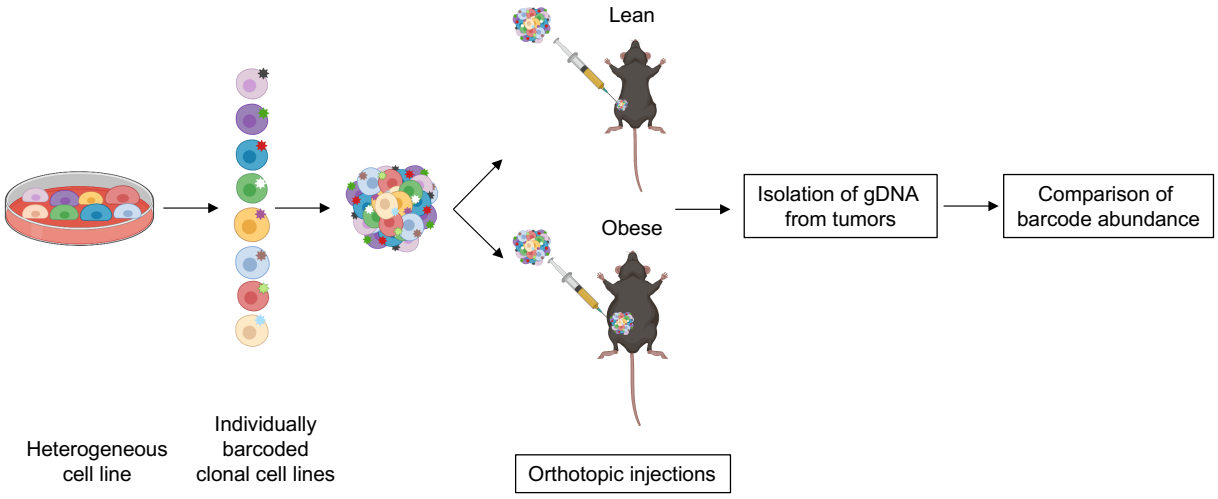

Figure 7.3.2 Schematic of barcoding experimental plan

7.4 Human-derived models.

All of the work described here and in previous chapters has relied on a mouse model of obesity-accelerated breast cancer. No one model can completely recapitulate human disease; thus, we are working to establish human-derived models to confirm and expand upon our findings. Specifically, we are establishing both an orthotopic model utilizing immortalized human-derived cell lines and a patient-derived xenograft (PDX) model of obesity-accelerated breast cancer.

One challenge associated with developing a human-derived mouse model is establishing obesity in an immunocompromised host. The NOD.Cg *Prkdc*^{scid} *Il2rg*^{tm1Wjl}/SzJ (NOD/SCID/Gamma, or NSG) mouse strain is a commonly used model in human derived cancer studies; however, NSG mice are more resistant to obesity and its comorbidities than C57BL6/J mice. Therefore, we adapted a protocol of high-fat diet feeding to generate female NSG animals with significantly higher body weight than chow control, which can be attributed to an accumulation of fat mass, as measured by echo MRI (Behan et al. 2013) (Figure 7.4.1 A-C).

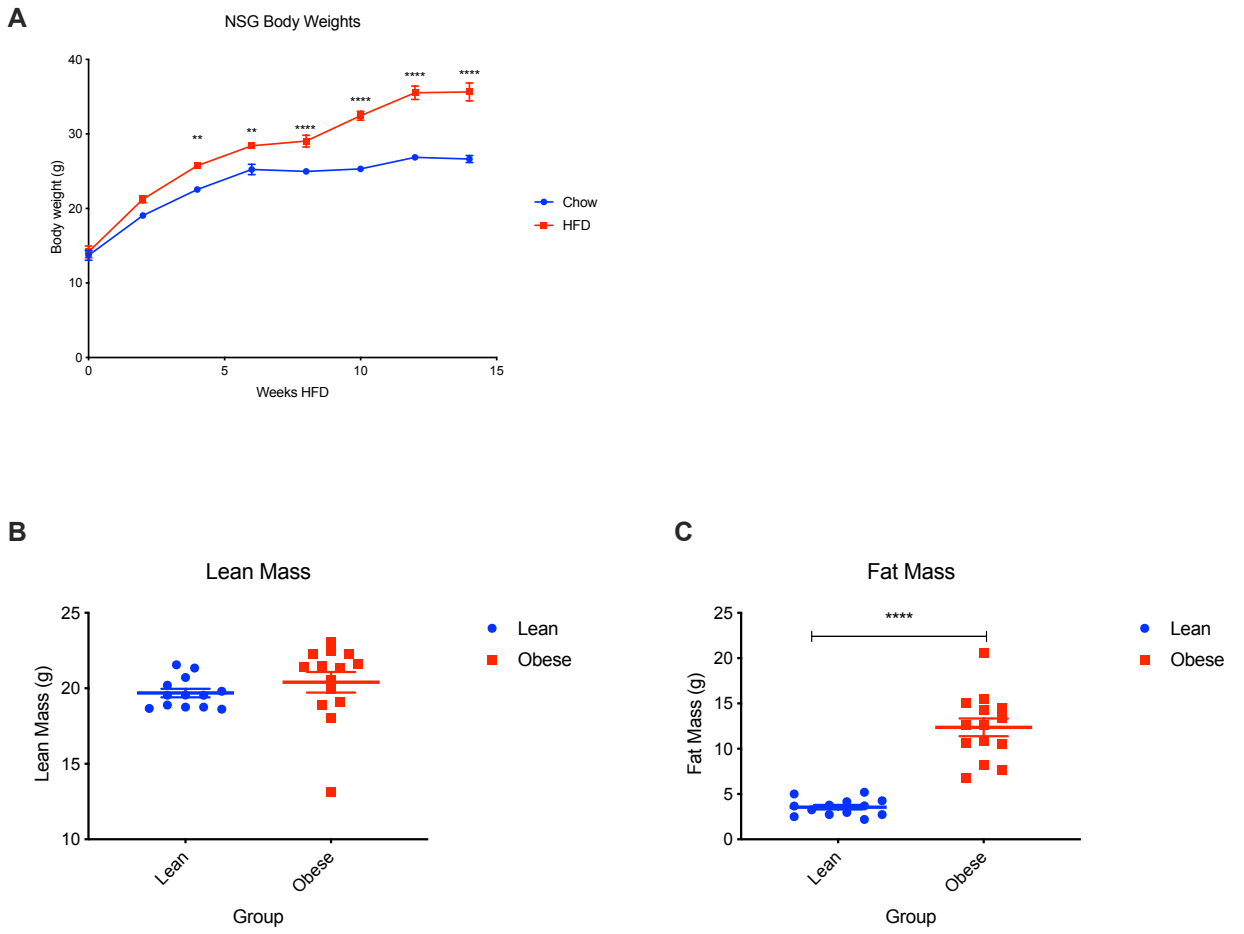

Figure 7.4.1 Diet induced obesity in female NSG animals.

A. Body weights of female NSG animals fed 60% high fat diet (n=13 or 14 animals per group). B. Lean mass of animals in A at sacrifice after 14 weeks of high fat feeding. C. Fat mass of animals in A at sacrifice after 14 weeks of high fat feeding. **p<0.01, ****p<0.0001.

Having established a model of diet-induced obesity in female NSG animals, the next step is to identify an immortalized human-origin cell line which displays obesity-accelerated growth *in vivo*. We will then use lentiviral methods to modulate Acsbg1 in these lines to determine whether Acsbg1 plays a similar role in driving obesity-associated tumor progression in human derived cell lines. Furthermore, we will establish an obesity-accelerated model of breast cancer from a PDX model, further enhancing the relevance of our findings to human disease. Finally, we will perform transcriptomic analysis of tumors generated from these studies to identify additional candidate genes and pathways that may link obesity and breast cancer.

7.5 Single-cell RNA sequencing

In this study and in the aims described above, we have focused on analyzing the neoplastic cells located in heterogeneous E0771 tumors. Our preliminary data suggest that many other cell types, like immune cells, fibroblasts, and adipocytes, make up a significant proportion

of the cell types in this environment (Chapters 3 and 4). Another series of future studies will be focused on better understanding how non-malignant, tumor-associated cell types may contribute to tumor growth in this model of obesity-accelerated breast cancer. Tumor immune cells have well established pro- and anti- tumor effects, and we know that the immune system is dysregulated in obesity, providing a strong rationale for studying the role of immune cells in the accelerated tumor progression in this model. I hypothesize that there are significant shifts in the numbers and phenotypes of immune and other non-cancer cell types within the tumor in obesity and that these shifts may play a significant role in promoting obesity-accelerated tumor progression. We will perform single-cell RNA sequencing on tumors isolated from lean or obese animals. This approach will allow us to identify unique cell populations within the tumor as well as shifts in gene expression within those populations in obesity.

7.6 Models of other obesity-accelerated cancers

This study has been entirely focused on investigating the mechanisms that drive obesity-driven progression in breast cancer. However, obesity is a significant risk factor for many other cancer types in both men and women (Chapter 1), and we hypothesize that our findings may be applicable to other obesity-driven cancer types, like pancreatic cancer, hepatocellular carcinoma, melanoma, and colorectal cancer. Specifically, we plan to assess the role of Acsbg1 in other obesity-dependent cancers both *in vitro* and *in vivo* with gain and loss of function experiments. In addition to probing the effects of modulating Acsbg1, we plan to use some of the methods previously described, namely RNA sequencing, to identify changes associated with obesity in these cancer types. We can then compare these datasets to identify an obesity-associated gene expression signature that may be more broadly associated with obesity across many cancer types.

The first step in this series of studies is to produce models of obesity-driven cancer for each of these cancer types. We have identified murine cell lines derived from a variety of obesity-associated tumor types that display increased cell viability when exposed to adipocyte conditioned media (Figure 7.6.1). This suggests that these cell lines may also be obesity sensitive *in vivo*.

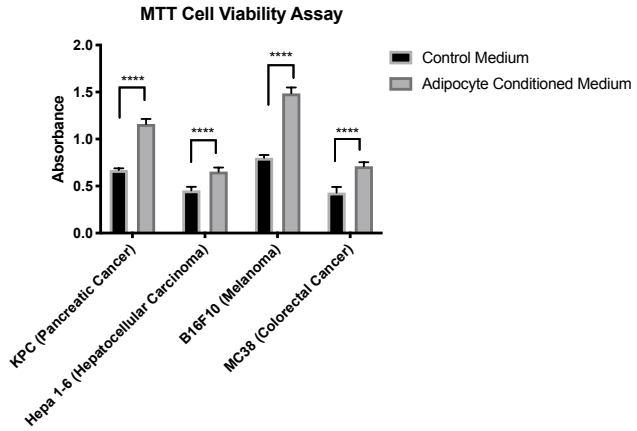

Figure 7.6.1 Cell viability of a panel of cancers treated with adipocyte conditioned medium.

****p<0.0001 Data here represent mean +/- standard error of the mean (SEM). n=4 wells per group.

The next step is to develop *in vivo* orthotopic models of each of these tumor types in lean and obese animals. We have started this process with a cell line derived from the KrasLSL.G12D/+; Pdx Cretg/+ (KC) model of pancreatic ductal adenocarcioma (PDAC) (Hingorani et al. 2003; Torres et al. 2013). Importantly, this orthotopic model involves surgical implantation of cancer cells into the pancreas, so we would be unable to measure tumor growth logitudinally with digital calipers as we did with E0771 tumors. Instead, we plan to use *in vivo* imaging (IVIS) to detect luciferase activity in these tumors over time. In this model, luciferase ativity is proportional to the size of the tumor. In a pilot experiment with luciferase-expressing KC cells, we found that tumors in obese animals grew to be significantly larger than in lean, suggesting that this may be a suitable model for obesity-accelerated pancreatic cancer (Figure 7.6.2). We plan to use similar approaches to produce in vivo models for a panel of obesity-sensitive cancers.

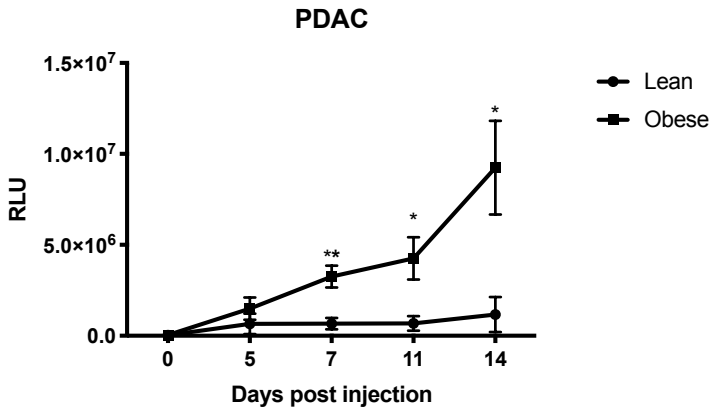

Figure 7.6.2 Luciferase activity detected by IVIS in orthotopic KC tumors in lean or obese animals over time.

Data here represent mean +/- standard error of the mean (SEM). *p<0.05, ** p<0.01.

7.7 Summary

The previous chapters described experiments aimed at better understanding the connection between obesity and breast cancer progression. Notably, these studies relied heavily on unbiased transcriptomic profiling of cancer cells isolated from tumors in lean or obese animals to determine candidate genes and pathways involved in this process. Using this approach, we identified an undescribed role for Acsbg1 in potentiating obesity-accelerated tumor progression in the orthotopic E0771 model. To further expand our work, we propose several new projects employing complementary approaches that would continue to enrich our understanding of the mechanisms underlying the connection between obesity and breast cancer. These projects include cell-type specific proteomic profiling, cell barcoding, single-cell RNA sequencing, and human-derived *in vivo* models, as well as expanding our findings to other types of obesity-associated cancers.

CHAPTER 8 MATERIALS AND METHODS

Cell culture

Unless otherwise noted, all cells were maintained in RPMI 1640 medium (Thermofisher) supplemented with 10% FBS (Gemini) and 1% penicillin/streptomycin (Thermofisher). Cells were incubated at 37°C with 5% CO_2 and passaged to maintain 40-80% confluence.

Preparing a stable mCherry$^+$ E0771 cell line

The mCherry plasmid was prepared by Benjamin Ostendorf in the laboratory of Dr. Sohail Tavazoie at The Rockefeller University by modifying the Phiv-Luc-ZsGreen (Addgene 39196) and replacing the ZsGreen1 reporter with mCherry. HEK-293T cells were plated at 70% confluence in a 10 cm plate and co-transfected for 16 hours with 10ug mCherry$^+$ plasmid DNA, 4 ug VSVG, and 8ug PsPax2 packaging vectors in 10mL serum and antibiotic free optiMEM (Thermofisher) with Fugene. Medium containing lentiviral particles was collected and filtered through a 0.4 μM filter. Parental E0771 cells were plated at 150,000 cells per well in a 6-well plate. The next morning, the media was changed to 100% viral supernatant with 8uM polybrene (Sigma-Aldrich) and the cells were incubated for 24 hours before being replenished with normal growth medium. The infected cells were expanded to 15 cm plates and mCherry+ cells were selected using FACS. A bulk fraction of mCherry+ cells was collected and passaged to form the mE0771 cell line.

Fluorescence Activated Cell Sorting (FACS)

Tumors were dissected and dissociated according to the manufacturer's instructions using the mouse tumor dissociation kit (Miltenyi). Cells were suspended in FACS buffer (PBS, 1% BSA, 0.1% 1M HEPES pH 7.4) and stained for live cells using DAPI exclusion. FACS was performed by the Rockefeller University Flow Cytometry Resource Center.

Mice

Female C57Bl6/J mice were purchased from the Jackson Laboratory (stock: 0664) at 6 weeks of age. They were maintained in The Rockefeller University Center for Comparative Bioscience Center. Unless otherwise noted, they were fed standard rodent chow diet, Pecola Rodent Diet 2.0 (Labdiets), and irradiated water, ad libitum. They were housed 4 animals per cage with standard enrichment.

Necropsy

Mice were euthanized at humane endpoint or the indicated time. Blood was collected using cardiac puncture and serum was isolated by centrifugation at 2000g for 15 minutes. Tumors were dissected and weighed, then bisected. One half was flash frozen, the other half was placed into a histology cassette and fixed using 10% neutral buffered formalin. The 4th mammary pads adjacent and contralateral to the tumor were collected.

High Fat feeding experiments

At 6 weeks of age, female C57BL6/J animals were randomized to continue a standard chow diet or switched to a diet comprising 60% calories from fat (Research diets, D12450J). The standard obesogenic diet contains 25g soybean oil, 20g lard, 72.8g sucrose per 1055.05g of diet. Animals were monitored bi-weekly for weight gain. After 8-10 weeks, animals on a high-fat diet

that reached a weight above 28.5 g were considered obese and were included in future studies of diet-induced obesity.

Injections

For E0771 orthotopic injections, cells were maintained in culture as normal. On the day of injection, cells were trypsinized using 0.5% trypsin (Gibco) and quenched with equal volume of standard, FBS containing medium. They were counted using trypan blue exclusion and the Countess II automatic cell counter (Thermofisher). 50,000 cells per animal were resuspended in 100 microliters per animal of serum and antibiotic free RPMI 1640 medium (Thermofisher) with equal volume phenol-red free growth factor reduced matrigel (Corning) and kept on ice until injection. The cell mixture was transferred to prechilled 27g insulin syringes by first removing the plunger of the syringe, then using a micropipette to place the cell mixture into the barrel of the syringe and replacing the plunger. 100 microliters of the cell mixture were injected into the left, fourth mammary gland of anesthetized lean or obese animals.

Tumor measurements

Subcutaneous, orthotopic mammary tumors were monitored twice weekly using digital calipers beginning on 7 days post injection. Tumor volume was calculated using the following formula: volume (mm3) = 0.5 x length x (width^2) where length is defined as the largest diameter and width is perpendicular to length. Animals reached humane endpoint when the tumor exceeded 1.5cm in the largest diameter or the tumor ulcerated through the skin.

Generation of a stable Acsbg1 OE mE0771 cell line

PLX-304 plasmids containing V5-tagged Acsbg1 or LacZ control were obtained from an ORF expression library (X. Yang et al. 2011). Lentivirus was prepared by cotransfecting HEK-293T cells with 10ug of the PLX-304 vector, 4ug VSVG (Addgene 8454) envelope protein and 8ug psPax2 (addgene 12260) with fugene in serum, antibiotic, and phenol-red free optiMEM medium (Thermofisher) overnight. After 16 hours the medium was changed to standard RPMI 1640 with 10% FBS and 1% penicillin/streptomycin. Lentivirus containing supernatant was collected and filtered through a 0.45 μM filter. 150,000 E0771 mCherry+ cells per well were plated in a 6-well plate. The next day, the growth medium was replaced with 100% lentiviral medium containing 8μM polybrene overnight. After 16 hours, the viral medium was replaced with growth medium for 24 hours. The growth medium was replaced with medium containing 20 ug/ml blasticidin. Selection was considered complete when a plate of uninfected mCherry$^+$ E0771 cells were killed. Overexpression was confirmed by immunoblot for V5 tag and Acsbg1.

Generation of a stable Acsbg1 KD mE0771 cell line

The pLKO.1 cloning plasmid was purchased (Addgene, 8453) and linearized by treatment with the restriction enzymes EcorI and Age1. Oligos encoding a non-targeting scrambled control (CTCAAGCCTGACTGGTCAAAG) or short hairpin targeting Acsbg1 (GCGCCTCAAAGAATTAATCAT) were ligated into the empty vector using T4 ligase. Lentivirus was prepared by cotransfecting HEK-293T cells with 10ug of the pLKO.1 vector, 4ug VSVG (Addgene 8454) envelope protein and 8ug psPax2(addgene 12260) with fugene in serum, antibiotic, and phenol-red free optiMEM medium (Thermofisher) overnight. After 16 hours the medium was changed to standard RPMI 1640 with 10% FBS and 1% penicillin/streptomycin. Lentivirus containing supernatant was collected and filtered through a 0.45 μM filter. 150,000

E0771 mCherry$^+$ cells per well were plated in a 6-well plate. The next day, the growth medium was replaced with 100% lentiviral medium containing 8μM polybrene overnight. After 16 hours, the viral medium was replaced with growth medium for 24 hours. The growth medium was replaced with medium containing 2mg/mL puromycin. Selection was considered complete when a well of uninfected cells were killed. The knockdown efficiency was determined by qPCR and of mCherry$^+$ cells sorted from tumors.

Triacsin C administration

Triacsin C was purchased from Cayman Chemical (10007448). 1g of lyophilized powder was dissolved in 1mL DMSO. The concentrated stock was then dissolved 20x in sterile, normal saline, and sterile filtered. Triacsin C or vehicle control was delivered to animals via intraperitoneal injection three times per week to achieve a dose of 2mg/kg/week. Animals were monitored 3 times weekly for weight loss and signs of toxicity.

RNA isolation and cDNA synthesis

Tissues and cells were homogenized in 1 mL Triazol (Qiagen). Tissues were homogenized using the biolyzer (Qiagen). 200uL chloroform was added. After brief vortexing, samples were incubated at -20°C for at least 20 minutes, up to overnight. They were then centrifuged at 4°C for 15 minutes. The aqueous layer was transferred to an RNAse free microcentrifuge tube, and an equal volume of sterile 70% ethanol was added to precipitate nucleic acids. This mixture was applied to RNeasy columns (Qiagen) and the RNA was purified according to the manufacturer's instructions, with on-column DNAse digestion. RNA was eluted in RNAse free water and was quantified using the nanodrop (Thermofisher). RNA was stored at -80°C until use. cDNA was synthesized using the High Capacity Reverse Transcriptase Kit (Thermofisher) according to the manufacturer's protocol. qPCR was performed using a 384 well format, the Quantstudio 6 Flex Real-Time PCR System (Thermofisher) and power Sybr green mastermix (Life Technologies). 18S or TBP was used as an internal control and relative concentration was determined by using the delta-delta Ct method.

RNA Sequencing

RNA sequencing was performed by the Rockefeller University Genomics Resource Center. RNA was isolated as above, and RNA integrity was assessed using the bioanalyzer (Agilent technologies). Samples with RIN above 8 were considered acceptable for library production, which was performed by the Rockefeller University Genomics Resource Center. Paired-end, ribosomal-RNA depleted RNA sequencing was performed using the Illumina HiSeq 2500. The data generated were aligned to the mouse genome (mm10) and analyzed using the DeSeq2 platform from Bioconductor.

Immunoblots

Tumor samples were homogenized using the Tissuelyser (Qiagen) with sterile beads and RIPA buffer supplemented with protease and phosphatase inhibitors. Protein quantification was determined by BCA assay and 20ug protein was resuspended in Laemmli buffer and heated at 95°C for 10 minutes. Samples were loaded in 4-20% gradient tris-glycine precast gels (Biorad) and resolved using 120V. The protein was then transferred to PDVF membranes on ice at 100V for 90 minutes. Transfer was verified using Ponceau red staining. The blots were then blocked

using superblock (Thermofisher) for 1 hour at room temperature. After blocking, the membranes were treated with primary antibodies overnight at 4°C. Blots were washed with TBS-0.1% tween and then treated with a secondary-HRP conjugated antibody at 1:10,000 dilution for 1 hour at room temperature. Blots were treated with Western Lighting Plus ECL (PerkinElmer) and imaged using Bio-Rad Gel doc (Biorad). Quantification of images was performed using imageJ.

ATP quantification

Cell Titer Glo assays were performed using a 96well plate format. 5,000 E0771 cells were plated per well of a 96 well plate. Before treatment, they were serum starved for 1 hour, then treated as indicated in serum-free medium. ATP was quantified using the Cell-Titer-Glo kit (Promega) according to the manufacturer's instructions and luminescence was quantified using a plate reader.

Cell proliferation assays

150,000 E0771 cells were plated into each well of a 6 well tissue culture plate. They were then treated as indicated and counted using trypan blue exclusion and the Countess II automatic cell counter (Thermofisher).

Immunohistochemistry

At the time of sacrifice, tumor samples were placed in histology cassettes and were fixed in 10% buffered formalin with shaking overnight at 4°C. The cassettes were washed three times in PBS and transferred to 70% ethanol. The fixed samples were then paraffin embedded, cut, and placed onto slides by the Laboratory of Comparative Pathology at Memorial Sloan Kettering Cancer Center. The slides were deparaffinized using xylene and rehydrated using decreasing concentration of ethanol. Antigen retrieval was performed using 10mM sodium citrate and 0.05% tween. Endogenous peroxidase activity was quenched using 1% hydrogen peroxide. The slides were blocked with 5% donkey serum for 30 minutes and incubated with primary antibody at 1:200 dilution overnight at 4°C. The slides were incubated with secondary antibody at 1:500 dilution for 1 hour at room temperature. The stain was then revealed using 3,3′-Diaminobenzidine (DAB) and hydrogen peroxide. The slides were counterstained using hematoxylin. The slides were dehydrated using increasing concentrations of ethanol and mounted with permount.

Imaging and quantification of slides

Sections were imaged using the Axioplan2 imaging upright microscope (Zeiss) located in the Rockefeller University Bio-imaging Resource Center. Representative images were taken at 4x, 10x, 20x, and 40x. For quantification of p-HH3 and cleaved caspase 3, and lipid droplets, several representative 20x images were taken per slide. Positive cells were counted using imageJ and the average was plotted as an individual value. For EdU incorporation, the number of positive cells was counted using imageJ and represented as a percentage of the number of DAPI positive foci.

Cryosectioning and Oil-Red-O

During necropsy, tumor samples were frozen in Tissue-Tek Optimal Cutting Temperature compound (VWR). Frozen blocks were delivered to the Laboratory of Comparative Pathology, where they were cryosectioned and oil-red-o staining was performed.

Metabolomics and lipidomics

Tumor samples were flash frozen in liquid nitrogen during necropsy. 100 ug of sample was homogenized in prechilled 500ul LC-MS grade methanol (Sigma) and 250 ul LC-MS grade water using pre-filled bead mill tubes (Fisher scientific) and the tissuelyzer homogenizer (Qiagen) until fully homogenized. 400uL pre-chilled LC-MS grade chloroform containing 50mM Metabolomics Amino Acid Standard (Cambridge isotope labs) was added. Samples were vortexed and centrifuged to separate the organic and aqueous phases. The top, polar phase was collected for polar metabolite analysis and the bottom, organic layer was collected for lipidomic analysis. Both fractions were dried using a speedvac located in the laboratory of Dr. Kivanç Birsoy at The Rockefeller University. The dried samples were stored at -80°C until use. Targeted polar metabolomics and untargeted lipidomics were performed by The Rockefeller University Proteomics Resource center using LC-MS.

EdU incorporation

Two hours prior to sacrifice, animals received 25 mg/kg EdU via intraperitoneal injection. Animals were sacrificed and dissected. Sections of tumor were placed in histology cassettes and fixed in 10% neutral buffered formalin overnight at 4°C. The next day, the cassettes were washed three times in PBS and transferred to 70% ethanol. The samples were processed by the laboratory for comparative pathology at Memorial Sloan Kettering. The slides were deparaffinized and permeabilized following the protocol for immunohistochemistry. EdU was detected using the Click-It EdU alexa fluor 647 kit (Thermo fisher). Nuclei were stained with incubation of 100ng/mL DAPI for 10 minutes at room temperature. The slides were mounted with ProLong Gold mounting medium (Thermofisher). Alexa 647 and DAPI were imaged using the Rockefeller University Bioimaging Resource Center.

Adipocyte conditioned medium experiments

5,000 cells of the indicated cell line were plated per well of a 96-well plate and incubated under standard conditions overnight. Medium was changed to adipocyte conditioned medium for 24 hours. The MTT assay was performed using the manufacturer's instructions (Sigma).

Oxygen consumption and Extracellular Acidification rate measurements

Oxygen consumption rate and extracellular acidification rates were measured using a 96 well format XF96 Extracellular Flux Analyzer (Seahorse Biosciences). 30,000 cells per well were plated 16 hours before the assay. Mitochondrial or glycolysis stress tests were performed according to the manufacturer's instructions. Oxygen consumption rate or extracellular acidification rate was normalized by cell count staining using NucBlue Reagent (Thermofisher).

Human tumor analysis

Analysis was performed by the Rockefeller University Bioinformatics Resource Center. Gene expression (previously processed with Partek Genomics Suite 6.6) and clinical information for each sample was obtained from Gene Expression Omnibus, using the series 15matrix file of the GSE78958 dataset. Gene expression for each sample was quantile normalized for analysis. Gene expression level changes between groups were tested with one-way ANOVA, followed by post-hoc testing with Tukey's honestly significant test. The p-values for each comparison were adjusted with a Bonferroni correction.

Statistics

For longitudinal tumor volume experiments, a linear mixed effects model for repeated measures was used to analyze data with fixed effects for group, time, and group-by-time interaction. An unstructured covariance matrix was used to model the changes in variances over unequally spaced measurements. A compound symmetry covariance matrix was used in the Acsbg1 KD experiment because it had insufficient degrees of freedom to estimate separate variances and covariances. Post-hoc testing was performed between select groups of interest at the last time point of each experiment. Cube root transformation was applied to skewed tumor volume distributions prior to analysis and chosen over log transformation to deal with tumor volume measurements of 0 mm^3.Residual plots were examined to evaluate the validity of model assumptions. Data analysis was performed using Proc Mixed in SAS Studio version 3.8. For all analyses, * $p< 0.05$, ** $p<0.01$, *** $p<0.001$, **** $p<0.0001$

For RT- qPCR experiments, data was analyzed via one-way ANOVA (one-factor three or more groups), or t-test (one-factor two groups). * $p< 0.05$, ** $p<0.01$, *** $p<0.001$, **** $p<0.0001$.

List of primary antibodies

Antigen	Company	Product Number	Application	Dilution
Actin	Gene-Tex	109639	Western Blot	1-10,000
Acsbg1	Thermofisher	MA5-25104	Western Blot IHC	1-1,000 1-200
Hif-1a	Cell Signaling	36169T	Western Blot	1-1,000
Cleaved-caspase3	Cell Signaling	9664	IHC	1-200
Phosphohistone H3	Millipore	05-636	IHC	1-200
Perilipin -1	Santa Cruz	47320	IHC	1-200

List of qPCR primers

Target	Forward sequence	Reverse Sequence
Slc6a8	GTGTGGAGATCTTCCGCCAT	CCCGTGGAGAGCCTCAATAC
TBP	GGGTATCTGCTGGCGGTTT	TGAAATAGTGATGCTGGGCACT
Acsbg1	ACTCGCAAACCAGCTCCTTA	CCGGGTTGTCCATAGTGCTT
18s	CGATGCTCTTAGCTGAGTGT	GGTCCAAGAATTTCACCTCT
Slc27a4	TGAGATGGCCTCAGCTATCTG	TGCCCGATGTGTAGATGTAGAA
Klf16	ATCCTGGCCGATCTGAGAGG	GTGCGAAGACTTGTAATAGGCT
Acads	CGTAGAGCTCTCGGTGTTCG	AGGTAATCCAAGCCTGCACC
Cebpd	GAACCCGCGGCCTTCTAC	GAAGAGTTCGTCGTGGCACA
Dgka	GATGAACAGATTTTGCCAGGGA	GTAGCAGTACACATCACTGAGAC
Pla2g7	CTTTTCACTGGCAAGACACATCT	CGACGGGGTACGATCCATTTC
Epsti1	CTGGGCTTGCAGCAAAACC	CTGCCTCTCCATCTTGGGG
Acads	CGTAGAGCTCTCGGTGTTCG	AGGTAATCCAAGCCTGCACC
Acadm	TGACAAAAGCGGGGAGTACC	GCACCCCTGTACACCCATAC
Acadl	CCGCCCGATGTTCTCATTCT	CGCCATGTTTCTCTGCGATG
Acadvl	GTAGCCTCCATCCGAAGCTC	CAGGCCCCCATTACTGATCC

Hadha	TGCATTTGCCGCAGCTTTAC	GTTGGCCCAGATTTCGTTCA
Hsd17b10	GGCTTGGTCGCGGTAGTAAC	CCTCTGAGTCAGGTACATCCA

List of cell lines

Cell line	Cell type	origin
E0771	Murine mammary carcinoma	CH3 biosystems
KPC	Murine PDAC	S. Tavazoie lab
UN-KC-6141	Murine PDAC	S. Batra lab
B16F10	Murine melanoma	S. Tavazoie lab
Hepa 1-6	Murine hepatoma	ATCC
MC38	Murine colorectal carcinoma	S. Tavazoie lab
HEK-293T	Human embryonic kidney	ATCC

CHAPTER 9 References

Ackerman, Sarah E. 2020. “The Role of Adipocytes in the Tumor Microenvironent in Obesity-Driven Breast Cancer Progression.” The Rockefeller University.

Ackerman, Sarah E, Olivia A Blackburn, François Marchildon, and Paul Cohen. 2017. “Insights into the Link Between Obesity and Cancer.” *Current Obesity Reports* 6 (2): 195–203. https://doi.org/10.1007/s13679-017-0263-x.

Agilent. 2017. “Glycolysis Stress Test Kit User,” no. July.

Alarmo, Emma Leena, Jenita Pärssinen, Johanna M. Ketolainen, Kimmo Savinainen, Ritva Karhu, and Anne Kallioniemi. 2009. “BMP7 Influences Proliferation, Migration, and Invasion of Breast Cancer Cells.” *Cancer Letters* 275 (1): 35–43. https://doi.org/10.1016/j.canlet.2008.09.028.

Alikhani, N., R. D. Ferguson, R. Novosyadlyy, E. J. Gallagher, E. J. Scheinman, S. Yakar, and D. Leroith. 2013. “Mammary Tumor Growth and Pulmonary Metastasis Are Enhanced in a Hyperlipidemic Mouse Model.” *Oncogene* 32 (8): 961–67. https://doi.org/10.1038/onc.2012.113.

Arnold, Melina, Nirmala Pandeya, Graham Byrnes, Prof Andrew G Renehan, Gretchen A Stevens, Prof Majid Ezzati, Jacques Ferlay, et al. 2015. “Global Burden of Cancer Attributable to High Body-Mass Index in 2012: A Population-Based Study.” *The Lancet. Oncology* 16 (1): 36–46. https://doi.org/10.1016/S1470-2045(14)71123-4.

Baglietto, Laura, Gianluca Severi, Dallas R. English, Kavitha Krishnan, John L. Hopper, Catriona McLean, Howard A. Morris, Wayne D. Tilley, and Graham G. Giles. 2010. “Circulating Steroid Hormone Levels and Risk of Breast Cancer for Postmenopausal Women.” *Cancer Epidemiology Biomarkers and Prevention* 19 (2): 492–502. https://doi.org/10.1158/1055-9965.EPI-09-0532.

Balaban, Seher, Robert F. Shearer, Lisa S. Lee, Michelle van Geldermalsen, Mark Schreuder, Harrison C. Shtein, Rose Cairns, et al. 2017. “Adipocyte Lipolysis Links Obesity to Breast Cancer Growth: Adipocyte-Derived Fatty Acids Drive Breast Cancer Cell Proliferation and Migration.” *Cancer & Metabolism* 5 (1): 1–14. https://doi.org/10.1186/s40170-016-0163-7.

Barone, Bethany B, Hsin-Chieh Yeh, Claire F Snyder, Kimberly S Peairs, Kelly B Stein, Rachel L Derr, Antonio C Wolff, and Frederick L Brancati. 2008. “Long-Term All-Cause Mortality in Cancer Patients with Preexisting Diabetes Mellitus: A Systematic Review and Meta-Analysis.” *JAMA* 300 (23): 2754–64. https://doi.org/10.1001/jama.2008.824.

Barone, Ines, Cinzia Giordano, Daniela Bonofiglio, Sebastiano Andò, and Stefania Catalano. 2020. “The Weight of Obesity in Breast Cancer Progression and Metastasis: Clinical and Molecular Perspectives.” *Seminars in Cancer Biology* 60 (September 2019): 274–84. https://doi.org/10.1016/j.semcancer.2019.09.001.

Behan, James W., Ehsan A. Ehsanipour, Xia Sheng, Rocky Pramanik, Xingchao Wang, Yao Te Hsieh, Yong Mi Kim, and Steven D. Mittelman. 2013. “Activation of Adipose Tissue Macrophages in Obese Mice Does Not Require Lymphocytes.” *Obesity* 21 (7): 1380–88. https://doi.org/10.1002/oby.20159.

Berg, a H, T P Combs, X Du, M Brownlee, and P E Scherer. 2001. “The Adipocyte-Secreted Protein Acrp30 Enhances Hepatic Insulin Action.” *Nature Medicine* 7 (8): 947–53. https://doi.org/10.1038/90992.

Bessman, S. 1985. “The Creatine-Creatine Phosphate Energy Shuttle.” *Annual Review of Biochemistry* 54 (1): 831–62. https://doi.org/10.1146/annurev.biochem.54.1.831.

Bhaskaran, Krishnan, Ian Douglas, Harriet Forbes, Isabel dos-Santos-Silva, David A Leon, and Liam Smeeth. 2014. "Body-Mass Index and Risk of 22 Specific Cancers: A Population-Based Cohort Study of 5·24 Million UK Adults." *Lancet* 384 (9945): 755–65. https://doi.org/10.1016/S0140-6736(14)60892-8.

Blasbalg, Tanya L., Joseph R. Hibbeln, Christopher E. Ramsden, Sharon F. Majchrzak, and Robert R. Rawlings. 2011. "Changes in Consumption of Omega-3 and Omega-6 Fatty Acids in the United States during the 20th Century." *American Journal of Clinical Nutrition* 93 (5): 950–62. https://doi.org/10.3945/ajcn.110.006643.

Blücher, Christina, and Sonja C. Stadler. 2017. "Obesity and Breast Cancer: Current Insights on the Role of Fatty Acids and Lipid Metabolism in Promoting Breast Cancer Growth and Progression." *Frontiers in Endocrinology* 8 (OCT): 1–7. https://doi.org/10.3389/fendo.2017.00293.

Bråkenhielm, Ebba, Niina Veitonmäki, Renhai Cao, Shinji Kihara, Yuji Matsuzawa, Boris Zhivotovsky, Tohru Funahashi, and Yihai Cao. 2004. "Adiponectin-Induced Antiangiogenesis and Antitumor Activity Involve Caspase-Mediated Endothelial Cell Apoptosis." *Proceedings of the National Academy of Sciences of the United States of America* 101 (8): 2476–81. https://doi.org/10.1073/pnas.0308671100.

Brown, N. S., and R. Bicknell. 2001. "Oxidative Stress: Its Effects on the Growth, Metastatic Potential and Response to Therapy of Breast Cancer." *Breast Cancer Research* 3 (5): 323–27. https://doi.org/10.1186/bcr315.

Brown, Raya S., and Richard L. Wahl. 1993. "Overexpression of Glut-1 Glucose Transporter in Human Breast Cancer an Immunohistochemical Study." *Cancer* 72 (10): 2979–85. https://doi.org/10.1002/1097-0142(19931115)72:10<2979::AID-CNCR2820721020>3.0.CO;2-X.

Bu, Dawei, Clair Crewe, Christine M Kusminski, Ruth Gordillo, Alexandra L Ghaben, Min Kim, Jiyoung Park, et al. 2019. "Human Endotrophin as a Driver of Malignant Tumor Growth." *JCI Insight* 5. https://doi.org/10.1172/jci.insight.125094.

Calle, Eugenia E, Carmen Rodriguez, Kimberly Walker-Thurmond, and Michael J Thun. 2003. "Overweight, Obesity, and Mortality from Cancer in a Prospectively Studied Cohort of U.S. Adults." *The New England Journal of Medicine* 348 (17): 1625–38. https://doi.org/10.1056/NEJMoa021423.

Cao, Y., K. B. Dave, T. P. Doan, and S. M. Prescott. 2001. "Fatty Acid CoA Ligase 4 Is Up-Regulated in Colon Adenocarcinoma." *Cancer Research* 61 (23): 8429–34.

Cavanagh, Brenton L., Tom Walker, Anwar Norazit, and Adrian C.B. Meedeniya. 2011. "Thymidine Analogues for Tracking DNA Synthesis." *Molecules* 16 (9): 7980–93. https://doi.org/10.3390/molecules16097980.

Chadee, Deborah N., Michael J. Hendzel, Cheryl P. Tylipski, C. David Allis, David P. Bazett-Jones, Jim A. Wright, and James R. Davie. 1999. "Increased Ser-10 Phosphorylation of Histone H3 in Mitogen-Stimulated and Oncogene-Transformed Mouse Fibroblasts." *Journal of Biological Chemistry* 274 (35): 24914–20. https://doi.org/10.1074/jbc.274.35.24914.

Chan, D. S.M., A. R. Vieira, D. Aune, E. V. Bandera, D. C. Greenwood, A. McTiernan, D. Navarro Rosenblatt, I. Thune, R. Vieira, and T. Norat. 2014. "Body Mass Index and Survival in Women with Breast Cancer—Systematic Literature Review and Meta-Analysis of 82 Follow-up Studies." *Annals of Oncology* 25 (10): 1901–14. https://doi.org/10.1093/annonc/mdu042.

Chang, Qing, Laura Daly, and Jacqueline Bromberg. 2014. “The IL-6 Feed-Forward Loop: A Driver of Tumorigenesis.” *Seminars in Immunology* 26 (1): 48–53. https://doi.org/10.1016/j.smim.2014.01.007.

Chen, Fei Yu, Hui Ying Ou, Shou Man Wang, Yu Hui Wu, Guo Jiao Yan, and Li Li Tang. 2013. “Associations between Body Mass Index and Molecular Subtypes as Well as Other Clinical Characteristics of Breast Cancer in Chinese Women.” *Therapeutics and Clinical Risk Management* 9 (1): 131–37. https://doi.org/10.2147/TCRM.S41203.

Chen, Lu, Linda S. Cook, Mei Tzu C. Tang, Peggy L. Porter, Deirdre A. Hill, Charles L. Wiggins, and Christopher I. Li. 2016. “Body Mass Index and Risk of Luminal, HER2-Overexpressing, and Triple Negative Breast Cancer.” *Breast Cancer Research and Treatment* 157 (3): 545–54. https://doi.org/10.1007/s10549-016-3825-9.

Chen, Wensen, Sumin Wang, Tian Tian, Jianling Bai, Zhibin Hu, Yan Xu, Jing Dong, Feng Chen, Xinru Wang, and Hongbing Shen. 2009. “Phenotypes and Genotypes of Insulin-like Growth Factor 1, IGF-Binding Protein-3 and Cancer Risk: Evidence from 96 Studies.” *European Journal of Human Genetics* 17 (12): 1668–75. https://doi.org/10.1038/ejhg.2009.86.

Cimpean, Anca Maria, Roberto Tamma, Simona Ruggieri, Beatrice Nico, Alina Toma, and Domenico Ribatti. 2017. “Mast Cells in Breast Cancer Angiogenesis.” *Critical Reviews in Oncology/Hematology* 115: 23–26. https://doi.org/10.1016/j.critrevonc.2017.04.009.

Cohen, Dara Hope, and Derek LeRoith. 2012. “Obesity, Type 2 Diabetes, and Cancer: The Insulin and IGF Connection.” *Endocrine-Related Cancer* 19 (5): 27–45. https://doi.org/10.1530/ERC-11-0374.

Coussens, Lisa, and Zena Werb. 2018. “Inflammation and Cancer.” *Environmental Health and Preventive Medicine* 23 (1). https://doi.org/10.1186/s12199-018-0740-1.

Cowen, Sarah, Sarah L McLaughlin, Gerald Hobbs, James Coad, Karen H Martin, I Mark Olfert, and Linda Vona-Davis. 2015. “High-Fat, High-Calorie Diet Enhances Mammary Carcinogenesis and Local Inflammation in MMTV-PyMT Mouse Model of Breast Cancer.” *Cancers* 7 (3): 1125–42. https://doi.org/10.3390/cancers7030828.

Dalamaga, M, K N Diakopoulos, and C S Mantzoros. 2012. “The Role of Adiponectin in Cancer: A Review of Current Evidence.” *Endocr Rev* 33 (4): 547–94. https://doi.org/10.1210/er.2011-1015.

Dirat, Béatrice, Ludivine Bochet, Marta Dabek, Danièle Daviaud, Stéphanie Dauvillier, Bilal Majed, Yuan Yuan Wang, et al. 2011. “Cancer-Associated Adipocytes Exhibit an Activated Phenotype and Contribute to Breast Cancer Invasion.” *Cancer Research* 71 (7): 2455–65. https://doi.org/10.1158/0008-5472.CAN-10-3323.

Ellis, Jessica M., Jennifer L. Frahm, Lei O. Li, and Rosalind A. Coleman. 2010. “Acyl-Coenzyme A Synthetases in Metabolic Control.” *Current Opinion in Lipidology* 21 (3): 212–17. https://doi.org/10.1097/MOL.0b013e32833884bb.

Erdmann, Ines, Kathrin Marter, Oliver Kobler, Sven Niehues, Julia Abele, Anke Müller, Julia Bussmann, et al. 2015. “Cell-Selective Labelling of Proteomes in Drosophila Melanogaster.” *Nature Communications* 6 (May). https://doi.org/10.1038/ncomms8521.

Ewertz, Marianne, Maj Britt Jensen, Katrín Á Gunnarsdóttir, Inger Højris, Erik H. Jakobsen, Dorte Nielsen, Lars E. Stenbygaard, Ulla B. Tange, and Søren Cold. 2011. “Effect of Obesity on Prognosis after Early-Stage Breast Cancer.” *Journal of Clinical Oncology* 29 (1): 25–31. https://doi.org/10.1200/JCO.2010.29.7614.

Ferguson, Rosalyn D, Ruslan Novosyadlyy, Yvonne Fierz, Nyosha Alikhani, Hui Sun, Shoshana

Yakar, and Derek Leroith. 2012. “Hyperinsulinemia Enhances C-Myc-Mediated Mammary Tumor Development and Advances Metastatic Progression to the Lung in a Mouse Model of Type 2 Diabetes.” *Breast Cancer Research : BCR* 14 (1): R8. https://doi.org/10.1186/bcr3089.

Font-Burgada, Joan, Beicheng Sun, and Michael Karin. 2016. “Obesity and Cancer: The Oil That Feeds the Flame.” *Cell Metabolism* 23 (1): 48–62. https://doi.org/10.1016/j.cmet.2015.12.015.

Frydenberg, H., I. Thune, T. Lofterød, E. S. Mortensen, A. E. Eggen, T. Risberg, E. A. Wist, et al. 2016. “Pre-Diagnostic High-Sensitive C-Reactive Protein and Breast Cancer Risk, Recurrence, and Survival.” *Breast Cancer Research and Treatment* 155 (2): 345–54. https://doi.org/10.1007/s10549-015-3671-1.

Fukushima, Shintaro, Mizuhiko Terasaki, Kiyohiko Sakata, Naohisa Miyagi, Seiya Kato, Yasuo Sugita, and Minoru Shigemori. 2009. “Sensitivity and Usefulness of Anti-Phosphohistone-H3 Antibody Immunostaining for Counting Mitotic Figures in Meningioma Cases.” *Brain Tumor Pathology* 26 (2): 51–57. https://doi.org/10.1007/s10014-009-0249-9.

Fuster, José J., Noriyuki Ouchi, Noyan Gokce, and Kenneth Walsh. 2016. “Obesity-Induced Changes in Adipose Tissue Microenvironment and Their Impact on Cardiovascular Disease.” *Circulation Research* 118 (11): 1786–1807. https://doi.org/10.1161/CIRCRESAHA.115.306885.

Gallagher, E. J., Z. Zelenko, B. A. Neel, I. M. Antoniou, L. Rajan, N. Kase, and D. LeRoith. 2017. “Elevated Tumor LDLR Expression Accelerates LDL Cholesterol-Mediated Breast Cancer Growth in Mouse Models of Hyperlipidemia.” *Oncogene* 36 (46): 6462–71. https://doi.org/10.1038/onc.2017.247.

Garcia-Bermudez, Javier, Lou Baudrier, Konnor La, Xiphias Ge Zhu, Justine Fidelin, Vladislav O. Sviderskiy, Thales Papagiannakopoulos, et al. 2018. “Aspartate Is a Limiting Metabolite for Cancer Cell Proliferation under Hypoxia and in Tumours.” *Nature Cell Biology* 20 (7): 775–81. https://doi.org/10.1038/s41556-018-0118-z.

Gaudet, Mia M., Michael F. Press, Robert W. Haile, Charles F. Lynch, Sally L. Glaser, Joellen Schildkraut, Marilie D. Gammon, W. Douglas Thompson, and Jonine L. Bernstein. 2011. “Risk Factors by Molecular Subtypes of Breast Cancer across a Population-Based Study of Women 56 Years or Younger.” *Breast Cancer Research and Treatment* 130 (2): 587–97. https://doi.org/10.1007/s10549-011-1616-x.

Gérard, Céline, and Kristy A. Brown. 2018. “Obesity and Breast Cancer – Role of Estrogens and the Molecular Underpinnings of Aromatase Regulation in Breast Adipose Tissue.” *Molecular and Cellular Endocrinology* 466: 15–30. https://doi.org/10.1016/j.mce.2017.09.014.

Gerdes, Johannes, Ulrich Schwab, Hilmar Lemke, and Harald Stein. 1991. “Production of a Mouse Monoclonal Antibody (B1N) Reactive with a Human Nuclear Antigen Associated with Cell Proliferation.” *Comptes Rendus de l’Academie Des Sciences - Serie III* 312 (7): 301–7. https://doi.org/10.1002/ijc.v31:1.

Goossens, Gijs H. 2017. “The Metabolic Phenotype in Obesity: Fat Mass, Body Fat Distribution, and Adipose Tissue Function.” *Obesity Facts* 10 (3): 207–15. https://doi.org/10.1159/000471488.

Grevengoed, Trisha J., Eric L. Klett, and Rosalind A. Coleman. 2014. “Acyl-CoA Metabolism and Partitioning.” *Annual Review of Nutrition* 34 (1): 1–30. https://doi.org/10.1146/annurev-nutr-071813-105541.

Gunter, Marc J., Donald R. Hoover, Herbert Yu, Sylvia Wassertheil-Smoller, Thomas E. Rohan, Joann E. Manson, Jixin Li, et al. 2009. "Insulin, Insulin-like Growth Factor-I, and Risk of Breast Cancer in Postmenopausal Women." *Journal of the National Cancer Institute* 101 (1): 48–60. https://doi.org/10.1093/jnci/djn415.

Hales, CM, MD Carroll, CD Fryar, and CL Ogden. 2020. "Prevalence of Obesity and Severe Obesity Among Adults: United States, 2017-2018." *NCHS Data Brief* 360 (360): 1–8. http://www.ncbi.nlm.nih.gov/pubmed/26633046.

Hao, Qian, Cong Dai, Yujiao Deng, Peng Xu, Tian Tian, Shuai Lin, Meng Wang, et al. 2018. "Pooling Analysis on Prognostic Value of PHH3 Expression in Cancer Patients." *Cancer Management and Research* 10: 2279–88. https://doi.org/10.2147/CMAR.S167569.

Hendzel, Michael J., Yi Wei, Michael A. Mancini, Aaron Van Hooser, Tamara Ranalli, B. R. Brinkley, David P. Bazett-Jones, and C. David Allis. 1997. "Mitosis-Specific Phosphorylation of Histone H3 Initiates Primarily within Pericentromeric Heterochromatin during G2 and Spreads in an Ordered Fashion Coincident with Mitotic Chromosome Condensation." *Chromosoma* 106 (6): 348–60. https://doi.org/10.1007/s004120050256.

Hingorani, Sunil R., Emanuel F. Petricoin, Anirban Maitra, Vinodh Rajapakse, Catrina King, Michael A. Jacobetz, Sally Ross, et al. 2003. "Preinvasive and Invasive Ductal Pancreatic Cancer and Its Early Detection in the Mouse." *Cancer Cell* 4 (6): 437–50. https://doi.org/10.1016/S1535-6108(03)00309-X.

Hu, Guoming, Shimin Wang, and Pu Cheng. 2018. "Tumor-Infiltrating Tryptase+ Mast Cells Predict Unfavorable Clinical Outcome in Solid Tumors." *International Journal of Cancer* 142 (4): 813–21. https://doi.org/10.1002/ijc.31099.

Iyengar, Neil M., Clifford A. Hudis, and Andrew J. Dannenberg. 2013. "Obesity and Inflammation: New Insights into Breast Cancer Development and Progression." *American Society of Clinical Oncology Educational Book*, no. 33: 46–51. https://doi.org/10.14694/edbook_am.2013.33.46.

Iyengar, Neil M, Clifford a Hudis, and Andrew J Dannenberg. 2015. "Obesity and Cancer: Local and Systemic Mechanisms." *Annual Review of Medicine* 66: 297–309. https://doi.org/10.1146/annurev-med-050913-022228.

Iyengar, Neil M, Xi Kathy Zhou, Ayca Gucalp, Patrick G Morris, Louise R Howe, Dilip D Giri, Monica Morrow, et al. 2016. "Systemic Correlates of White Adipose Tissue Inflammation in Early-Stage Breast Cancer." *Clinical Cancer Research: An Official Journal of the American Association for Cancer Research* 22 (9): 2283–89. https://doi.org/10.1158/1078-0432.CCR-15-2239.

Iyengar, Puneeth, Paolo Bonaldo, and Phillipp Scherer. 2005. "Adipocyte-Derived Collagen VI Affects Early Mammary Tumor Progression in Vivo, Demonstrating a Critical Interaction in the Tumor/Stroma Microenvironment." *JCI* 115 (5): 8–10. https://doi.org/10.1172/JCI200523424.The.

Iyer, Narayan V., Lori E. Kotch, Faton Agani, Sandra W. Leung, Erik Laughner, Roland H. Wenger, Max Gassmann, et al. 1998. "Cellular and Developmental Control of O2 Homeostasis by Hypoxia- Inducible Factor 1α." *Genes and Development* 12 (2): 149–62. https://doi.org/10.1101/gad.12.2.149.

Jeschke, Jana, Heather M. O'Hagan, Wei Zhang, Rajita Vatapalli, Marilia Freitas Calmon, Ludmila Danilova, Claudia Nelkenbrecher, et al. 2013. "Frequent Inactivation of Cysteine Dioxygenase Type 1 Contributes to Survival of Breast Cancer Cells and Resistance to Anthracyclines." *Clinical Cancer Research* 19 (12): 3201–11. https://doi.org/10.1158/1078-

0432.CCR-12-3751.
Jögi, Annika, Anna Ehinger, Linda Hartman, and Sara Alkner. 2019. “Expression of HIF-1α Is Related to a Poor Prognosis and Tamoxifen Resistance in Contralateral Breast Cancer.” *PLoS ONE* 14 (12): 1–17. https://doi.org/10.1371/journal.pone.0226150.
Johnstone, Cameron N, Yvonne E Smith, Yuan Cao, Allan D Burrows, Ryan S N Cross, Xiawei Ling, Richard P Redvers, et al. 2015. “Functional and Molecular Characterisation of EO771.LMB Tumours, a New C57BL/6-Mouse-Derived Model of Spontaneously Metastatic Mammary Cancer.” *Disease Models & Mechanisms* 8 (3): 237–51. https://doi.org/10.1242/dmm.017830.
Jung, Un Ju, and Myung Sook Choi. 2014. “Obesity and Its Metabolic Complications: The Role of Adipokines and the Relationship between Obesity, Inflammation, Insulin Resistance, Dyslipidemia and Nonalcoholic Fatty Liver Disease.” *International Journal of Molecular Sciences* 15 (4): 6184–6223. https://doi.org/10.3390/ijms15046184.
Kadowaki, Takashi, Toshimasa Yamauchi, Naoto Kubota, Kazuo Hara, Kohjiro Ueki, and Kazuyuki Tobe. 2006. “Adiponectin and Adiponectin Receptors in Insulin Resistance, Diabetes, and the Metabolic Syndrome.” *The Journal of Clinical Investigation* 116 (7): 1784–92. https://doi.org/10.1172/JCI29126.
Kahn, Barbara B, Jeffrey S Flier, Barbara B Kahn, and Jeffrey S Flier. 2000. “Obesity and Insulin Resistance Find the Latest Version : Obesity and Insulin Resistance” 106 (4): 473–81. https://doi.org/10.1172/JCI10842.
Kazak, Lawrence, Edward T. Chouchani, Mark P. Jedrychowski, Brian K. Erickson, Kosaku Shinoda, Paul Cohen, Ramalingam Vetrivelan, et al. 2015. “A Creatine-Driven Substrate Cycle Enhances Energy Expenditure and Thermogenesis in Beige Fat.” *Cell* 163 (3): 643–55. https://doi.org/10.1016/j.cell.2015.09.035.
Kim, A Young, Yun Sok Lee, Kang Ho Kim, Jae Ho Lee, Hee Kyu Lee, Su-Hwa Jang, Seong-Eun Kim, et al. 2010. “Adiponectin Represses Colon Cancer Cell Proliferation via AdipoR1- and -R2-Mediated AMPK Activation.” *Molecular Endocrinology (Baltimore, Md.)* 24 (7): 1441–52. https://doi.org/10.1210/me.2009-0498.
Kim, Ji Ye, Hyang Sook Jeong, Taek Chung, Moonsik Kim, Ji Hee Lee, Woo Hee Jung, and Ja Seung Koo. 2017. “The Value of Phosphohistone H3 as a Proliferation Marker for Evaluating Invasive Breast Cancers: A Comparative Study with Ki67.” *Oncotarget* 8 (39): 65064–76. https://doi.org/10.18632/oncotarget.17775.
Kitahara, Cari M., Amy Berrington De González, Neal D. Freedman, Rachel Huxley, Yejin Mok, Sun Ha Jee, and Jonathan M. Samet. 2011. “Total Cholesterol and Cancer Risk in a Large Prospective Study in Korea.” *Journal of Clinical Oncology* 29 (12): 1592–98. https://doi.org/10.1200/JCO.2010.31.5200.
Klop, Boudewijn, Jan Willem F. Elte, and Manuel Castro Cabezas. 2013. “Dyslipidemia in Obesity: Mechanisms and Potential Targets.” *Nutrients* 5 (4): 1218–40. https://doi.org/10.3390/nu5041218.
Kolb, Ryan, Liem Phan, Nicholas Borcherding, Yinghong Liu, Fang Yuan, Ann M Janowski, Qing Xie, et al. 2016. “Obesity-Associated NLRC4 Inflammasome Activation Drives Breast Cancer Progression.” *Nature Communications* 7. https://doi.org/10.1038/ncomms13007.
Kuemmerle, Nancy B., Evelien Rysman, Portia S. Lombardo, Alison J. Flanagan, Brea C. Lipe, Wendy A. Wells, Jason R. Pettus, et al. 2011. “Lipoprotein Lipase Links Dietary Fat to Solid Tumor Cell Proliferation.” *Molecular Cancer Therapeutics* 10 (3): 427–36.

https://doi.org/10.1158/1535-7163.MCT-10-0802.
LeRoith, Derek, and Charles T. Roberts. 2003. “The Insulin-like Growth Factor System and Cancer.” *Cancer Letters* 195 (2): 127–37. https://doi.org/10.1016/S0304-3835(03)00159-9.
Liberti, Maria V, and Jason W Locasale. 2016. “The Warburg Effect: How Does It Benefit Cancer Cells? (Vol 41, Pg 211, 2016).” *Trends in Biochemical Sciences* 41 (3, SI): 287. https://doi.org/10.1016/j.tibs.2016.01.004.
Link, A. James, Mandy K.S. Vink, Nicholas J. Agard, Jennifer A. Prescher, Carolyn R. Bertozzi, and David A. Tirrell. 2006. “Discovery of Aminoacyl-TRNA Synthetase Activity through Cell-Surface Display of Noncanonical Amino Acids.” *Proceedings of the National Academy of Sciences of the United States of America* 103 (27): 10180–85. https://doi.org/10.1073/pnas.0601167103.
Liu, Yan, Michael J. Conboy, Melod Mehdipour, Yutong Liu, Thanhtra P. Tran, Aaron Blotnick, Prasanna Rajan, Thalie Cavalcante Santos, and Irina M. Conboy. 2017. “Application of Bio-Orthogonal Proteome Labeling to Cell Transplantation and Heterochronic Parabiosis.” *Nature Communications* 8 (1). https://doi.org/10.1038/s41467-017-00698-y.
Lopes-Marques, Mónica, André M. Machado, Raquel Ruivo, Elza Fonseca, Estela Carvalho, and L. Filipe C. Castro. 2018. “Expansion, Retention and Loss in the Acyl-CoA Synthetase ‘Bubblegum’ (Acsbg) Gene Family in Vertebrate History.” *Gene* 664 (April): 111–18. https://doi.org/10.1016/j.gene.2018.04.058.
López-Ibáñez, Javier, Florencio Pazos, and Mónica Chagoyen. 2016. “MBROLE 2.0-Functional Enrichment of Chemical Compounds.” *Nucleic Acids Research* 44 (W1): W201–4. https://doi.org/10.1093/nar/gkw253.
Madak-Erdogan, Zeynep, Shoham Band, Yiru C. Zhao, Brandi P. Smith, Eylem Kulkoyluoglu-Cotul, Qianying Zuo, Ashlie Santaliz Casiano, et al. 2019. “Free Fatty Acids Rewire Cancer Metabolism in Obesity-Associated Breast Cancer via Estrogen Receptor and MTOR Signaling.” *Cancer Research* 79 (10): 2494–2510. https://doi.org/10.1158/0008-5472.CAN-18-2849.
Mahdavi, Alborz, Graham D. Hamblin, Granton A. Jindal, John D. Bagert, Cathy Dong, Michael J. Sweredoski, Sonja Hess, Erin M. Schuman, and David A. Tirrell. 2016. “Engineered Aminoacyl-TRNA Synthetase for Cell-Selective Analysis of Mammalian Protein Synthesis.” *Journal of the American Chemical Society* 138 (13): 4278–81. https://doi.org/10.1021/jacs.5b08980.
Majorini, Maria Teresa, Valeria Cancila, Alice Rigoni, Laura Botti, Matteo Dugo, Tiziana Triulzi, and Loris De. 2020. “Infiltrating Mast Cell-Mediated Stimulation of Estrogen Receptor Activity in Breast Cancer Cells Promotes the Luminal Phenotype Word Count : 5756 Words , 7 Figures , 47 References (1 Supplementary Table and 3 Supplementary.” https://doi.org/10.1158/0008-5472.CAN-19-3596.
Makoukji, Joelle, Nadine J. Makhoul, Maya Khalil, Sally El-Sitt, Ehab Saad Aldin, Mark Jabbour, Fouad Boulos, et al. 2016. “Gene Expression Profiling of Breast Cancer in Lebanese Women.” *Scientific Reports* 6: 1–13. https://doi.org/10.1038/srep36639.
Maloberti, Paula M., Alejandra B. Duarte, Ulises D. Orlando, María E. Pasqualini, Angela R. Solano, Carlos Lopez-Otín, and Ernesto J. Podesta. 2010. “Functional Interaction between Acyl-Coa Synthetase 4, Lipooxygenases and Cyclooxygenase-2 in the Aggressive Phenotype of Breast Cancer Cells.” *PLoS ONE* 5 (11). https://doi.org/10.1371/journal.pone.0015540.
Mashek, Douglas G., Lei O. Li, and Rosalind A. Coleman. 2007. “Long-Chain Acyl-CoA

Synthetases and Fatty Acid Channeling." *Future Lipidology* 2 (4): 465–76. https://doi.org/10.2217/17460875.2.4.465.
Mashima, Tetsuo, Tomoko Oh-hara, Shigeo Sato, Mikiko Mochizuki, Yoshikazu Sugimoto, Kanami Yamazaki, Jun Ichi Hamada, et al. 2005. "P53-Defective Tumors with a Functional Apoptosome-Mediated Pathway: A New Therapeutic Target." *Journal of the National Cancer Institute* 97 (10): 765–77. https://doi.org/10.1093/jnci/dji133.
McIlwain, David R., Thorsten Berger, and Tak W. Mak. 2015. "Caspase Functions in Cell Death and Disease." *Cold Spring Harbor Perspectives in Biology* 7 (4). https://doi.org/10.1101/cshperspect.a026716.
Melvin, Jennifer C., Lars Holmberg, Sabine Rohrmann, Massimo Loda, and Mieke Van Hemelrijck. 2013. "Serum Lipid Profiles and Cancer Risk in the Context of Obesity: Four Meta-Analyses." *Journal of Cancer Epidemiology* 2013: 18–20. https://doi.org/10.1155/2013/823849.
Miyoshi, Yasuo, Tohru Funahashi, Sachiyo Tanaka, Tetsuya Taguchi, Yasuhiro Tamaki, Iichiro Shimomura, and Shinzaburo Noguchi. 2006. "High Expression of Leptin Receptor MRNA in Breast Cancer Tissue Predicts Poor Prognosis for Patients with High, but Not Low, Serum Leptin Levels." *International Journal of Cancer* 118 (6): 1414–19. https://doi.org/10.1002/ijc.21543.
Monaco, Marie E., Chad J. Creighton, Peng Lee, Xuanyi Zou, Matthew K. Topham, and Diana M. Stafforini. 2010. "Expression of Long-Chain Fatty Acyl-CoA Synthetase 4 in Breast and Prostate Cancers Is Associated with Sex Steroid Hormone Receptor Negativity." *Translational Oncology* 3 (2): 91–98. https://doi.org/10.1593/tlo.09202.
Mookerjee, Shona A., Renata L.S. Goncalves, Akos A. Gerencser, David G. Nicholls, and Martin D. Brand. 2015. "The Contributions of Respiration and Glycolysis to Extracellular Acid Production." *Biochimica et Biophysica Acta - Bioenergetics* 1847 (2): 171–81. https://doi.org/10.1016/j.bbabio.2014.10.005.
Morris, Patrick G, Clifford A Hudis, Dilip Giri, Monica Morrow, Domenick J Falcone, Xi Kathy Zhou, Baoheng Du, et al. 2011. "Inflammation and Increased Aromatase Expression Occur in the Breast Tissue of Obese Women with Breast Cancer." *Cancer Prevention Research (Philadelphia, Pa.)* 4 (7): 1021–29. https://doi.org/10.1158/1940-6207.CAPR-11-0110.
Murano, I., G. Barbatelli, V. Parisani, C. Latini, G. Muzzonigro, M. Castellucci, and S. Cinti. 2008. "Dead Adipocytes, Detected as Crown-like Structures, Are Prevalent in Visceral Fat Depots of Genetically Obese Mice." *Journal of Lipid Research* 49 (7): 1562–68. https://doi.org/10.1194/jlr.M800019-JLR200.
Nadanaciva, Sashi, Payal Rana, Gyda C. Beeson, Denise Chen, David A. Ferrick, Craig C. Beeson, and Yvonne Will. 2012. "Assessment of Drug-Induced Mitochondrial Dysfunction via Altered Cellular Respiration and Acidification Measured in a 96-Well Platform." *Journal of Bioenergetics and Biomembranes* 44 (4): 421–37. https://doi.org/10.1007/s10863-012-9446-z.
National Cancer Institute. 2020. "Cancer Stat Facts: Female Breast Cancer." Cancer Stat Facts. 2020. https://seer.cancer.gov/statfacts/html/breast.html.
Nelson, Erik R., Suzanne E. Wardell, Jeff S. Jasper, Sunghee Park, Sunil Suchindran, Matthew K. Howe, Nicole J. Carver, et al. 2013. "27-Hydroxycholesterol Links Hypercholesterolemia and Breast Cancer Pathophysiology." *Science* 342 (6162): 1094–98. https://doi.org/10.1126/science.1241908.
Neuhouser, Marian L., Aaron K. Aragaki, Ross L. Prentice, Jo Ann E. Manson, Rowan

Chlebowski, Cara L. Carty, Heather M. Ochs-Balcom, et al. 2015. “Overweight, Obesity, and Postmenopausal Invasive Breast Cancer Risk: A Secondary Analysis of the Women’s Health Initiative Randomized Clinical Trials.” *JAMA Oncology* 1 (5): 611–21. https://doi.org/10.1001/jamaoncol.2015.1546.

Neuhouser, Marian L, Aaron K Aragaki, Ross L Prentice, E Joann, Rowan Chlebowski, Cara L Carty, M Heather, et al. 2016. “HHS Public Access” 1 (5): 611–21. https://doi.org/10.1001/jamaoncol.2015.1546.Overweight.

Newman, Aaron M., Chloé B. Steen, Chih Long Liu, Andrew J. Gentles, Aadel A. Chaudhuri, Florian Scherer, Michael S. Khodadoust, et al. 2019. “Determining Cell Type Abundance and Expression from Bulk Tissues with Digital Cytometry.” *Nature Biotechnology* 37 (July). https://doi.org/10.1038/s41587-019-0114-2.

Ngo, John T., Julie A. Champion, Alborz Mahdavi, I. Caglar Tanrikulu, Kimberly E. Beatty, Rebecca E. Connor, Tae Hyeon Yoo, Daniela C. Dieterich, Erin M. Schuman, and David A. Tirrell. 2009. “Cell-Selective Metabolic Labeling of Proteins.” *Nature Chemical Biology* 5 (10): 715–17. https://doi.org/10.1038/nchembio.200.

Nielsen, Sune F., Børge G. Nordestgaard, and Stig E. Bojesen. 2012. “Statin Use and Reduced Cancer-Related Mortality.” *New England Journal of Medicine* 367 (19): 1792–1802. https://doi.org/10.1056/NEJMoa1201735.

Nieman, Kristin M., Hilary A. Kenny, Carla V. Penicka, Andras Ladanyi, Rebecca Buell-Gutbrod, Marion R. Zillhardt, Iris L. Romero, et al. 2011. “Adipocytes Promote Ovarian Cancer Metastasis and Provide Energy for Rapid Tumor Growth.” *Nature Medicine* 17 (11): 1498–1503. https://doi.org/10.1038/nm.2492.

Park, Jiyoung, Christine M. Kusminski, Streamson C. Chua, and Philipp E. Scherer. 2010. “Leptin Receptor Signaling Supports Cancer Cell Metabolism through Suppression of Mitochondrial Respiration in Vivo.” *The American Journal of Pathology* 177 (6): 3133–44. https://doi.org/10.2353/ajpath.2010.100595.

Park, Jiyoung, and Philipp E. Scherer. 2012. “Adipocyte-Derived Endotrophin Promotes Malignant Tumor Progression.” *Journal of Clinical Investigation* 122 (11): 4243–56. https://doi.org/10.1172/JCI63930.

Pathmanathan, Nirmala, and Rosemary L. Balleine. 2013. “Ki67 and Proliferation in Breast Cancer.” *Journal of Clinical Pathology* 66 (6): 512–16. https://doi.org/10.1136/jclinpath-2012-201085.

Pei, Zhengtong, Nadia A. Oey, Maartje M. Zuidervaart, Zhenzhen Jia, Yuanyuan Li, Steven J. Steinberg, Kirby D. Smith, and Paul A. Watkins. 2003. “The Acyl-CoA Synthetase ‘Bubblegum’ (Lipidosin): Further Characterization and Role in Neuronal Fatty Acid β-Oxidation.” *Journal of Biological Chemistry* 278 (47): 47070–78. https://doi.org/10.1074/jbc.M310075200.

Petrova, Varvara, Margherita Annicchiarico-Petruzzelli, Gerry Melino, and Ivano Amelio. 2018. “The Hypoxic Tumour Microenvironment.” *Oncogenesis* 7 (1). https://doi.org/10.1038/s41389-017-0011-9.

Picon-Ruiz, Manuel, Cynthia Morata-Tarifa, Janeiro J. Valle-Goffin, Eitan R. Friedman, and Joyce M. Slingerland. 2017. “Obesity and Adverse Breast Cancer Risk and Outcome: Mechanistic Insights and Strategies for Intervention.” *CA: A Cancer Journal for Clinicians* 67 (5): 378–97. https://doi.org/10.3322/caac.21405.

Pierce, Brandon L, Rachel Ballard-Barbash, Leslie Bernstein, Richard N Baumgartner, Marian L Neuhouser, Mark H Wener, Kathy B Baumgartner, et al. 2009. “Elevated Biomarkers of

Inflammation Are Associated with Reduced Survival among Breast Cancer Patients." *Journal of Clinical Oncology: Official Journal of the American Society of Clinical Oncology* 27 (21): 3437–44. https://doi.org/10.1200/JCO.2008.18.9068.

Pierobon, Mariaelena, and Cara L. Frankenfeld. 2013. "Obesity as a Risk Factor for Triple-Negative Breast Cancers: A Systematic Review and Meta-Analysis." *Breast Cancer Research and Treatment* 137 (1): 307–14. https://doi.org/10.1007/s10549-012-2339-3.

Porter, Alan G., and Reiner U. Jänicke. 1999. "Emerging Roles of Caspase-3 in Apoptosis." *Cell Death and Differentiation* 6 (2): 99–104. https://doi.org/10.1038/sj.cdd.4400476.

Protani, Melinda, Michael Coory, and Jennifer H. Martin. 2010. "Effect of Obesity on Survival of Women with Breast Cancer: Systematic Review and Meta-Analysis." *Breast Cancer Research and Treatment* 123 (3): 627–35. https://doi.org/10.1007/s10549-010-0990-0.

Qu, Q., F. Zeng, X. Liu, Q. J. Wang, and F. Deng. 2016. "Fatty Acid Oxidation and Carnitine Palmitoyltransferase I: Emerging Therapeutic Targets in Cancer." *Cell Death and Disease* 7 (5): 1–9. https://doi.org/10.1038/cddis.2016.132.

Renehan, Andrew G, Margaret Tyson, Matthias Egger, Richard F Heller, and Marcel Zwahlen. 2008. "Body-Mass Index and Incidence of Cancer: A Systematic Review and Meta-Analysis of Prospective Observational Studies." *The Lancet* 371 (9612): 569–78. https://doi.org/10.1016/S0140-6736(08)60269-X.

Romar, George A., Thomas S. Kupper, and Sherrie J. Divito. 2016. "Research Techniques Made Simple: Techniques to Assess Cell Proliferation." *Journal of Investigative Dermatology* 136 (1): e1–7. https://doi.org/10.1016/j.jid.2015.11.020.

Salic, Adrian., and Timothy Mitchison. 2008. "A Chemical Method for Fast and Sensitive Detection of DNA Synthesis in Vivo: Commentary." *Proceedings of the National Academy of Sciences* 6 (2): 157–58. https://doi.org/10.1089/adt.2008.9995.

Schwab, Luciana P., Danielle L. Peacock, Debeshi Majumdar, Jesse F. Ingels, Laura C. Jensen, Keisha D. Smith, Richard C. Cushing, and Tiffany N. Seagroves. 2012. "Hypoxia-Inducible Factor 1α Promotes Primary Tumor Growth and Tumor-Initiating Cell Activity in Breast Cancer." *Breast Cancer Research* 14 (1): 1–25. https://doi.org/10.1186/bcr3087.

Semenza, Gregg L. 2013. "HIF-1 Mediates Metabolic Responses to Intratumoral Hypoxia and Oncogenic Mutations Find the Latest Version : Review Series HIF-1 Mediates Metabolic Responses to Intratumoral Hypoxia and Oncogenic Mutations." *Journal of Clinical Investigation* 123 (9): 3664–71. https://doi.org/10.1172/JCI67230.3664.

Semenza, Gregg L., Peter H. Roth, Hon Ming Fang, and Guang L. Wang. 1994. "Transcriptional Regulation of Genes Encoding Glycolytic Enzymes by Hypoxia-Inducible Factor 1." *Journal of Biological Chemistry* 269 (38): 23757–63.

Shahar, Suzana, Rabeta Mohd Salleh, Ahmad Rohi Ghazali, Poh Bee Koon, and Wan Nazaimoon Wan Mohamud. 2010. "Roles of Adiposity, Lifetime Physical Activity and Serum Adiponectin in Occurrence of Breast Cancer among Malaysian Women in Klang Valley." *Asian Pacific Journal of Cancer Prevention* 11 (1): 61–66.

Sheng, Yi, Chon Hwa Tsai-Morris, Jie Li, and Maria L. Dufau. 2009. "Lessons from the Gonadotropin-Regulated Long Chain Acyl-CoA Synthetase (GR-LACS) Null Mouse Model: A Role in Steroidogenesis, but Not Result in X-ALD Phenotype." *Journal of Steroid Biochemistry and Molecular Biology* 114 (1–2): 44–56. https://doi.org/10.1016/j.jsbmb.2008.12.011.

Sieri, Sabina, Paola Muti, Agnoli Claudia, Franco Berrino, Valeria Pala, Sara Grioni, Carlo Alberto Abagnato, et al. 2012. "Prospective Study on the Role of Glucose Metabolism in

Breast Cancer Occurrence." *International Journal of Cancer* 130 (4): 921–29. https://doi.org/10.1002/ijc.26071.
Simpson, Evan R., and Kristy A. Brown. 2013. "Obesity and Breast Cancer: Role of Inflammation and Aromatase." *Journal of Molecular Endocrinology* 51 (3). https://doi.org/10.1530/JME-13-0217.
Smith, Ian E, and Mitch Dowset. 2003. "Aromatase Inhibitors in Breast Cancer Prevention." *New England J* 48 (12): 1605–10. https://doi.org/10.1177/1060028014548416.
Sridharan, Gokul, and Akhil A. Shankar. 2012. "Toluidine Blue: A Review of Its Chemistry and Clinical Utility." *Journal of Oral and Maxillofacial Pathology* 16 (2): 251–55. https://doi.org/10.4103/0973-029X.99081.
Steinberg, Steven J., Janine Morgenthaler, Ann K. Heinzer, Kirby D. Smith, and Paul A. Watkins. 2000. "Very Long-Chain Acyl-CoA Synthetases: Human 'bubblegum' Represents a New Family of Proteins Capable of Activating Very Long-Chain Fatty Acids." *Journal of Biological Chemistry* 275 (45): 35162–69. https://doi.org/10.1074/jbc.M006403200.
Sun, Shichao, Yao Sun, Xiaoping Rong, and Lei Bai. 2019. "High Glucose Promotes Breast Cancer Proliferation and Metastasis by Impairing Angiotensinogen Expression." *Bioscience Reports* 39 (6): 1–9. https://doi.org/10.1042/BSR20190436.
Sung, Young Kwan, Sun Young Hwang, Mi Kyung Park, Han Ik Bae, Woo Ho Kim, Jung Chul Kim, and Moonkyu Kim. 2003. "Fatty Acid-CoA Ligase 4 Is Overexpressed in Human Hepatocellular Carcinoma." *Cancer Science* 94 (5): 421–24. https://doi.org/10.1111/j.1349-7006.2003.tb01458.x.
Tameemi, Wafaa Al, Tina P. Dale, Rakad M. Kh Al-Jumaily, and Nicholas R. Forsyth. 2019. "Hypoxia-Modified Cancer Cell Metabolism." *Frontiers in Cell and Developmental Biology* 7 (January): 1–15. https://doi.org/10.3389/fcell.2019.00004.
Tang, Pei Zhong, Chon Hwa Tsai-Morris, and Maria L. Dufau. 2001. "Cloning and Characterization of a Hormonally Regulated Rat Long Chain Acyl-CoA Synthetase." *Proceedings of the National Academy of Sciences of the United States of America* 98 (12): 6581–86. https://doi.org/10.1073/pnas.121046998.
Technologies, Agilent. 2019. "Mito Stress Test Kit User Guide Seahorse."
Tőkés, Tímea, Anna Mária Tőkés, Gyöngyvér Szentmártoni, Gergő Kiszner, Dorottya Mühl, Béla Ákos Molnár, Janina Kulka, Tibor Krenács, and Magdolna Dank. 2019. "Prognostic and Clinicopathological Correlations of Cell Cycle Marker Expressions before and after the Primary Systemic Therapy of Breast Cancer." *Pathology and Oncology Research*. https://doi.org/10.1007/s12253-019-00726-w.
Tomoda, H., K. Igarashi, J. C. Cyong, and S. Omura. 1991. "Evidence for an Essential Role of Long Chain Acyl-CoA Synthetase in Animal Cell Proliferation: Inhibition of Long Chain Acyl-CoA Synthetase by Triacsins Caused Inhibition of Raji Cell Proliferation." *Journal of Biological Chemistry* 266 (7): 4214–19.
Toro, Allyson L., Nicholas S. Costantino, Craig D. Shriver, Darrell L. Ellsworth, and Rachel E. Ellsworth. 2016. "Effect of Obesity on Molecular Characteristics of Invasive Breast Tumors: Gene Expression Analysis in a Large Cohort of Female Patients." *BMC Obesity* 3 (1): 1–9. https://doi.org/10.1186/S40608-016-0103-7.
Torres, María P., Satyanarayana Rachagani, Joshua J. Souchek, Kavita Mallya, Sonny L. Johansson, and Surinder K. Batra. 2013. "Novel Pancreatic Cancer Cell Lines Derived from Genetically Engineered Mouse Models of Spontaneous Pancreatic Adenocarcinoma: Applications in Diagnosis and Therapy." *PLoS ONE* 8 (11): 1–12.

https://doi.org/10.1371/journal.pone.0080580.
Ulanet, Danielle B, Dale L Ludwig, C Ronald Kahn, and Douglas Hanahan. 2010. "Insulin Receptor Functionally Enhances Multistage Tumor Progression and Conveys Intrinsic Resistance to IGF-1R Targeted Therapy." *Proceedings of the National Academy of Sciences of the United States of America* 107 (24): 10791–98. https://doi.org/10.1073/pnas.0914076107.
Vaisse, C, J L Halaas, C M Horvath, J E Darnell, Markus Stoffel, and J M Friedman. 1996. "Leptin Activation of Stat3 in the Hypothalamus of Wild-Type and Ob/Ob Mice but Not Db/Db Mice." *Nature Genetics* 14 (1): 95–97. https://doi.org/10.1038/ng0996-95.
Vaupel, P., K. Schlenger, C. Knoop, and M. Hockel. 1991. "OxygeNationof Human Tumors: Evaluation Of Tissue Oxygen Distribution In Breast Cancers By Computerized O2 Tension Measurements'." *Cancer Research* 51 (12): 3316–22.
Vaysse, Charlotte, Jon Lomo, Oystein Garred, Froydis Fjeldheim, Trygve Lofteroed, Ellen Schlichting, Anne McTiernan, et al. 2017. "Inflammation of Mammary Adipose Tissue Occurs in Overweight and Obese Patients Exhibiting Early-Stage Breast Cancer." *Npj Breast Cancer* 3 (1): 1–9. https://doi.org/10.1038/s41523-017-0015-9.
Wang, Guang L., Bing Hua Jiang, Elizabeth A. Rue, and Gregg L. Semenza. 1995. "Hypoxia-Inducible Factor 1 Is a Basic-Helix-Loop-Helix-PAS Heterodimer Regulated by Cellular O2 Tension." *Proceedings of the National Academy of Sciences of the United States of America* 92 (12): 5510–14. https://doi.org/10.1073/pnas.92.12.5510.
Wang, Yuan Yuan, Philippe Valet, Catherine Muller, Yuan Yuan Wang, Camille Attané, Delphine Milhas, Béatrice Dirat, et al. 2017. "Mammary Adipocytes Stimulate Breast Cancer Invasion through Metabolic Remodeling of Tumor Cells Find the Latest Version : Mammary Adipocytes Stimulate Breast Cancer Invasion through Metabolic Remodeling of Tumor Cells." *JCI Insight* 2 (4): 1–21.
Ward, Zachary J., Sara N. Bleich, Angie L. Cradock, Jessica L. Barrett, Catherine M. Giles, Chasmine Flax, Michael W. Long, and Steven L. Gortmaker. 2019. "Projected U.S. State-Level Prevalence of Adult Obesity and Severe Obesity." *New England Journal of Medicine* 381 (25): 2440–50. https://doi.org/10.1056/NEJMsa1909301.
Whelan, Jay, and Kevin Fritsche. 2013. "Linoleic Acid." *American Society for Nutrition*, 311–12. https://doi.org/10.3945/an.113.003772.311.
White, Alexandra J., Hazel B. Nichols, Patrick T. Bradshaw, and Dale P. Sandler. 2015. "Overall and Central Adiposity and Breast Cancer Risk in the Sister Study." *Cancer* 121 (20): 3700–3708. https://doi.org/10.1002/cncr.29552.
Whiteman, David C., and Louise F. Wilson. 2016. "The Fractions of Cancer Attributable to Modifiable Factors: A Global Review." *Cancer Epidemiology* 44: 203–21. https://doi.org/10.1016/j.canep.2016.06.013.
Williams, Ellen P., Marie Mesidor, Karen Winters, Patricia M. Dubbert, and Sharon B. Wyatt. 2015. "Overweight and Obesity: Prevalence, Consequences, and Causes of a Growing Public Health Problem." *Current Obesity Reports* 4 (3): 363–70. https://doi.org/10.1007/s13679-015-0169-4.
Wolf, Beni B., Martin Schuler, Fernando Echeverri, and Douglas R. Green. 1999. "Caspase-3 Is the Primary Activator of Apoptotic DNA Fragmentation via DNA Fragmentation Factor-45/Inhibitor of Caspase-Activated DNase Inactivation." *Journal of Biological Chemistry* 274 (43): 30651–56. https://doi.org/10.1074/jbc.274.43.30651.
Yamashita, Atsushi, Yasuhiro Hayashi, Naoki Matsumoto, Yoko Nemoto-Sasaki, Saori Oka,

Takashi Tanikawa, and Takayuki Sugiura. 2014. “Glycerophosphate/Acylglycerophosphate Acyltransferases.” *Biology* 3 (4): 801–30. https://doi.org/10.3390/biology3040801.
Yang, Xiaoping, Jesse S. Boehm, Xinping Yang, Kourosh Salehi-Ashtiani, Tong Hao, Yun Shen, Rakela Lubonja, et al. 2011. “A Public Genome-Scale Lentiviral Expression Library of Human ORFs.” *Nature Methods* 8 (8): 659–61. https://doi.org/10.1038/nmeth.1638.
Yang, Yu-an, Howard Yang, Ying Hu, Peter Watson, Huaitian Liu, Thomas R. Geiger, Miriam R. Anver, et al. 2017. “Abstract 1846: Immunocompetent Mouse Allograft Models for Development of Therapies to Target Breast Cancer Metastasis Therapies to Target Breast Cancer Metastasis” 8 (19): 1846–1846. https://doi.org/10.1158/1538-7445.am2017-1846.
Ying, Xuexiang, Yunpo Sun, and Pingqing He. 2015. “Bone Morphogenetic Protein-7 Inhibits EMT-Associated Genes in Breast Cancer.” *Cellular Physiology and Biochemistry* 37 (4): 1271–78. https://doi.org/10.1159/000430249.
Young, Kwan Sung, Kyung Park Mi, Hyung Hong Su, Young Hwang Sun, Hee Kwack Mi, Chul Kim Jung, and Kyu Kim Moon. 2007. “Regulation of Cell Growth by Fatty Acid-CoA Ligase 4 in Human Hepatocellular Carcinoma Cells.” *Experimental and Molecular Medicine* 39 (4): 477–82. https://doi.org/10.1038/emm.2007.52.
Zaidi, Nousheen, Leslie Lupien, Nancy B. Kuemmerle, William B. Kinlaw, Johannes V. Swinnen, and Karine Smans. 2013. “Lipogenesis and Lipolysis: The Pathways Exploited by the Cancer Cells to Acquire Fatty Acids.” *Progress in Lipid Research* 52 (4): 585–89. https://doi.org/10.1016/j.plipres.2013.08.005.
Zhang, Maomao, Julie S. Di Martino, Robert L. Bowman, Nathaniel R. Campbell, Sanjeethan C. Baksh, Theresa Simon-Vermot, Isabella S. Kim, et al. 2018. “Adipocyte-Derived Lipids Mediate Melanoma Progression via FATP Proteins.” *Cancer Discovery* 8 (8): 1006–25. https://doi.org/10.1158/2159-8290.CD-17-1371.
Zhong, Hua, Angelo M. De Marzo, Erik Laughner, Michael Lim, David A. Hilton, David Zagzag, Peter Buechler, William B. Isaacs, Gregg L. Semenza, and Jonathan W. Simons. 1999. “Overexpression of Hypoxia-Inducible Factor 1α in Common Human Cancers and Their Metastases.” *Cancer Research* 59 (22): 5830–35.